AN ABSTRACT OF THE THESIS OF

Yi Wang for the degree of Master of Science in Wood Science presented on July 20, 2007.

Title: Morphological Characterization of Wood Plastic Composite (WPC) with Advanced Imaging Tools: Developing Methodologies for Reliable Phase and Internal Damage Characterization.

Abstract approved:

Lech Muszyński

Wood plastic composites (WPCs) are composite materials made from thermoplastic polymers, wood flour, and a small amount of process- and property-enhancing additives; they are principally used in the automotive industry and as secondary building materials. Although the WPC market is expected to keep growing, it is still relatively small when compared with other building materials. Challenges for increasing the market share of WPCs include relatively low tensile strength and stiffness, significant long-term creep deformations and weak creep rupture properties. A significant barrier to obtain better understanding of the composite performance and internal bond durability is the lack of reliable tools and procedures for direct quantitative measurement of the micro-mechanical response of this heterogeneous material. The objective of this study was to use advanced imaging tools, including X-ray computed tomography (CT) and conventional microscopy for quantitative morphological characterization of WPCs, with the focus on developing methodologies for reliable characterization of component phases and internal damage generated by accelerated weathering and cyclic loading.

One of the primary concerns in X-ray CT scanning of WPCs is the poor contrast between the wood and polyethylene, which is the most common polymer for the WPC matrix. The objective of the first part of the thesis was to investigate the applicability of fine gold particles as contrast agent. Specifically, the effects of adding gold nano- and micro-particles, and commonly used surfactant on the mechanical properties of WPCs was assessed. Technically pure gold micro-particles was found to be an effective contrast agent for X-ray CT scanning of wood/HDPE composites. When used without surfactant, the addition of 1% gold particles did not impair the tensile properties of the composites.

In order to establish effective experimental methodologies for morphological characterization of WPCs in the second part of the project, various imaging tools, including X-ray CT scanning, optical and electron microscopy were applied to examine wood particles embedded in the polymer matrix. Scans and images of uncompounded wood particles were used for reference. Such a combination of the imaging tools assisted in confirmation of the existence of an extensive wood/polymer interphase within the wood particles. Using the X-ray CT scanning, the combined volume of the interphase was quantitatively determined to be about 56% of the wood particle volume. This knowledge is critically needed for the proper assessment of the wood particle content from the CT scans.

The third part of the thesis reports on a research which is not part of the original MS project, and is still in progress. This part was included to demonstrate how the conclusions and methods derived in the previous two parts are applied in further research. Here, the X-ray CT scanning technique is applied to examine the morphological changes in WPCs resulting from accelerated weathering treatment and cyclic loading. It was found that significant initial tensile modulus loss in wood/PVC composites may be induced by the relatively low number of accelerated soak-dry and freeze-thaw weathering cycles. Although no significant modulus loss was observed for the specimens subjected to cyclic tensile loading, the reduced residual strength indicated a significant damage accumulation.

In summary, X-ray CT scanning was found to be a promising and effective nondestructive technique for 3D in situ examination and morphological characterization of WPCs. The experimental methodologies employing various imaging tools (including X-ray CT scanning and 2D microscopy) and digital image processing methods are capable of characterizing WPCs, its component phases and the interphase returning statistically meaningful quantitative data.

Morphological Characterization of Wood Plastic Composite (WPC) with Advanced Imaging Tools: Developing Methodologies for Reliable Phase and Internal Damage Characterization

by
Yi Wang

A THESIS

submitted to

Oregon State University

in partial fulfillment of
the requirement for the
degree of

Master of Science

Presented July 20, 2007
Commencement June, 2008

Master of Science thesis of Yi Wang presented on July 20, 2007.

APPROVED:

Major Professor, representing Wood Science

Head of the Department of Wood Science and Engineering

Dean of the Graduate School

I understand that my thesis will become part of the permanent collection of Oregon State University libraries. My signature below authorizes release of my thesis to any reader upon request.

Yi Wang, Author

ACKNOWLEDGEMENTS

This research was funded in part by McIntire-Stennis Project #: OREZ-FP-821-U and OSU General Research Fund grant 2004/05. The pine flour was donated by American Wood Fibers (Schofield, WI). I would like to express sincere appreciation to my major professor, Dr. Lech Muszyński for his guidance and patience in the last two years, and my minor professor, Dr. John Simonsen for his valuable advice and help. Dr. Brian Bay, Dr. Dan Berry in the Department of Mechanical Engineering at OSU provided great help with their X-ray CT and mechanical testing facilities. Dr. Urszula Iwaniec and Jamie C. Hunter in Bone Research Laboratory at OSU helped me with numerous access to their MicroCT scanner. Dr. John Lu helped me with specimen fabrication and mechanical testing. Dr. Kate McCulloh assisted me in microscopic examination. Milo Clauson helped me in the mechanical testing and experiments. Connie Love and Camille Freitag assisted me in the durability experiments. Henrik Lund Frandsen, Aurélien Sevrain also helped me with my experiments. Without their kind assistance and help, it would be impossible to finish this thesis. Special thanks should be given to all the faculty and staff in Wood Science Department community, with whom I spent really wonderful two years in Corvallis. I would also like to say thank you to my wife, Li Liu for her support and assistance during this research.

CONTRIBUTION OF AUTHORS

Dr. Lech Muszyński was involved with the writing of Chapter 3-5. Dr. John Simonsen was involved with the writing of Chapter 3.

TABLE OF CONTENTS

LIST OF FIGURES

LIST OF FIGURES (Continued)

Figure Page

LIST OF TABLES

LIST OF APPENDICES

Page

LIST OF APPENDIX FIGURES

LIST OF APPENDIX FIGURES (Continued)

Figure Page

LIST OF APPENDIX FIGURES (Continued)

Morphological Characterization of Wood Plastic Composite (WPC) with Advanced Imaging Tools: Developing Methodologies for Reliable Phase and Internal Damage Characterization.

CHAPTER 1 -- INTRODUCTION

Background

Wood plastic composites (WPCs) are relatively new composite materials made of wood flour, thermoplastic polymer, and small amounts of additives. It was first developed several decades ago as a way of utilizing post-consumer recycled plastics such as polyethylene milk jugs and grocery bags, and sawdust, generated as a waste product of lumber mills and furniture factories. Currently, high density polyethylene (HDPE, virgin or recycled) are predominantly used to make commercial WPC products, some other thermoplastics, including poly (vinyl chloride) (PVC) and polypropylene (PP) are also used in the WPC market. Other polymers, such as polystyrene and acrylonitrile-butadiene-styrene (ABS) are also being used. Small amount of thermoset resins such as phenol-formaldehyde or diphenyl methane diisocyanate are sometimes used in composites with a high wood content (Clemons 2002).

Besides wood and polymer, some additives are added in small amounts to enhance processing and performance of WPCs. The most often used additives include compatibilizers, lubricants, colorants, pigments, and foaming agents, etc. The majority of WPCs are manufactured by profile extrusion, while other processing technologies such as injection molding and compression molding are also used. Since the typical sizes of wood particles used for WPCs range from 10 to 80 mesh, and the polymer content of polymers is relatively high, WPCs are morphologically closer to concrete or short-fiber reinforced composites than conventional wood fiberboard or particleboard. Therefore, different approaches are needed to deal with the research or testing for WPCs.

As a material composed of wood and polymer, WPCs show many advantages over neat plastics, such as improved stiffness, creep resistance, and thermal stability, and so on. However, they also have some limitations, like increased sensitivity to moisture and long-term deformation. WPCs were initially used in automobile and secondary building applications that had relatively low structural requirements and were not

regulated by building codes, such as picnic tables, decking, and some other products. Arising from the complaints about the treated lumber product attributes such as long-term maintenance, surface characteristics, and straightness, WPC decking gained relative success. In addition, WPCs were believed to be resistant to biodegradation, which raised hopes for the development of a material that could replace increasingly scrutinized treated wood in structures exposed to the elements (Clemons 2002; Wolcott and Smith 2004).

Although the WPC market is expected to keep growing rapidly, the market potential for WPCs still remains untapped at less than 5% of all building materials (Dagher 2005; Morton et al. 2003; Rossi 2005). To compete with other predominant building materials (such as solid wood, glulam, and LVL), it is important that WPC properties can be improved to satisfy the building code requirements. Challenges include relatively lower tensile strength and lower stiffness, but most importantly longer-term creep deformations and creep rupture properties (Dagher 2005; Smith and Wolcott 2006; Wolcott and Smith 2004).

It is widely believed that the key to increasing the volume of the WPC products and the future of the market is the development of highly engineered WPCs characterized by better structural performance such as stiffness and duration of load (DOL) response (Dagher 2005). In advancing WPC technology to allow for structural applications, it is critical to understand how WPCs perform under load and changing environments. A significant barrier in this development is the lack of reliable tools and procedures for direct quantitative measurement of the micro-mechanical response of this heterogeneous material.

The mechanical and physical properties of WPCs may be engineered to some extent by changing component characteristics and proportions, filler orientation and distribution, and by fine tuning the processing parameters. However, composite design is limited by the naturally variable wood properties and the limited selection of thermoplastics that may be used with wood, which decomposes at temperatures above

200 °C. Consequently, research efforts in WPCs have been mostly focused on improving the internal bonding between the wood particles and the matrix. The hydrophilic wood particles are generally incompatible with hydrophobic thermoplastic polymers. The incompatibility between wood and polymer matrix is a major problem for interfacial adhesion between these two component materials, which is of critical importance for the mechanical properties of the composite (Bledzki et al. 1998; Jiang and Kamdem 2004). To examine the role of the interface on WPCs properties, a number of micro-mechanical studies on single-fiber/polymer systems have been conducted (Egan and Shaler 2000; Eichhorn and Young 2004; Rials et al. 2001; Shaler et al. 1997; Stamboulis et al. 1999; Tze et al. 2003). The above research provided valuable fundamental background information, including the basic failure behavior of the interface and the micro-mechanical value (the apparent shear strength) for particular compositions. However, these results cannot substitute for a direct in situ knowledge of how larger particles of much more diverse geometry interact with a solid polymer matrix. Such studies also cannot answer the important question of what is the statistical significance of the variability and distribution of filler particles in the material.

Digital images carry large amount of information, therefore, various 2D and 3D imaging tools are being applied to understand the interfacial characteristics of WPCs destructively or nondestructively. Scanning electron microscopy (SEM) is one of the most commonly used image techniques (Oksman and Clemons 1998; Ray et al. 2002; Redondo et al. 2003; Rials et al. 2001; Tripathy et al. 2000). Other 2D and 3D imaging techniques including transmission electron microcopy (TEM), energy-dispersive X-ray analysis (EDX), atomic force microscopy (AFM), and three dimensional confocal laser scanning microscopy (CLSM) have been successfully used to obtain qualitative understanding of the interaction between wood and polymer in WPCs (Michaeli et al. 2000). Those studies demonstrated how imaging tools helped to obtain qualitative understanding of the interaction between wood and polymer in WPCs. However, in most of these studies, conclusions were drawn from assessment of small areas of

interest. Little discussion was offered on how these regions of interest were selected and whether they could be representative of the material under investigation. Such assessment is rarely supported by an objective quantitative analysis on the statistical significance and spatial distribution of the observed features.

High-resolution X-ray computed tomography (CT) created new opportunities for nondestructive, in situ analysis of particulate composites. X-ray CT scanners are capable of returning digital images carrying spatial information coded in discrete grayscale values representing densities and X-ray attenuations assigned to millions of voxels arranged in arrays (Park et al. 2003; Pétraud et al. 2003). The combination of high-resolution nondestructive imaging techniques like X-ray CT with machine vision tools provides the means for a quantitative characterization of the internal structure of heterogeneous composites as well as an assessment of the deformation and damage that occurs because of climate exposure and loading. Machine vision-based characterization of 3D samples of particulate composites and fibrous materials have already been proposed by some researchers (Bertilsson et al. 1992; Kamke and Lee 2007; Peix et al. 1997; Shaler et al. 2003; Yang and Lindquist 2000). However, most of the proposed algorithms assumed a high contrast and relatively well defined interfaces between component materials.

HDPE is the predominantly used polymer in commercial WPC products; in this study, it was selected as the starting point for examination of internal structure and micro-mechanics of WPCs with the help of X-ray CT scanning. However, due to similar X-ray attenuation in wood and HDPE, only weak contrast can be obtained between those two components in X-ray CT scanning of wood/HDPE composites. In our preliminary study, gold along with a surfactant used in the process of generating the gold particles were added to wood/HDPE composite to improve the CT scanning contrast between wood and HDPE. It was found that although scanning contrast could be improved significantly, the gain was achieved with the price of reduced mechanical properties.

Objectives

The general objective of this study was to develop experimental tools and procedures for 3D morphological characterization and evaluation of micro-damage accumulation in wood plastic composites (WPCs). The specific objectives were:

1. To examine the effects of adding gold particles and surfactant on the mechanical properties of resulting wood/HDPE composite and their effects on the X-ray CT scanning contrast between wood and HDPE component.

2. To establish an effective experimental methodology for quantitative morphological characterization of WPCs that would properly account for the existence of interphase between the wood particles and the polymer matrix.

3. To investigate effective methods for quantitative characterization of the morphological changes in WPCs resulting from accelerated weathering and cyclic mechanical loading, and to correlate the structural changes to the mechanical property loss in these degradation treatments.

Thesis Structure and Units

This thesis is written in manuscript format. It has seven chapters. Chapter 1 is the general introduction. Chapter 2 is the comprehensive literature review. Chapter 3 discusses the suitability of using gold as an X-ray CT scanning contrast agent for wood/HDPE composites, the effect of gold and surfactant on the mechanical properties and X-ray CT scanning contrast of the resulting composites. Chapter 3 has been accepted by *Holzforschung* journal for publication. Chapter 4 discusses the methodology for quantitative characterization of wood/polymer interphase in WPCs on various scale levels using digital image tools. Chapter 4 will be submitted to *Holzforschung* journal after the final revision. Chapter 5 describes a project that is still in progress, and its completion is out of the scope of this thesis. This chapter is concerned with assessing durability of WPCs using X-ray CT scanning. The methodology and the preliminary experimental results were presented and discussed.

Chapter 5 is also prepared for publication. Chapter 6 is the general conclusion, which summarizes the conclusions from previous chapters, and is followed by bibliography, and appendices.

CHAPTER 2 -- LITERATURE REVIEW

Wood Plastic Composites (WPCs) and Applications

Clemons (2002) defined wood plastic composites (WPCs) as any composites that contain wood and thermoset or thermoplastic polymers. Nevertheless, the term "WPC" is most often used to represent particulate wood/thermoplastic composites. WPCs were first developed several decades ago as a way of utilizing post-consumer recycled plastics such as polyethylene milk jugs and grocery bags, and sawdust, generated as a waste product of lumber mills and furniture factories (Clemons 2002). WPCs were initially used in automobile and secondary building applications that had relatively low structural requirements and were not regulated by building codes, such as picnic tables, decking, and some other products. Arising from the complaints about the treated lumber product attributes such as long-term maintenance, surface characteristics and straightness, WPC decking were introduced. Among all the WPC products, decking (Figure 2.1a) is the largest application with nearly two-thirds of the extruded WPC market in the United States in 2005, followed by window and door frames (11%) (Figure 2.1b), with addition of some other applications, such as fencing, docks, and so on (Smith and Wolcott 2006).

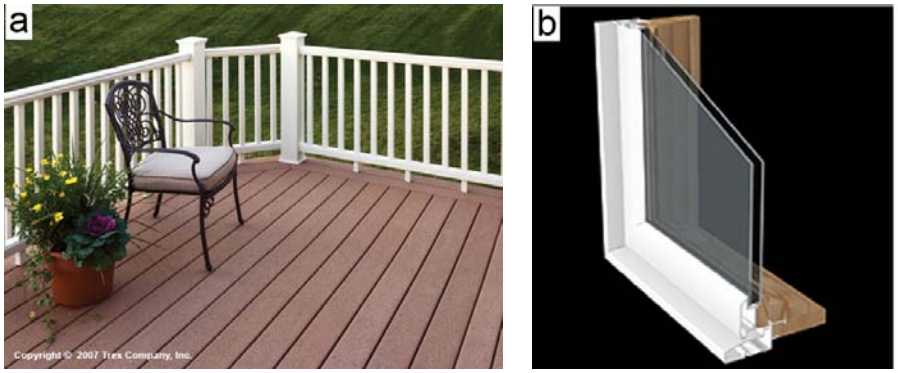

Figure 2.1 Application of wood plastic composites: (a) Decking, (b) Window frame.

Source: Figure 2.1a is from http://www.trex.com/, Figure 2.1b is from http://www.commercialwindows.umn.edu/materials_assemblies1.php

A typical WPC compound contains 50-70% wood flour by weight. Wood flour is finely divided ground wood with a flour-like consistency made by grinding planer shavings, chips, and sawdust. Typical particle sizes are 10 to 80 mesh (Clemons 2002). The aspect ratio (length/diameter) of the wood particles is in the range of 1:1 to

4:1 (Patterson 2001). The combination of wood flour and thermoplastics results in a particulate composite with wood particles embedded in polymer matrix.

Because of the limited thermal stability of wood, only thermoplastics that melt or can be processed at temperature below 200 °C (392 °F) are commonly used in WPCs (Clemons 2002). The most widely used thermoplastics for WPCs are polyethylene (PE), poly (vinyl chloride) (PVC) and polypropylene (PP). Among these polymers, PE (virgin and recycled) accounts for 83% of market share, followed by PVC (9%) and PP (7%) (Morton et al. 2003). Currently, most WPCs made with PE are used in exterior building components, such as decking, fencing, siding, and so on. WPCs made with PP are typically used in automotive applications. Wood/PVC composites are mainly used in window manufacturing as well as some decking applications (Clemons 2002).

Different types of additives, such as compatibilizers, lubricants, colorants, pigments, and foaming agents may be required to blend the plastic with wood or to achieve the desired composite properties. Compatibilizers (or coupling agents) are the most often used additives. Since the hydrophilic wood particles are generally incompatible with hydrophobic thermoplastic polymers. Compatibilizers are added to influence the internal bonding between the wood and polymer matrix. It helps to improve the dispersion, flow, and mechanical properties of the composite when increased performance is required. The most common compatibilizers used today are maleic anhydride grafted polypropylene (MAPP) and maleic anhydride grafted polyethylene (MAPE) (Rowell 2006).

Lubricants reduce friction in the compounding and forming process, and thus increase throughput and improve WPC surface appearance. Standard lubricants for polyolefins and PVC, such as ethylene bis-stearamide (EBS), zinc strearate, paraffin waxes, and oxidized PE, can be used for WPCs. Colorants are used to provide both a wood-like appearance and UV resistance. Pigment levels must be 1% to 3% or higher to overcome color staining from the wood. Color concentrates tailored for WPCs

typically include lubricant and often are customized multifunctional packages that may include coupling agents, antimicrobials, and UV stabilizers. Foaming agents are also of great interest because chemical foaming reduces weight and materials cost as well as improve surface appearance, processing speed, machinability, and ease of surface finishing of products. Another category of additive is antifungal biocides that protect either the plastic component and maintain its surface appearance or that preserve the wood component from decay and also reduce moisture absorption (Sherman 2004).

Besides the expected enhancing effects of additives, they might adversely affect the properties of the components or the interface (Clemons 2002; Colom et al. 2003; Gardner et al. 2004; Geng et al. 2004; Lee et al. 2004; Manchado et al. 2003; Newson and Maine 2004; Wolcott and Smith 2004; Zafeiropoulos et al. 2002). In most studies, the wood/polymer interaction was discussed from the chemical point of view. Although mechanical coupling is considered a major mechanism in adhesion, no known studies have addressed its role in WPCs (Wolcott 2003).

The manufacture of wood plastic composites is often a two-step process (Clemons 2002). The raw materials are first mixed together in a process called compounding, and the compounded material is then formed into a product. The majority of WPCs are manufactured by profile extrusion (Figure 2.2a), in which molten composite material is forced through a die to make a continuous profile of the desire shape (Figure 2.2b). Other processing technologies such as injection molding and compression molding are also used to produce WPCs, but the total poundage is much less than what is produced with extrusion.

In comparison with solid wood, WPCs are believed to have following advantages: 1. Good moisture resistance and dimensional stability when exposed to moisture; 2. Resistance to rot and insects; 3. Longer life and low maintenance; 4. No finishing required (color can be added during processing); 5. Relatively easy to make complex shapes by profile extrusion or injection molding; 6. Easy installation (easy machining,

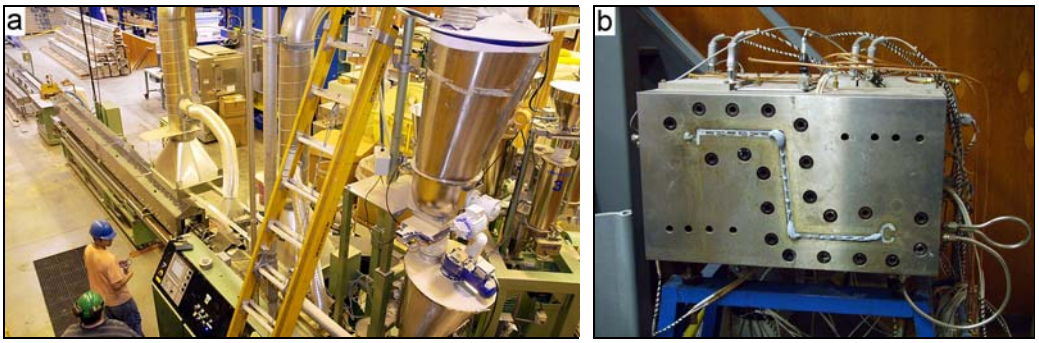

Figure 2.2 Extrusion facilities at the University of Maine: (a) Extrusion line, (b) Profile die.

Source: Figure 2.2 a,b are from the University of Maine website: http://www.aewc.umaine.edu/equipment/woodtruder.htm

no splinters or cracks); 7. No toxic chemical contents (particularly compared with conventional chemical treated lumber).

On the other hand, WPCs have certain limitations when compared with both components. In comparison with solid wood, these are: 1. Generally WPCs are more expensive to produce due to the cost of the polymers; 2. Mechanical properties such as creep resistance, stiffness and strength are lower than solid wood, 3. Higher thermal expansion than wood; 4. Limited use in exterior applications; 5. The majority of WPCs do not have the aesthetic appeal of real wood (Clemons 2002; Dagher 2005; Jiang and Kamdem 2004; Smith and Wolcott 2006; Wolcott 2003).

As products and market develop, WPCs are expanding from decking and railing systems to fenestration applications and exterior covering applications. It is expected that the WPC market will keep growing rapidly in the coming years (Smith and Wolcott 2006). However, the market potential for WPCs still remains untapped at less than 5% of the building material (Morton et al. 2003; Rossi 2005). To compete with other predominant wood-based building materials (such as solid wood, glulam, and I-joists), it is important that WPCs properties can be improved to satisfy the building code requirements. Challenges include relatively lower tensile strength and lower stiffness, but most importantly longer-term creep deformations and creep rupture properties (Dagher 2005; Smith and Wolcott 2006; Wolcott and Smith 2004).

Effects of Wood Particle Characteristics on WPC Properties

As the major component of WPCs, wood flour plays an important role on the properties of the resulting composites. WPC properties are significantly affected by wood flour quality and characteristics, of which species and size of wood particles are two of the most important factors.

Effects of Wood Species

Berger and Stark (1997) investigated the mechanical properties of PP filled with wood flours of different species (ponderosa pine, loblolly pine, maple and oak). The following properties were measured: Izod impact energy (notched and unnotched), flexural strength and MOE, tensile strength and MOE, tensile elongation, mold shrinkage, and heat deflection (264 psi). The species' effects on the performances of the resulting composites were examined. It was concluded that hardwood flours provided an improvement in tensile properties and heat deflection temperature (the temperature at which a polymer or plastic sample deforms under a specified load) over softwood flour, however, ponderosa pine wood flour provides the best overall mechanical property enhancements compared with other species.

Effects of Wood Particle Sizes

Generally, commercial wood flours have a specific but broad particle distribution, because extra screening to narrow the particle size distribution would result in higher manufacturing cost. As a result, a comparison of mesh sizes from a commercial wood flour supplier results in an overlap of particle size. This in turn made it difficult to characterize properties based on specific particle sizes using commercial wood flour, particularly at larger mesh sizes (smaller particle sizes) (Stark and Berger 1997).

Extensive research effort (quoted below) has been made to examine the effects of wood particles sizes (expressed mostly as the sieve mesh size) on the properties of the composites. However, different effects of particle sizes were often observed by different researchers.

On one hand, some researchers reported favorable effects of fine wood particles on composite properties: Maiti and Singh (1986) reported that compared with wood flour of coarse size (355 to 425 μm), finer particles (less than 180 μm) offered higher tensile strength and hardness, while lower impact strength for resulting wood/HDPE composites. Later, Myers et al. (1991) found that fine wood particles (40 mesh) provided higher tensile and flexural strength than coarse particles (20 mesh) for wood/PP composites. Ismail et al. (1997) concluded that composites filled with smaller wood flours showed higher tensile strength, tensile modulus and tear strength for wood/expoxidized natural rubber composites. Similarly, Takatani et al. (2000) found that smaller wood flours (120 mesh) provided better strength and water resistance than larger wood flours (20 mesh). Kim et al. (2005) observed that as the particle size decreased, the tensile strength of the wood/Polybutylene succinate (PBS) composites slightly increased, while the impact strength decreased.

On the other hand, opposite effects of wood particle sizes were observed in some other studies: Zaini et al. (1996) reported that wood/PP composites, larger-sized wood particles showed higher modulus, tensile and impact strength. Later Zhu et al. (2001) concluded that wood/HDPE composites' flexural strength decrease with the decrease of wood particle size. Similarly, Ichazo et al (2006) observed that larger particles (300-425 μm) offered better overall balance of mechanical and dynamic properties than the small particles (250-300 μm).

In above studies, raw materials used were obtained from commercial sources, which might have particle size overlaps. To address this problem, Stark and Berger (1997) focused their research on the effect of discrete, non-overlapping particle size distributions on the mechanical properties of the wood flour/polypropylene composites. They found that the trends in property performance for screened wood flour-filled polypropylene are the same as those for commercial wood flour-filled polypropylene. Particle sizes did not affect specific gravity, but flow index, flexural and tensile modulus and strength, heat deflection temperature and notched impact

energy increased with increasing particle size, whereas unnotched impact energy decreased.

Later Stark and Rowlands (2003) examined the effects of wood particle sizes (35, 70, 120 and 235 mesh) on the mechanical properties of resulting composites. They found that aspect ratio, instead of wood particle size, had the greatest effect on strength and stiffness of the composite. It is generally expected that composites filled with wood particles of larger aspect ratios have superior mechanical properties to those filled with particles of much lower aspect ratios.

Comparison between Wood Flour and Wood Fibers

The basic difference between a wood fiber and a wood flour is that the wood fiber has an aspect ratio (length/diameter) of 10:1 to 20:1 (as high as 100:1 for some softwood), while wood flour generally has an aspect ratio of 1:1 to 4:1 (Patterson 2001). In general, wood flour is used as filler for plastic, with tends to increase the stiffness of the composite, but does not always improve its strength. Natural fibers, such as wood fibers, can be used to reinforce rather than fill plastics, which increase strength as well as stiffness.

Since wood and other lignocellulosic fibers typically have higher aspect ratio than that of wood flour, at a critical fiber length, stress is transferred from the matrix to the fiber, resulting in a stronger composite (Stark and Rowlands 2003). In the same study (Stark and Rowlands 2003), the mechanical properties of wood flour-filled and wood fiber-reinforced polypropylene composite were compared. The use of wood fiber in polypropylene composites resulted in higher strength than with wood flour, which indicate that higher aspect ratio enhanced stress transfer from the matrix to the fiber.

In summary, a lot work has been done to understand the role of wood species and wood particle sizes on the properties of the resulting composites. Conflicting conclusions were drawn from some of the studies. Although it is generally expected that composites filled with fibers have superior mechanical properties to those filled

with particles of much lower aspect ratio. The exact mechanisms behind the effects of the bio-particle geometry on the composite micro-mechanics remain unclear.

Durability of Wood Plastic Composites

The development of WPCs has been driven primarily by the need for durable wood materials that can function in exterior environments without preservative treatment (Wolcott 2003). WPCs are often advertised as durable building product that resists cracking and warping and require less maintenance that traditional pressure-treated wood decking. Many manufacturers provide at 15 years warranty time which is more competitive when compared with treated wood. However, since the common product (like decking) service life is generally shorter than warranty time, the real long-term performance can hardly be evaluated accurately. Product problems within the warranty made most of the advertised advantages of WPCs open for debate (DeRosa 2004). As WPCs are increasingly used in exterior applications, long-term performance is one of the most important considerations (Smith and Wolcott 2006), especially for structural applications. In a survey conducted on the WPCs application in the U.S. recreational bridge market, it was found that durability is the most important attributes for recreational bridge decking material, and plays the most important role in new product adoption (McGraw and Smith 2007).

Generally, in-service condition can expose WPCs to various degrading factors, including moisture and temperature change, ultraviolet (UV) light, atmosphere gases, and biological degradation (such as termites and fungal attacks, etc.). In the past decade, extensive research efforts have been made to investigate how WPCs were affected by various environmental exposures and how can WPCs be protected against these degradation factors.

Moisture Absorption

Moisture absorption poses problems not only in composite processing, but also in the field application. It is sometimes claimed that moisture is not a problem for wood plastic composites because the wood is encapsulated in polymer matrix. In the case of

total encapsulation, polymers would protect the wood from moisture because they are hydrophobic. However, this external protective barrier is relatively easy to compromise by machining, damage or surface wear, even composites with relatively low wood content (30% weight ratio) are reported to absorb water (Balatinecz and Park 1997).

Balatinecz and Park (1997) examined the effects of moisture exposure (by exposure in boiling water for 48 h) on the mechanical properties of the resulting composites, and found that water absorption resulted in decrease in tensile and flexural properties, while increase in impact strength. Stark (2001) examined the influence of different relative humidities (RH 30%, 56%, and 90%) on the mechanical properties (tensile, flexural, and impact properties) of composites made from PP with 20% and 40% wood flour. It was concluded that higher wood content resulted in more moisture absorption, and might cause more decrease in mechanical properties, which was attributed to the possible degradation of the wood/PP interface and/or the moisture absorption in wood. Lin et al. (2002) examined the moisture absorption and mechanical properties of wood flour/PP composites and found that the tensile strength, flexural strength and modulus, and the impact strength change in different trend as the composites were immersed in water.

Temperature Change

Temperature is also an important factor that might influence the long-term performance of WPCs. Accelerated degradation treatments (either higher or lower than ambient temperature) were applied to assess the durability of WPCs. Balatinecz and Park (1997) examined the effects temperatures on the mechanical properties of the resulting composites, and found that temperatures higher than ambient (23 °C) resulted in decreased strength and modulus. Pilarski and Matuana (2005; 2006) examined the effects of accelerated freeze-thaw actions on the durability of wood plastic composites made with PVC and HDPE matrix. The durability of exposed samples was assessed in terms of flexural properties, density, and dimensional

stability. For wood/PVC and wood/HDPE composites, similar results were obtained. The cyclic freeze-thaw actions did not affect the density. However, the stiffness of the composites was significantly affected by the freeze-thaw treatment, which was attributed to the decreased interfacial adhesion due to the water portion of the cycling.

Ultraviolet (UV) Radiation

UV light is another source of degradation that needs to be taken account for WPCs used in exterior applications. The effects of UV radiation on wood/HDPE composites (Johnson et al. 1999; Lundin et al. 2001; Stark and Matuana 2003), wood/PVC composites (Matuana and Kamdem 2002; Matuana et al. 2001), and wood/PP composites (Johnson et al. 1999; Selden et al. 2004) were examined. All the above studies concluded that wood fibers are effective sensitizers and their incorporation into the polymer promote and/or accelerates photodegradation of the polymer matrix.

Fungal Attack

The wood in WPCs is considered to be susceptible to moisture absorption and degradation. Despite the claims of rot resistance, some in-service wood plastic composite did experience rot problems (Morris and Cooper 1998). Research (Mankowski and Morrell 2000; Pendleton et al. 2002) has been conducted to examine the effects of fungal attack on wood/HDPE composites. It was found that composites with higher wood content were more susceptible to fungal attack.

Natural Exposure

Besides the above accelerated degradation treatments, research has also been done to investigate the effects natural exposure on the durability of WPCs. Schauwecker et al. (2006) examined the WPCs that have been in field for 10 years. Surface hardness, presence of microorganisms, and wood content were examined to evaluate the degradation effects. Oberdorfer and Golser (2005) studied the environmental impact on high wood content WPCs in full scale tests. Water absorption, thickness swelling,

tensile strength, and fastener withdrawal capacity were measured to evaluate the material degradation.

In most of the above studies on the durability of WPCs, the degradation effects were evaluated indirectly from measuring the mechanical and/or physical property changes during the treatments or natural exposures. The degradation was often assessed via chemical composition examination or 2D microscopic analysis, which only contained indirect and limited information on the internal structural changes resulting from the treatments or natural exposures. Considering the heterogeneous and complex nature of WPCs, multi-scale, nondestructive evaluation with statistical significance will be preferable to obtain better understanding of the inner structure changes of WPCs subjected to environmental exposures.

Characterization of WPCs and Wood/Polymer Interface

Different processing and loading regimes affect spatial distributions of phases, particle alignments, and void contents. Severe weathering cycles, surface wear, and/or mechanical loading can result in a variety of damage mechanisms ranging from distributed micro cracking to localized crack bands and macro-cracks, which mechanically weaken the internal structure and breach the protective layers of polymer. The principal types of internal micro-damage are identified as either fracture within the polymer matrix or the wood particle; or as failure at the wood/polymer interface (Landis et al. 2004).

The strength and toughness of fiber-reinforced materials are determined by the interface between the fibers and matrix., which is defined as an imaginary surface forming a common boundary between the phases (a wood particle and the surrounding polymer matrix). A strong interface creates a material that displays good composite action between the matrix and the fiber. A weaker interface reduces the efficiency of stress transfer from the matrix to the fiber, which acts merely as a filler and as a result the strength and stiffness are lower than in the composites (Jacob et al. 2005). In WPCs, the hydrophilic wood particles are generally incompatible with hydrophobic

thermoplastic polymers. The incompatibility between wood and polymer matrix is a major problem for interfacial adhesion between these two component materials, which is of critical importance for the mechanical properties of the resulting composite (Bledzki et al. 1998; Jiang and Kamdem 2004). Extensive research (as quoted below) has been conducted to understand the nature of the interfacial bond and its characterization. The interface characterization techniques return information about the chemical composition and the morphology of the interface as well as the fiber/matrix interactions.

Various methods have been developed for the characterization of internal micro-damage accumulation as well as fiber/polymer interface in the fiber/polymer composites. Thee principal categories of characterization methods listed in literature are: micro-mechanical techniques, physical characterization, chemical characterization, mechanical tests, microscopic techniques, and X-ray computed tomography (CT) technique.

Micro-mechanical Techniques

The fiber-matrix bonding can be evaluated by measuring the interfacial shear strength, which is a critical factor that controls the toughness, mechanical properties, and inter-laminate shear strength of composite materials. The following methods were used to measure the interfacial shear strength in fiber polymer composites:

Single Fiber Pull-out Test

The aim of single fiber pull-out test is to measure the force required to pull out a fiber embedded in a matrix, this value can be used to evaluate the interfacial shear strength between the fiber and the matrix. The single fiber pull-out problems have been extensively studied to investigate the interfacial adhesion quality and elastic stress transfer between fibers and matrix (Joseph et al. 2002; Manchado et al. 2003; Stamboulis et al. 1999; Tripathy et al. 2000; Valadez et al. 1999; Velde and Kiekens 2001; Zafeiropoulos et al. 2002). From single fiber pull-out test, much information can

be derived that is related to the fundamental aspects of the fiber/matrix mechanical interaction. However, since this kind of test only involves a single fiber, it is not suitable for the characterization of wood flour plastic composite, in which the wood particles embedded in the polymer matrix are generally composed of large amount of fibers and have different geometrical features (e.g. significantly lower aspect ratio). Besides, this type of test can be hardly applied to particles of relatively low aspect ratio, which are used for WPCs.

Micro-debond Test

In this test, a micro-bead of the matrix is deposited onto a fiber, then the fiber with the micro-bead is mounted in a micro-vice by placing the micro bead under the micro-vice blades and the fiber is pulled out. Then interfacial shear strength can be calculated from the measured force (Craven et al. 2000; Egan and Shaler 2000; Luo and Netravali 2001; Shaler et al. 1997). Micro-debond test is the modification of the single fiber pull-out test, and it is suitable for fibers with very large aspect ratios. The aspect ratio of wood flour range from 3 to 5, therefore it is not suitable for wood flour plastic composite characterization.

Single Fiber Fragmentation Test

Single fiber fragmentation test involves embedding a single fiber along the centerline of a dog-bone shaped specimen of matrix material. The specimen is then strained along the fiber axis. With the minimum length of the fractured fiber fragments at the end of the test and the stress needed to obtain this minimum length, the interfacial shear strength can be calculated (Tripathy et al. 2000; Valadez et al. 1999; Zafeiropoulos et al. 2002). This is the most realistic test from the point of view of the interfacial pressure. The fiber is neither pushed nor pulled directly, and so fiber Poisson effects are similar to that occurring in a fiber composite. However, as analyzed in the previous two micro-mechanical methods, this method cannot be used

for wood flour plastic composite, because of the wood particles' geometrical feature-much smaller aspect ratios compared to wood fibers.

Physical Characterization

Physical properties are generally connected to material structure and performances, so the measurement of physical property changes can be used to evaluate material structural changes.

Appearance Inspection

The surface color change of wood/PVC composite samples before and after accelerated ultraviolet (UV) weathering treatment was examined using reflectometer and chroma meter to evaluate the degradation effect (Matuana and Kamdem 2002; Matuana et al. 2001; Stark 2005)

Physical Property Measurement

Density changes, thickness swelling, and water sorption can be measured to evaluate the degradation introduced from environmental exposure (Clemons and Ibach 2004; Johnson et al. 1999).

X-ray Energy Dispersive Analysis

When an electron beam of sufficient energy bombards a specimen, an X-ray spectrum characteristic for a chemical and physical composition of a sample is generated and may be used for characterization of chemicals present on the surface. From their energy and intensity, the atomic number and relative concentration of a particular element can be determined. Wright and Mathias (Wright and Mathias 1993) examined a balsa WPC composite containing 1:1 copolymer of ethyl-(hydroxyl methyl) acrylate (EHMA) and ethyl (chloro methyl) acrylate with X-ray energy dispersive analysis. Chlorine was detected from the X-ray analysis, this indicated the presence of the polymer within the wood cell walls.

Porosity Measurement

Porosity is an important measure of the void content in material. The predominant method used to measure porosity in WPCs is mercury intrusion porosimetry (MIP). Mercury porosimetry characterizes a material's porosity by applying various levels of pressure to a sample immersed in mercury. MIP forces mercury into the pores of a material by gradually increasing pressure. At each discrete pressure increment, the volume of mercury intruded into the pores is recorded (Willis et al. 1998). The pressure required to intrude mercury into the sample's pores is inversely proportional to the size of the pores. Porosimetry can provide information about the surface area and porosity of solids; therefore, it has been used to evaluate quantitatively the porosity in the WPC samples before and after exposure. For wood/HDPE composite, after freeze-thaw exposures, general increase in porosity was observed and was attributed to the decrease in bonding between the matrix and fibers (Pilarski and Matuana 2006). This method, however, assumes that all pores in the volume are connected with the surface pore systems, which might not be true for composite with complex structures, like WPCs.

Swelling Techniques

Swelling technique is another method to analyze the interfacial adhesion in fiber-reinforced elastomer composites. The swelling ratio in any direction forming an angle θ with the fiber orientation can be determined from the dimensional swelling ratios in the longitudinal and transverse directions. The extend of swelling in hybrid fiber reinforced polymer composite was correlated to the interfacial adhesion (Jacob et al. 2004; Kumar and Thomas 2001).

Physical properties are an effective measurement of the composite structural composition characterization. However, in many cases, only small fraction of the sample volume can be analyzed as representative, which might be reasonable for

homogeneous materials. Proper representation of heterogeneous bio-composites like WPCs via this kind of analysis is charged with much greater uncertainty.

Chemical Characterization

Chemical composition analyses are often used to detect WPCs component changes after weathering exposure or to identify interface in the composites.

Contact Angle Measurement

Contact angle on the surface of the exposed specimens can be correlated to surface wettability of a material. For material suffered from photodegradation, they have lower contact angle values and are more hydrophilic, the increased wettability of specimen surface implies changes on the surface chemical composition (Matuana and Kamdem 2002). Changes in contact angle may also signal increased porosity and appearance of micro-cracks on the sample surface.

Spectroscopic Techniques

Fourier transform infrared (FTIR) spectroscopy and X-ray photoelectron spectroscopy (XPS) were used to measure and compare different surface functional groups, and to quantify the surface chemical changes as the measure of accelerated UV degradation (Matuana and Kamdem 2002).

Pyrolysis gas chromatography-mass spectrometry (Py-GC-MS) is a technique that thermally cracks the polymeric material into smaller molecular fragments (characteristics of the parent polymer) which can be separated and analyzed by GC-MS. It was applied to analyze the chromatograms and mass spectra and to quantify the wood content in the weathered WPC samples (Fabiyi et al. 2005).

For the fiber/polymer interface characterization, electron spectroscopy for chemical analysis with X-ray photoelectron spectroscopy (ESCA/XPS), Fourier transform spectroscopy (FTIR) (Colom et al. 2003; Hristov and Vasileva 2003; Velde and Kiekens 2001; Zhou et al. 2003), laser Raman spectroscopy (LRS) (Eichhorn and

Young 2003, 2004), nuclear magnetic resonance (NMR) (Wright and Mathias 1993) and photoacoustic spectroscopy have been successfully applied to explore the boundary regions around wood fibers and to detect whether a chemical reaction between wood fiber and polymer matrix had occurred.

Thermal Analysis Methods

The thermodynamic analysis methods used for characterization of reinforced polymers are differential scanning calorimetry (DSC) (Manchado et al. 2003; Zhou et al. 2003), wettability study, inverse gas chromatography (IGC) measurement, zeta potential measurement (Pothan and Thomas 2003). In the research examining UV aging of wood/PP composites, DSC was utilized to measure the exposure's effect on transition temperature and melting endotherms, which can reflect the molecular chain reactions and crystallization characteristics in the polymer matrix (Selden et al. 2004).

From these chemical characterization methods, valuable information about the chemical composition of the volume of interest can be extracted. However, use of the chemical analysis tools is subject to the same limitation as in the case of physical characterization methods for the characterization of WPCs - the chemical characterization results might deviate from the actual material characteristics due to the complexity and heterogeneity of WPCs. Proper representation of WPC materials is subjected to greater uncertainty.

Mechanical Characterization

In weathering exposure, material degradation is often accompanied by the loss of mechanical properties. Material bulk mechanical properties were usually measured through mechanical testing to characterize degradation of WPCs. The most often measured properties include: bending strength, flexural modulus, Izod impact strength (Pilarski and Matuana 2006; Simonsen et al. 1998). In a study on the durability of WPC with high wood content, tensile strength perpendicular to the board surface

(internal board strength and surface soundness) and fastener withdrawal capacity were measured to quantify the effects of weathering on WPC (Oberdorfer and Golser 2005).

For the characterization of fiber/polymer interface, the interfacial bonding between fibers and polymer matrix were indirectly characterized from measuring the material bulk mechanical properties (Joseph et al. 1996; Selke and Wichman 2004). The bio-fiber/polymer interface is also characterized indirectly by dynamic mechanical analysis (DMA) (Hristov and Vasileva 2003; Pothan and Thomas 2003; Rials et al. 2001; Zhou et al. 2003).

Stress relaxation experiments are also proved to be effective methods for the characterization of the fiber/polymer interface. It was observed that the nature of the relaxation curve depends on the nature of the interface. Chemical treatment of the fibers reduced the rate of stress relaxation, which was associated with the improved fiber-matrix adhesion due to better interlocking between the two components (Pothan et al. 2004).

For homogenous material, these mechanical testing methods can effectively describe the mechanical characteristics of a material. However, for heterogeneous materials with complex structures, like wood flour polymer composite, these methods can only provide indirect and limited insight into the nature of the mechanical interaction between wood particles and polymer matrix, failure mechanism, and the long-term performance of the composites.

Microscopic Techniques

Scanning Electron Microscopy (SEM)

SEM is an important microscopic imaging technique for research in which high resolution images are crucial for analysis of morphological features. In numerous investigations focusing on interfacial mechanical characteristics of WPCs, SEM images of the fractured surfaces were used to examine the interfacial features and

predict the bonding strength based on whether the wood particles were pulled out of the matrix or broken (Oksman and Clemons 1998; Ray et al. 2002; Redondo et al. 2003; Rials et al. 2001; Tripathy et al. 2000).

SEM images of exposed surfaces of WPC specimens were examined to compare the surface quality of specimens before and after exposure and qualitatively correlate to the damage resulted from the weathering process (Pilarski and Matuana 2005, 2006; Stark et al. 2004).

Optical Microscopy

Conventional optical microscopy was often used to examine environmental degradation effects on WPCs. The depth of the surface layer that has different color from the core material was considered as depth of degradation, and was measured from optical microscopic image of specimen cross section (Lundin et al. 2001). Micrographs of the exposed WPC sample surfaces were examined to qualitatively characterize the material degradation by fungal attack (Clemons and Ibach 2004).

Other Microscopic Methods

Michaeli et al. (2000) used a combination of SEM, transmission electron microcopy (TEM), energy-dispersive X-ray analysis (EDX) and atomic force microscopy (AFM) to detect the fiber/matrix boundary layer of the individual wood fibers coated with coupling agent. Grigsby et al. (Grigsby et al. 2005) applied confocal laser scanning microscopy (CLSM) to obtain 3D images of wood fiber/plastic composites surfaces, from which the fiber/plastic interphase were successfully visualized and characterized qualitatively.

Most of the above microscopic methods provided effective ways to obtain 2D qualitative characterization of the areas of interest. However, in many cases, only small areas of interest were examined, from which a trained eye picks up clues to support or reject hypotheses based on results from other tests. Quantitative analysis on

the statistical significance and spatial distribution of the observed features is rarely offered (Muszynski 2007).

X-ray Computed Tomography (CT) Technique

Conventionally, material characterization was performed on 2D level with the help of optical or electron microscopy. In some cases, 3D information can be drawn form 2D measurements, such as some simple cases (spheres, cube, etc). However, in most cases of material science, enough information cannot be drawn from 2D characterization merely, because the connectivity of phases is a 3D parameter, which cannot be obtained from 2D measurements. Another constraint of 2D characterization is that artifacts might be introduced in sample preparation; this in turn will create misleading characteristics. Finally, although in situ 2D characterization can be realized, it is also constrained because of the different stress and strain conditions between a real section in bulk and a free surface for 2D characterization (Salvo et al. 2003). Therefore, it is desirable to use 3D characterization to obtain better understanding of complex materials.

X-ray CT (XCT) scanning technique is an important 3D, nondestructive examination method. X-rays are electromagnetic radiations having wavelengths roughly within the range from 0.005 to 10 μm. At the short-wavelength end, they overlap with γ–rays, which is called soft X-ray, at the long-wavelength end they approach ultraviolet radiation, which is called hard X-ray (Grieken and Markowicz 1993). X-ray has very high penetrating capability and can penetrate even very dense solids, like metals, stones, and minerals. When X-ray penetrates a material, its intensity (energy per unit area per unit time) becomes attenuated due to the absorption and scattering of X-ray by the atoms of the material. Different materials attenuate X-ray at different rates. Therefore, by penetrating X-ray into different materials and measuring their attenuations (the difference between the intensity before and after penetration), the types of the materials can be determined (Wang et al. 2004).

Computed tomography (CT) uses multiple X-ray projections in order to reconstruct 3D distributions of materials of various attenuations within the sample. Figure 2.3 illustrates the principle of X-ray CT. An X-ray tomography imaging system usually consists of three components: X-ray source, specimen manipulator, and X-ray detector (Figure 2.3a). By rotating the specimen 360°, the attenuation of the X-ray in many orientations can be registered by the detector. From a set of projections, a cross-sectional image is reconstructed by a back-projection algorithm (Figure 2.3b). With sequential cross-sectional slices taken (Figure 2.3c), 3D CT images can be reconstructed (Figure 2.3d).

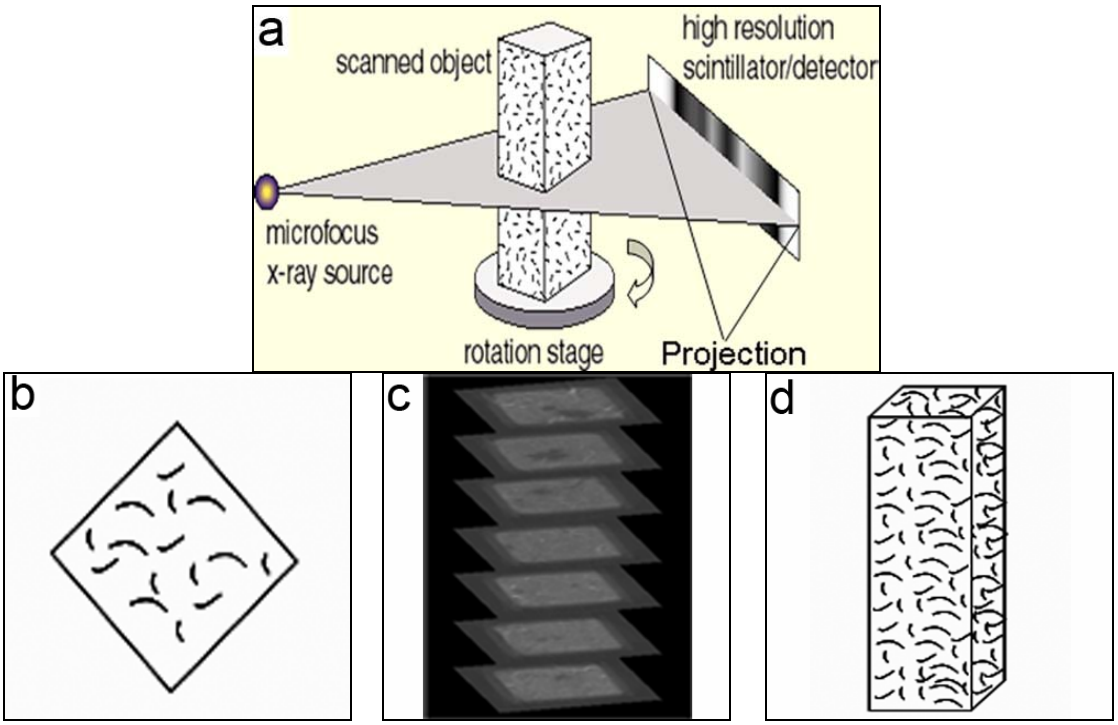

Figure 2.3 Principle of X-ray computed tomography (CT): (a) X-ray CT scanning set-up, (b) Reconstructed slice, (c) Reconstructed image stack, (d) Reconstructed 3D image volume.

Source: Figure 2.3a is from Shaler et al. (2003), Figure 2.3c is from www.ph.surrey.ac.uk/.../plant_tomo.html.

X-ray CT's Application

X-ray CT techniques have been used in diagnostic medicine, as well as in imaging and microscopic nondestructive evaluation of materials such as ceramics, electrical insulators, plastics, wood and other materials (Rao et al. 1999; Wang et al. 2007).

In material science, X-ray CT has been used for imaging morphological structure and phase distribution of concrete, heterogeneous metal alloys and inorganic metal and ceramic composites reinforced with continuous and discontinuous second phases, as well particulates, chopped fiber, continuous fiber and monofilament reinforced composites, and their response to deformation and damage (Carmeliet et al. 2004; Morse et al. 2004; Stock 1999)

The high sensitivity of X-ray CT to density change is utilized to characterize edge profiles, porosity, delaminations, micro-cracking, internal damage initiation and propagation due to mechanical and thermal stress (Bayraktar et al. 2006; London et al. 1990; Morse et al. 2004; Schilling et al. 2005; Stock 1999). Specifically in wood research, X-ray techniques have been used for nondestructive evaluation (NDE), log quality assessment, wood density profile measurement, and moisture flux in wood (Macedo et al. 2002).

High resolution (up to 5-10 μm) X-ray CT is also termed micro-tomography (XMT) and allows reconstructions of sample interiors with the spatial and contrast resolution comparable with microscopic imagery (Stock 1999). High resolution X-ray CT was used for multi-scale morphological characterization of aggregates, void structure, void connectivity of the interfacial zone, and for computational simulation of mixture properties in concrete and asphalt-concrete (Carmeliet et al. 2004; Wang et al. 2004). Song et al. (Song et al. 2005) used XMT to develop a comprehensive methodology for the characterization of damage and healing in asphalt mastics. Similar methods are used for characterization of fiber and particulate composites with elastomer and

polymer matrices (Bayraktar et al. 2006; Schilling et al. 2005; Shaler et al. 1997; Stock 1999).

In most of the above applications of X-ray CT in material characterization, the proposed algorithms assumed a high contrast and relatively well defined interfaces between component materials. Application of similar approaches to 3D scans of WPCs proved to be a challenge due to relatively low contrast between the component materials (Landis et al. 2004; Shaler et al. 2003).

X-ray CT Image Contrast

The basic parameter which quantifies the penetration or absorption of X-ray is the linear attenuation coefficient μ, defined as: $\mu = \delta^{-1} \ln(I_0 / I)$, where I_0 is the initial X-ray intensity and I is the incident intensity remaining after the X-ray passes through a thickness, δ, of sample. Materials with larger μ values will absorb more X-ray radiation, and fewer photons will reach the detector. In this way, materials with different μ values will correspond to the different light intensities on the detector, and thus reflect the heterogeneity of the subject (Macedo et al. 2002).

The apparent contrast between the phases in X-ray CT imaging depends on the materials' X-ray attenuation capacity and is correlated to the materials' molecular composition, density, X-ray beam energy and the signal-to-noise ratio. At a given energy level divergent densities and/or atomic numbers make materials easy to differentiate under X-ray, while similar densities and molecular compositions provide only low contrast images (Ketchman and Carlson 2001).

In theory, the contrast could be enhanced by doping one of the components with a small amount of a highly attenuating substance. One such doping material which has been successfully used as a contrast agent in X-ray microscopic imaging for biological specimens is gold (Chapman et al. 1994). In an effort to improve the X-ray CT scanning (resolution was 2.4 μm per pixel) contrast of the wood/thermoset polymer

interphase, Kamke and Lee (2007) examined the yellow-poplar wood bonded with PF resin with ferric chloride added, and obtained enhanced contrast.

Conclusions

The following conclusions were drawn from the literature review.

1. Extensive research has been conducted to examine the effects of bio-fiber sizes on the properties of the resulting reinforced plastic composites, and it is generally accepted that wood particle with larger aspect ratio can provide better mechanical properties. However, the exact mechanisms behind the effects of the bio-particle geometry on the composite micro-mechanics remain unclear.

2. In most studies, the wood/polymer interaction was discussed from the chemical point of view (the chemistry of bonding in the imaginary wood/polymer interface). Although mechanical interlocking is commonly considered a major mechanism in adhesion, no known studies have addressed its role in WPCs (Wolcott 2003)

3. Although many interesting techniques have been successfully applied for characterization of the wood/polymer bond area, none offered the capacity of nondestructive in situ evaluation comparable to X-ray CT techniques. However, the full potential of this XCT has not been fully utilized in the area of morphological characterization of WPCs.

CHAPTER 3 -- GOLD AS AN X-RAY CT SCANNING CONTRAST AGENT: EFFECT ON THE MECHANICAL PROPERTIES OF WOOD PLASTIC COMPOSITES

Yi Wang, Lech Muszyński, and John Simonsen

Manuscript accepted by *Holzforschung*.

Manuscript # HOLZ-D-07-00041

Gold as an X-ray CT Scanning Contrast Agent: Effect on the Mechanical Properties of Wood Plastic Composites

Yi Wang*, Lech Muszyński and John Simonsen

Department of Wood Science & Engineering

Oregon State University

Corvallis, OR 97331

* Corresponding author

119 Richardson Hall, Oregon State University, Corvallis, OR 97331-5751

Email: yi.wang@oregonstate.edu

Abstract

Wood plastic composites (WPCs) are typically composed of wood particles, thermoplastic polymers, and small amounts of additives. Further improvement of WPC technology requires a better understanding of their mechanical performance and durability on the micro level. X-ray computed tomography (CT) and advanced imaging techniques can provide visualization and support characterization of the internal structure, deformation and damage accumulation in WPCs under loading and various environmental exposures. However, both wood and thermoplastics are weakly attenuating materials for X-ray and good contrast between these two components is difficult to obtain. Chemically inert gold nano-particles and micro-particles were investigated as contrast agents in order to improve X-ray CT scanning contrast between wood and thermoplastics.

In this study, the effect of adding 1% (weight) gold nano- and micro-particles on the tensile properties of wood/HDPE composites was examined. Samples with and without surfactant, which was used in the gold particle synthesis process and supposed to improve their dispersion in the polymer, were tested in tension and scanned on a custom desktop X-ray CT system. It was concluded that the addition of gold particles did not impair the WPC tensile properties. However, some of the tensile properties were significantly affected when the surfactant was included. Gold micro-particles were shown to disperse well without surfactant and significantly improve the X-ray CT scanning contrast between wood and polymer, while gold nano-particles (without surfactant) did not disperse well and no contrast improvement was observed.

Introduction

Wood plastic composites (WPCs) are heterogeneous materials comprised of wood particles, thermoplastic polymers, and small amounts of modifying additives. Currently, WPCs are used principally in the automotive industry (interior details) and as secondary building materials in applications with limited structural requirements. Though the volume of WPC production, driven by consumer demand, is growing

rapidly, it constitutes but a small segment of the overall forest products market. This is due to limitations in the production process, relatively high cost and the fact that the in-service performance and durability of WPCs is still being debated.

It is widely believed that the key to increasing the volume of the WPC materials and the future of the market is the development of highly engineered WPCs characterized by better structural performance in areas such as stiffness and duration of load (DOL) response (Dagher 2005). In advancing WPC technology to allow for structural applications, it will be critical to understand how WPCs perform under load and changing environments. In addition, WPCs are believed to be resistant to biodegradation, which raises hopes for the development of a material that can replace increasingly scrutinized treated wood in structures exposed to the elements (Clemons 2002; Wolcott and Smith 2004). A significant barrier in this development is the lack of reliable tools and procedures for direct quantitative measurement of the micro-mechanical response of this heterogeneous material.

The mechanical and physical properties of WPCs may be engineered to some extent by changing component characteristics, proportions, filler orientation, and processing parameters. However, composite design is limited by the naturally variable wood properties and the limited selection of thermoplastics that may be used with wood. Consequently, research efforts in this area have been mostly focused on improving the internal bonding between the wood and the matrix. The hydrophilic wood particles are generally incompatible with hydrophobic thermoplastic polymers. This incompatibility is usually addressed by the addition of chemical modifiers (coupling agents or compatibilizers) which influence the internal bonding between the wood and polymer matrix. On the other hand, modifiers and agents added to act as lubricants, protective treatments or fire retardants may adversely affect the properties of the components or the interface (Clemons 2002; Colom et al. 2003; Gardner et al. 2004; Geng et al. 2004; Lee et al. 2004; Manchado et al. 2003; Newson and Maine 2004; Wolcott and Smith 2004; Zafeiropoulos et al. 2002). In most studies, the wood/polymer interaction was discussed from the chemical point of view. Although

mechanical coupling is considered a major mechanism in adhesion, no known studies have addressed its role in WPCs (Wolcott 2003).

On the micro-mechanical level, the spatial distributions of components, particle alignments, and void spaces are affected by various processing and in-use service regimes. Severe weathering cycles, surface wear and/or mechanical loading can result in a variety of damage mechanisms ranging from distributed micro-cracking to localized crack bands and macro-cracks either within the polymer matrix or the wood particle; or as failure at the wood/polymer interface (Landis et al. 2004). As these internal fractures accumulate with time they mechanically weaken the internal structure and breach the protective layers of polymer, which exposes the wood particles to further degradation.

Although certain imaging methods, such as scanning electron microscopy (SEM) and nuclear magnetic resonance (NMR) have been utilized for qualitative assessment of fractured surfaces and inner structures of WPC materials, the quantitative relationship between the composite morphology and the macro-mechanical performance is still poorly understood.

Micro-mechanical studies on single-fiber/polymer systems (Egan and Shaler 2000; Eichhorn and Young 2004; Rials et al. 2001; Shaler et al. 1997; Stamboulis et al. 1999; Tze et al. 2003) provide valuable fundamental background information, but cannot substitute for a direct in situ knowledge of how larger particles of much more diverse geometry interact with a solid polymer matrix. Such studies also cannot answer the important question of what is the statistical significance of the variability and distribution of filler particles in the material.

Recent progress in high resolution X-ray computed tomography (CT) created new opportunities for nondestructive, in situ analysis of particulate composites. CT scanners are capable of returning digital images carrying spatial information coded in millions of discrete grayscale values (voxels) arranged in arrays, which represent local

densities and X-ray attenuations (Park et al. 2003; Pétraud et al. 2003). X-ray scanning techniques have been used in diagnostic medicine, as well as in imaging and the microscopic nondestructive evaluation of materials such as ceramics, electrical insulators, plastics, wood and other materials (Rao et al. 1999). In wood research, X-ray techniques have been used for nondestructive evaluation (NDE), log quality assessment, wood density profile measurement and moisture flux in wood (Macedo et al. 2002).

The combination of high-resolution nondestructive imaging techniques like X-ray micro-tomography (XMT) with machine vision tools provides the means for a quantitative morphological characterization of heterogeneous composites as well as an assessment of the deformation and damage resulting from climate exposure and mechanical loading. In fact machine vision-based methods have been used for characterization of 3D samples of certain particulate composites and fibrous materials (Bertilsson et al. 1992; Peix et al. 1997; Thompson et al. 2006; Yang and Lindquist 2000). However, most of the proposed algorithms assumed a high contrast and relatively well defined interfaces between component materials. Application of similar approaches to 3D scans of WPCs proved to be a challenge due to relatively low contrast between the component materials (Landis et al. 2004; Shaler et al. 2003).

The apparent contrast between the components in CT imaging depends on the materials' X-ray attenuation and is correlated to the materials' molecular composition, density, X-ray beam energy and the signal-to-noise ratio. At a given energy level, divergent densities and/or atomic numbers provide easy differentiation by X-rays, while similar densities and molecular compositions provide only low contrast images (Ketchman and Carlson 2001). The basic parameter which quantifies the penetration or absorption of X-rays is the linear attenuation coefficient μ defined as: $\mu = \delta^{-1} \ln(I_0 / I)$, where I_0 is the incident X-ray intensity and I is the intensity remaining after the X-ray passes through a thickness, δ, of sample. Materials with larger μ values will absorb more X-ray radiation, and fewer photons will reach the

detector. In this way, materials with different μ values will correspond to the different light intensities on the detector, and thus the subject contrast.

The approximate μ values for various compounds and mixtures can be readily calculated from tabularized values determined experimentally for elements (Hubbell and Seltzer 1996). Linear attenuation coefficients of wood (represented as cellulose), high density polyethylene (HDPE), polypropylene (PP) and poly(vinyl chloride) (PVC) for the energy output range of 20 to 160 keV (which is the operational range for the desktop X-ray CT scanning system used in this study) are shown in Figure 3.1a. It is evident that while a significant contrast between wood and PVC can be obtained, HDPE and PP have almost the same X-ray attenuation as wood. At the same time, about 84% of WPC materials use HDPE matrices while PVC and PP share about 9% and 7% respectively of the total WPC market. Therefore, this study is focused on improving the contrast between wood and HDPE to enhance morphological characterization of the composite.

In theory, the contrast could be enhanced by doping one of the components with a small amount of a highly attenuating substance. It is essential that the doping particles be smaller than the resolution of the scanner and well dispersed, so that the result appears as an increased contrast of the mixture rather than as individual high contrast particles. It is also very important that the doping material be chemically inert with respect to the components of the composite (including additives), so that the mechanical properties of the composite and its interaction with the environment are not affected.

As an effort to improve the X-ray CT scanning (resolution was 2.4 μm per pixel) contrast of the wood/thermoset polymer interphase, Kamke and Lee (2007) examined the yellow-poplar wood bonded with PF resin with ferric chloride added, and obtained enhanced contrast. Gold has been successfully used as a contrast agent in X-ray microscopic imaging for biological specimens is gold (Chapman et al. 1994). The effect of adding various amounts of gold to the HDPE matrix on the linear attenuation

coefficient of the mixture can be theoretically predicted. As seen from Figure 3.1b, adding 0.1% gold to HDPE may reduce the contrast between the mixture and wood, while increasing gold content to 1% is expected to improve the contrast significantly.

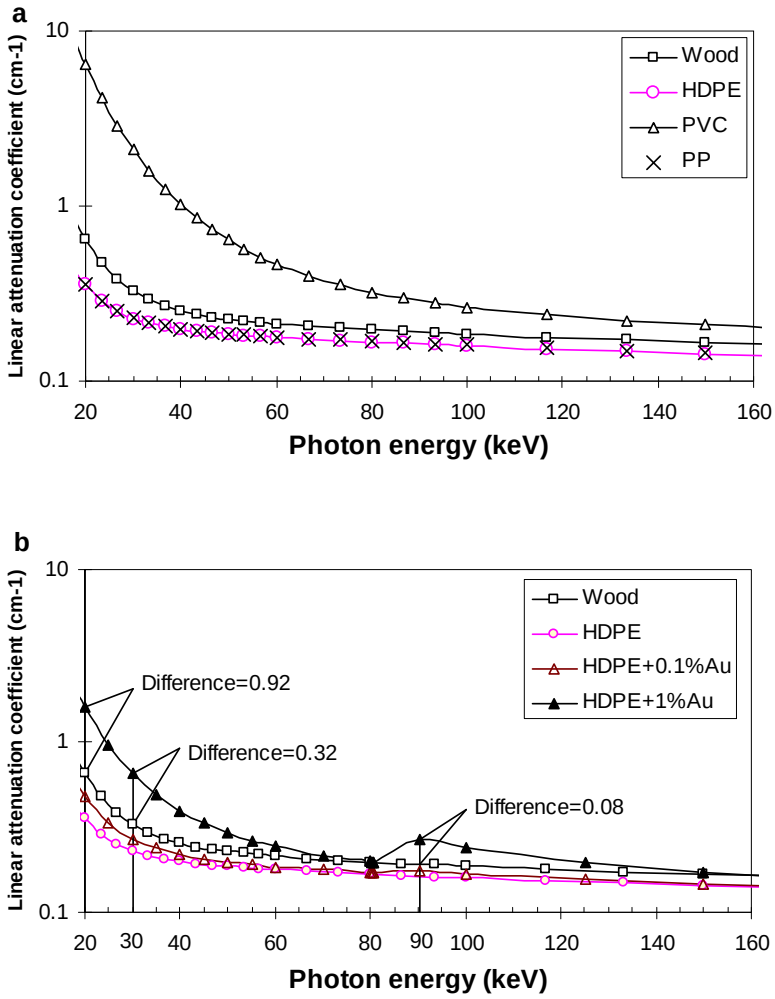

Figure 3.1 X-ray linear attenuation coefficients of: (a) Wood, HDPE, PVC, and PP, (b) Wood, HDPE, mixture of HDPE and gold (weight ratio 59/1), mixture of HDPE and gold (weight ratio 59.9/0.1).

The difference in the μ values between wood and the mixture of HDPE + 1% gold at 20 keV is 0.92 cm^{-1}, and it decreases to less than 0.01 cm^{-1} with the X-ray energy increasing from 20 to 80 keV. Because of a discontinuity in the attenuation coefficient characteristics of gold, the difference in the μ values increases again as X-ray energy increases from 80 to 90 keV. At 90 keV, this difference reaches the peak of 0.08 cm^{-1}.

In this research, X-ray source output energy of 30 keV was used for scanning, which is the lowest energy allowing exposure time at or below 5 s. At 30 keV the difference in μ values between wood and the mixture of HDPE + 1% gold is 0.32 cm^{-1}.

In the preliminary experiments with gold-doped WPCs, results from mechanical tests suggested that the addition of custom-synthesized gold nano-particles significantly weakened the strength and elastic properties of the resulting WPCs (Geng et al. 2005). In that preliminary study gold nano-particles were synthesized in the OSU lab following a procedure described by Brust (1994), which included the addition of tetra-n-octyl ammonium bromide as a surfactant. The surfactant was also believed to help in dispersing the gold particles in the polymer. It was hypothesized, though not confirmed, that the deterioration of the mechanical properties was caused by the addition of the surfactant rather than the presence of gold particles.

The objective of this study was to investigate the effect of gold nano- and micro-particles, and surfactant on the mechanical properties of wood/HDPE composites and neat HDPE polymer matrix as observed under monotonic and cyclic tensile tests. The effect of gold particles on the contrast of X-ray CT scanning images was also assessed.

Materials and Methods

Materials:

The WPC specimens were manufactured using a wood/HDPE ratio of 40/60 (weight). In order to separate the effect of gold particles (nano-particles and micro-particles) and surfactant (tetra-n-octyl ammonium bromide) added to the composite formulations, specimens with 1% (of specimen weight) of technically pure gold particles with and without the surfactant were fabricated. In order to evaluate the effect of the surfactant on the composite and on the matrix alone, WPC and neat matrix polymer specimens without gold particles but with the addition of the surfactant were fabricated. Finally, wood/HDPE composites and neat HDPE specimens without any additives were prepared for reference. The materials and sample designations are summarized in Table 3.1.

The wood flour was Pine, 40 mesh, donated by American Wood Fibers (Schofield, WI). Prior to use, the wood flour was dried at 103 °C for 24 h. The polymer was high density polyethylene (HDPE), Fortiflex HP-54-60-FLK (density 954 kg m^{-3}; melt flow index 0.50 g per 10 min) from BP Solvay Polymers North American (Houston, TX). Technically pure gold micro-particles (spherical gold powder, 0.8–1.5 μm in diameter) and nano-particles (50–130 nm in diameter) were purchased from Alfa-Aesar (Ward Hill, MA).

Specimen Preparation:

The components were first mixed at ambient temperature in batches of 46 g. The mixture was then compounded in a Brabender IntelliTorque mixer with bowl mixer and rotor blades attached (C.W. Brabender Instruments, Inc., S. Hackensack, NJ). The mixer was preheated to 170 ºC. The speed of the rotors in the bowl was 30 rpm. The mixture was blended for 5 min until a constant torque was reached and then the blending continued for about 5 min. The contents were then removed and stored for subsequent compression molding (Detailed description on the WPC sample fabrication is given in Appendix A).

A steel mold with the dimensions of 101.6 × 101.6 × 2.5 mm^3 was used to compress the mixture into boards in a hot press preheated to 180 °C. The initial pressure was 0.04 MPa and then raised to 0.60 MPa over 2 min and held for an additional 10 min. After that the mold was gradually cooled under pressure in ambient conditions for 24 h. After being removed from the mold, the WPC panels were cut and machined into dog-bone shaped specimens (narrow cross section of 8.0 × 2.5 mm^2).

Mechanical Tests

The specimens were subjected to monotonic and cyclic tensile tests, as planned for the research on the durability of WPCs (to be reported in a separate publication).

Table 3.1 Specimen composition.

Group	Description	Weight percentage (%)				
		HDPE	Wood flour	Gold micro-particles	Gold nano-particles	Surfactant
H	Neat HDPE	100	–	–	–	–
HS	HDPE + Surfactant	99.7	–	–	–	0.3
R	Reference WPC	60	40	–	–	–
RS	WPC + Surfactant	59.7	40	–	–	0.3
M	WPC + Gold micro-particles	59	40	1	–	–
N	WPC + Gold nano-particles	59	40	–	1	–
NS	WPC + Gold nano-particles + Surfactant	58.7	40	–	1	0.3

The monotonic tensile tests were performed in the displacement control mode at a constant rate of 0.5 mm min^{-1}. After the grips were tightened, the specimens were preloaded to 10 N for several seconds, followed by monotonic loading until failure.

In the cyclic tests, the specimens were pre-stressed to 0.60 MPa before the cyclic loading began. In the first four cycles the stress was cycled between 0.60 MPa and 4.80 MPa. Beginning with the fifth cycle, the peak stress was increased by 1.20 MPa for each consecutive cycle with the minimum stress kept at 0.60 MPa. Nominal average tensile stress values were calculated from the real time load cell force readings and the initial individual cross section measurements for each specimen.

The tests were performed on an Instron 5500 Series EM universal testing machine. The ambient temperature in the testing lab was 25 ± 0.5 °C and the humidity was 27 ± 3%.

Deformations and strains were measured with optical equipment based on the digital image correlation method (Vic-3D by Correlated Solutions, Inc., West Columbia, SC). The system included two horizontally configured digital cameras, an image acquisition unit and VIC-3D analytical software. During the tests, sequential images were recorded every 1 s until failure. Then the displacement and strain fields for areas of interest on the specimen surfaces were calculated by comparing the images of deformed specimens with those of the reference undeformed specimens. In order to enhance the analysis, a random black and white speckle pattern was applied to the specimen surfaces before testing using a black and white paint spray. Since in this study only the total deformations were of interest, uniform strain and stress distributions were assumed and the average strain values from the full-field strain distributions were used for further analysis.

Data Analysis

From the stress and strain data of the monotonic tensile tests, ultimate tensile strength (UTS) was calculated according to ASTM standard D 638-03 (ASTM 2004). Initial

tangent modulus (E_t) was calculated from the derivative at the origin of a second order polynomial curve fitted to the original stress and strain data. Work to maximum load (W_m) was calculated from the area enclosed by the stress-strain curve and the maximum stress. A typical stress-strain curve from monotonic tensile test is shown in Figure 3.2.

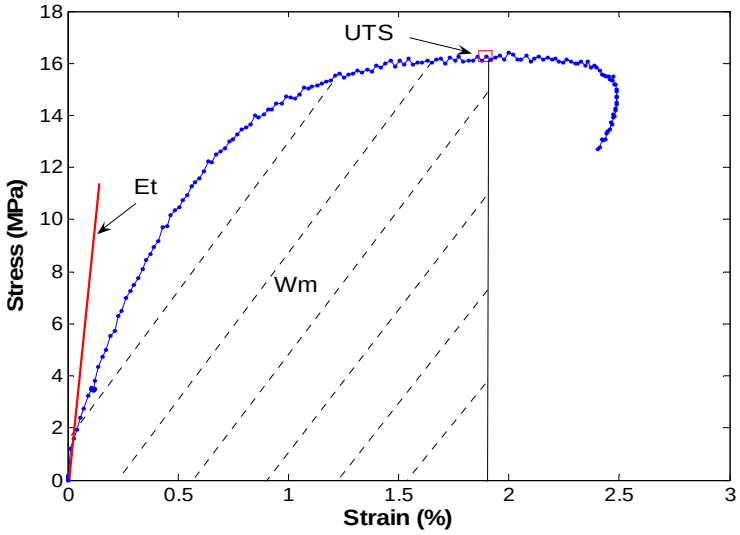

Figure 3.2 Calculation of tensile properties from monotonic tensile test.

From the stress and strain data of the cyclic tensile tests, an envelope curve was drawn by connecting the peak stress points of each cycle (Figure 3.3). Maximum tensile stress (σ_{max}) was calculated from the original stress-strain curve and work to maximum load (W_c) was calculated from the area enclosed by the envelope curve and σ_{max}. An equivalent initial modulus E_e was calculated by connecting the origin and the $0.4\sigma_{max}$ point on the envelope curve following the general procedures used for calculation of elastic shear stiffness for shear walls in ASTM standard E 2126-05 (ASTM 2005).

The calculated mechanical properties from monotonic and cyclic tensile tests were analyzed statistically. To investigate the effect of adding surfactant, properties of the specimens with and without surfactant were compared using the two-sample t-test. For the effect of gold particles, properties of specimens with gold micro-particles and

nano-particles were compared with the reference WPC specimens using the two-sample t-test. The analysis was performed at the 0.05 significance level.

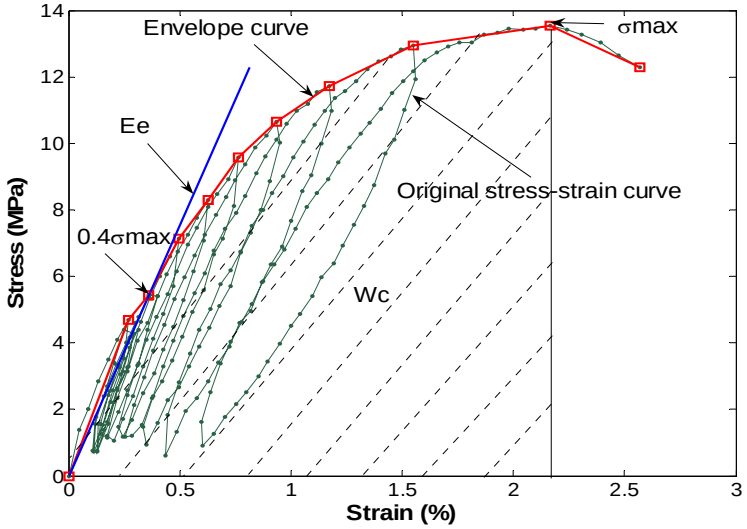

Figure 3.3 Calculation of tensile properties from cyclic tensile test.

X-ray CT Scanning

The effect of adding gold particles with and without surfactant on X-ray CT scanning contrast was compared by scanning the specimens in the Fein Focus FXE-160.20 custom X-ray system in the Department of Mechanical Engineering at OSU. The system includes a micro focus X-ray source, rotational sample stage, and a detector connected to a digital camera. The minimum resolution of the system is 20 μm. In order to achieve the best possible contrast between the wood particles and the polymer matrix, the X-ray source output energy level was set to 30 keV and 267 μA. The exposure time for a single projection was 3400 ms. The 3D reconstructions of the specimen cross sections were calculated from projection images taken at 1600 angular positions in 360°. In order to suppress the random noise, the projections for each angular position were calculated as averages from 5 exposures.

Results and Discussion

Monotonic Tensile Test

Ultimate Tensile Strength (UTS)

The average UTS values for all the groups were between 12 and 20 MPa. The results and statistical analyses are shown in Figure 3.4a and Table 3.2 respectively.

For WPC specimens with and without gold and the neat HDPE specimens, the addition of surfactant caused a significant decrease in UTS (1.83 MPa between H and HS groups, 2.09 MPa between R and RS groups, 1.08 MPa between N and NS groups). This indicated that the surfactant might have interacted with the polymer matrix, filler or wood/polymer interface, thus lowered the UTS of the resulting WPCs, both with and without gold particles.

No significant differences in the UTS values between WPC groups with and without gold (R, M and N) were observed. This confirmed that at the X-ray energy level used in this study, the addition of chemically pure gold particles did not affect the strength of the resulting WPC composites, regardless of the gold particle sizes.

Initial Tangent Modulus (E_t)

E_t was calculated from the initial linear region on the stress-strain curve. It can be used to evaluate the initial stiffness of elastic-plastic materials. The results are shown in Figure 3.4b and the statistical analysis results are shown in Table 3.2.

For neat HDPE, the addition of the surfactant did not significantly affect its initial stiffness (E_t), while for reference WPC, the initial stiffness was significantly affected by the addition of surfactant (0.6 GPa decrease between R and RS groups). This indicated that the surfactant did not impair the stiffness of HDPE polymer, but might influence the stiffness of reference WPC specimens by affecting wood or wood/HDPE interface. For WPC with gold nano-particles, difference can also be observed but it is not statistically significant. This suggested the possible effect of surfactant on this

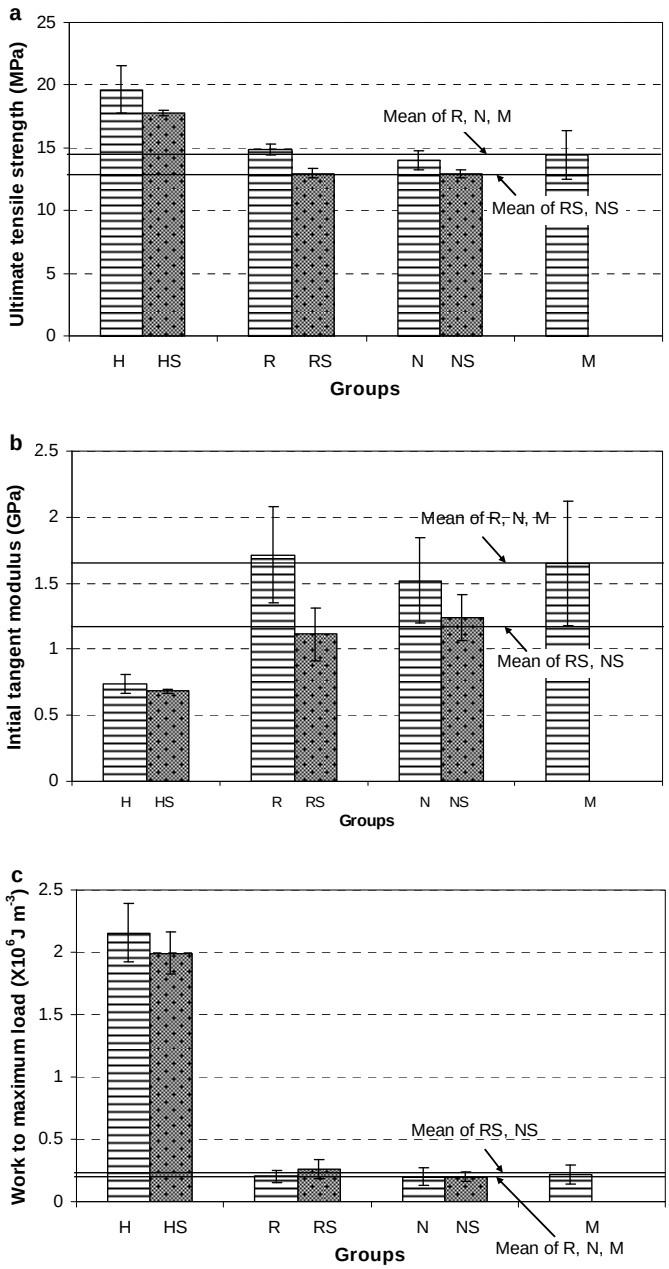

Figure 3.4 Monotonic tensile test results: (a) Ultimate Tensile Strength (UTS), (b) Initial tangent modulus (E_t), (c) Work to maximum load (W_m). The error bars represent one standard deviation of the data.

Note: H: Neat HDPE, HS: HDPE with surfactant, R: reference wood/HDPE composite, RS: wood/HDPE composite with surfactant, M: wood/HDPE composite with gold micro-particles, N: wood/HDPE composite with gold nano-particles, NS: wood/HDPE composite with gold nano-particles and surfactant

Table 3.2 Statistical analysis results from monotonic tensile tests.

	H vs. HS	R vs. RS	N vs. NS	M vs. R	N vs. R	M vs. N	M, N and R vs. NS and RS
Comparison of UTS							
Two-sided p-value	0.04	<0.01	0.01	0.61	0.05	0.64	<0.01
Significantly different?	Yes	Yes	Yes	No	No	No	Yes
Difference (MPa)	1.83	2.09	1.08	0.43	0.83	0.40	1.58
Comparison of E_t							
Two-sided p-value	0.14	<0.01	0.10	0.79	0.34	0.58	<0.01
Significantly different?	No	Yes	No	No	No	No	Yes
Difference (GPa)	0.06	0.60	0.28	0.07	0.20	0.13	0.45
Comparison of W_m							
Two-sided p-value	0.23	0.17	0.96	0.67	0.96	0.67	0.37
Significantly different?	No	No	No	No	No	No	No
Difference ($\times 10^6$J m^{-3})	0.16	0.06	<0.01	0.02	<0.01	0.02	0.02

Note: H: Neat HDPE, HS: HDPE with surfactant, R: reference wood/HDPE composite, RS: wood/HDPE composite with surfactant, M: wood/HDPE composite with gold micro-particles, N: wood/HDPE composite with gold nano-particles, NS: wood/HDPE composite with gold nano-particles and surfactant

group of specimens. Comparison between the pooled result of M, N and R groups and the pooled result from NS and RS groups (Figure 3.4b and Table 3.2) showed a clearer picture: the surfactant's effect is significant for the group averages. This indicated adding surfactant to WPC with gold nano-particles affected its initial stiffness but the effect is insignificant at the 0.05 level.

It is reasonable to suppose that the surfactant ammonium head group binds to the wood surface, resulting in a wood surface coated with a hydrocarbon tail. This would result in a lower surface energy for wood and, while it might provide for improved wetting of HDPE, it might also provide for a weaker interface since the octyl hydrocarbon group on the surfactant might be too short to effectively interact with the HDPE matrix. Typically, elastic modulus is not affected by interface changes, since there is no slippage between the matrix and filler in the elastic portion of the stress-strain regime. However, for especially weak interfaces, the matrix and filler may not even be in contact, resulting in weaker properties overall, as was observed. To explore the surfactant's roles on the stiffness of the WPCs, further experiments will be necessary.

Comparison of the initial tangent modulus (E_t) between WPC groups without the surfactant (R, N and M groups) led to conclusions similar to the UTS values: neither the presence of gold nor the particle size had any significant effect on the initial stiffness of the resulting WPC composites. It is clear that gold particles did not affect the elastic properties of the WPCs, even though different gold particle sizes were employed.

Work to Maximum Load (W_m)

Work to maximum load reflects the energy absorbed by the material during the test and the toughness of the composite. The values of W_m are shown in Figure 3.4c and the statistical analysis results are shown in Table 3.2.

For the neat HDPE and WPC with and without gold, no significant differences were observed in W_m between groups with and without the surfactant. In this case the reduction in strength and stiffness is compensated by the increase in elongation to break. Thus the areas under the respective curves are similar, even though the UTS and E_t were significantly affected.

There is also no statistically significant difference in W_m values between reference WPC (R group) and WPC with gold particles (M and N groups).

The results from the monotonic tensile tests suggested that the addition of the surfactant possibly impaired the HDPE polymer matrix and wood/HDPE interface. This effect is reflected by the decrease of UTS between groups with and without surfactant. However, for the initial tangent modulus (E_t), similar results were observed, except that the surfactant's effect in the neat HDPE was insignificant. Further experiments will be necessary to explore how the surfactant affects the stiffness of HDPE and wood/HDPE composites. On the other hand, the addition of gold with different particle sizes did not have a significant effect on tensile strength, elastic modulus, or toughness of WPCs. It confirms that adding small amounts of fine gold particles (without surfactant) to WPC formulations as an X-ray attenuation contrast agent will not affect the tensile properties of the resulting WPCs.

Cyclic Tensile Test

Maximum Tensile Stress (σ_{max})

The maximum tensile stress (σ_{max}) values determined in cyclic tensile tests for all groups are shown in Figure 3.5a and the statistical analysis results are shown in Table 3.3.

Significant decreases in the maximum tensile stress (σ_{max}) were detected between the groups with and without surfactant (0.68 MPa between H and HS group, 3.37 MPa between R and RS groups, and 3.54 MPa between N and NS groups). On the other

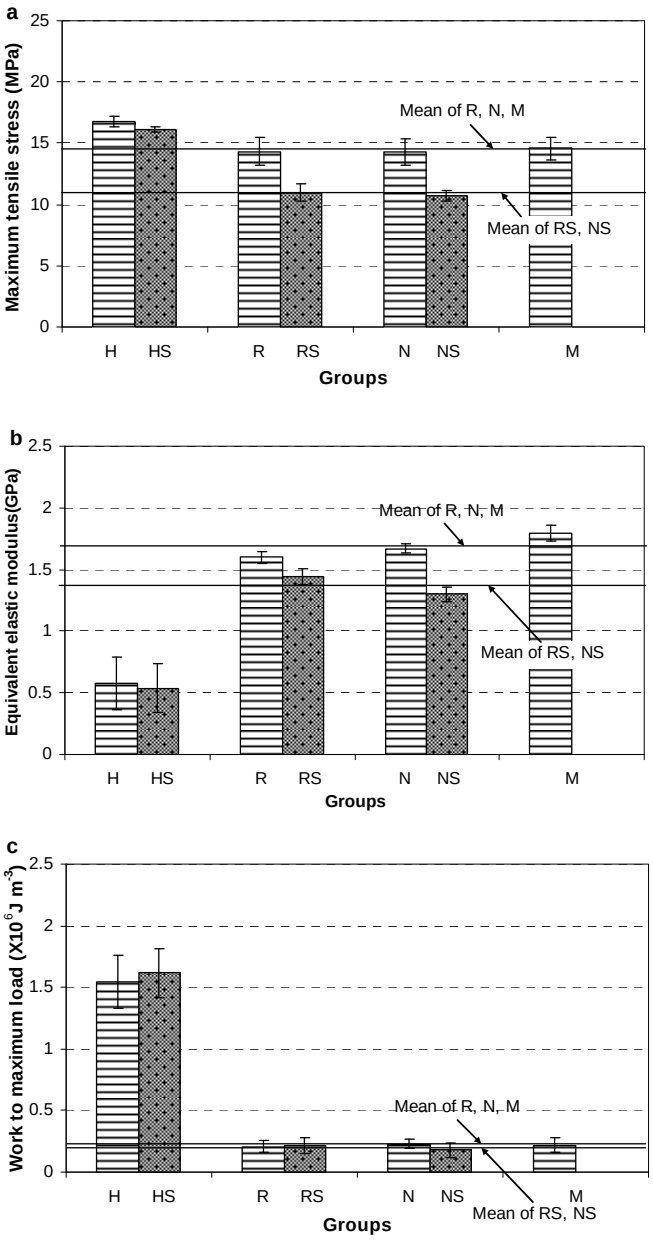

Figure 3.5 Cyclic tensile test results: (a) Maximum tensile stress (σ_{max}), (b) Equivalent elastic modulus (E_e), (c) Work to maximum load (W_c). The error bars represent one standard deviation of the data.

Note: H: Neat HDPE, HS: HDPE with surfactant, R: reference wood/HDPE composite, RS: wood/HDPE composite with surfactant, M: wood/HDPE composite with gold micro-particles, N: wood/HDPE composite with gold nano-particles, NS: wood/HDPE composite with gold nano-particles and surfactant

Table 3.3 Statistical analysis results from cyclic tensile tests.

	H vs. HS	R vs. RS	N vs. NS	M vs. R	N vs. R	M vs. N	M, N and R vs. NS and RS
Comparison of σ_{max}							
Two-sided p-value	0.02	<0.01	<0.01	0.71	0.93	0.62	<0.01
Significantly different?	Yes	Yes	Yes	No	No	No	Yes
Difference (MPa)	0.68	3.37	3.54	0.25	0.06	0.31	3.54
Comparison of E_e							
Two-sided p-value	0.12	0.01	<0.01	0.10	0.42	0.33	<0.01
Significantly different?	No	Yes	Yes	No	No	No	Yes
Difference (GPa)	0.04	0.16	0.38	0.20	0.07	0.13	0.31
Comparison of W_c							
Two-sided p-value	0.56	0.89	0.13	0.71	0.35	0.56	0.30
Significantly different?	No	No	No	No	No	No	No
Difference($\times 10^6$J m^{-3})	0.07	<0.01	0.05	0.01	0.02	0.07	0.02

Note: H: Neat HDPE, HS: HDPE with surfactant, R: reference wood/HDPE composite, RS: wood/HDPE composite with surfactant, M: wood/HDPE composite with gold micro-particles, N: wood/HDPE composite with gold nano-particles, NS: wood/HDPE composite with gold nano-particles and surfactant

hand, the addition of chemically pure gold particles and gold particle size did not affect the maximum stress (σ_{max}) significantly. These results were similar to those obtained in the monotonic tensile tests and supported our previously stated conclusions.

Equivalent Elastic Tensile Modulus (E_e)

In cyclic tensile tests, equivalent elastic tensile modulus (E_e) was calculated by connecting the origin and $0.4\sigma_{max}$ on the envelope stress-strain curve, as shown in Figure 3.3. The calculated E_e values for all groups are shown in Figure 3.5b and the statistical analysis results are shown in Table 3.3.

For neat HDPE specimens, the average E_e of specimens with the surfactant was lower than that of specimens without surfactant, but the effect was not statistically significant. However, adding surfactant to the formulation had a significantly negative effect on the initial tangent modulus (E_e) for all WPC specimen groups with or without gold (0.16 GPa between R and RS groups, 0.38 GPa between N and NS groups, and 0.31 GPa between pooled result of M, N and R groups and pooled result of NS and RS groups). This indicates that the surfactant is possibly affecting the wood or wood/HDPE interface, as discussed in section 1.2.

Upon comparing the E_e values of WPC specimens with and without gold particles, it was found that neither the addition of chemically pure gold particles nor the size of the gold particles had a significant effect on E_e values. These conclusions supported the conclusions of the monotonic testing.

Work to Maximum Load (W_c)

Work to maximum load (W_c) values obtained from cyclic tensile tests on all groups are shown in Figure 3.5c and the statistical analysis results are shown in Table 3.3. No

significant differences were observed in W_c values between groups with and without surfactant (H and HS groups, R and RS groups, N and NS groups).

Similarly, there were no differences in W_c between reference WPC (R group) and WPCs with gold particles of different sizes (M and N groups). This indicated that addition of surfactant and gold particles had no significant effect on the toughness of either neat polymer or WPC composites.

From the above cyclic testing results, it can be concluded that the addition of surfactant deteriorated the maximum tensile stress (σ_{max}) and equivalent elastic modulus (E_e) of WPC with and without gold. However, including the surfactant did not affect the work to maximum load (W_c) of both neat HDPE and WPC composites. The addition of gold and the size of the gold particles did not have significant effect on the maximum stress (σ_{max}), elastic properties or toughness of WPC composites. These results corroborated the conclusions from monotonic tests.

X-ray CT Scanning Contrast Effects:

The reconstructed X-ray CT scanning images of the WPC containing gold micro-particles and nano-particles are shown in Figure 3.6a and Figure 3.7a respectively. In both cases the gold particles were not completely dispersed in the polymer matrix, but formed agglomerates large enough to be detected as separate components in the CT scanning images using a relatively low resolution (20 μm). Nevertheless, in the scanned images of WPC with gold micro-particles (Figure 3.6a), visibly fewer agglomerates and an improved contrast between wood particles and polymer matrix could be observed. This allowed the polymer matrix to be clearly differentiated from the wood particles using the grayscale threshold method. The segmented wood component and gold component are shown in Figure 3.6b,c respectively. While not all the particles were well dispersed in the polymer matrix, dispersion was sufficient to allow adequate attenuation for computer separation of the two components.

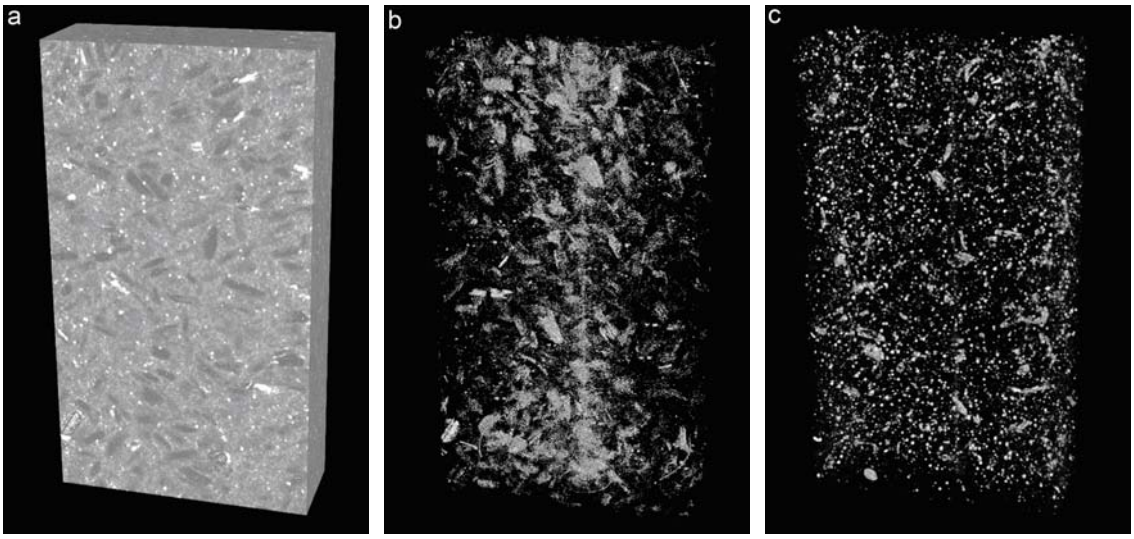

Figure 3.6 Image processing from reconstructed X-ray CT image of WPC with gold micro-particles: (a) Specimen volume, (b) Segmented wood component, (c) Segmented gold component.

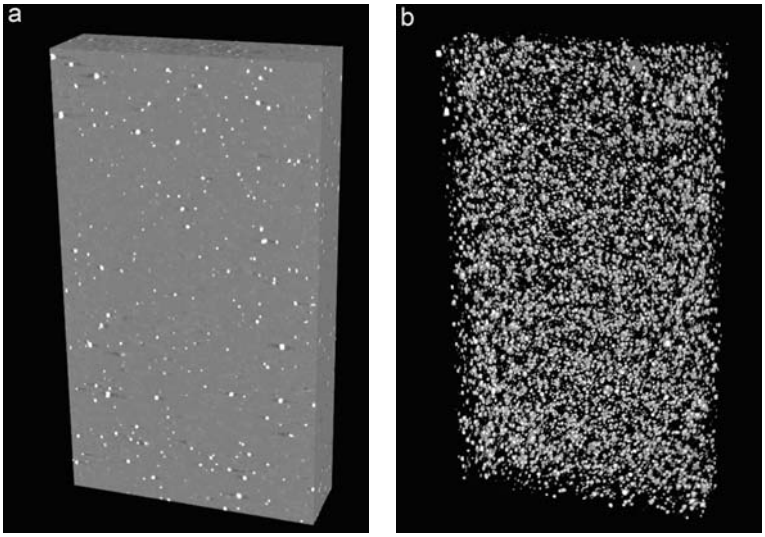

Figure 3.7 Image processing from reconstructed X-ray CT image of WPC with gold nano-particles: (a) Specimen volume, (b) Segmented gold component.

This was not the case for WPC doped with gold nano-particles (Figure 3.7a), from which it was concluded that most or all of the gold nano-particles agglomerated into sizes equal to or greater than 20 μm, which is the smallest size that can be identified by the scanner. An interesting observation was that the addition of the surfactant did not improve the dispersion of the gold nano-particles or the apparent contrast of the doped composite specimens (NS group). This may indicate that the surfactant

preferentially binds to the wood surface instead of the gold particle surface. However, additional testing would be required to investigate this supposition.

Conclusions

This study examined the effects of adding surfactant and gold particles of two different sizes on the tensile properties of WPC composites and X-ray CT scanning contrast. The following conclusions were drawn from the experimental work:

1. The addition of small amounts (1% weight) of technically pure gold particles to WPC formulations in order to improve the X-ray CT scanning contrast between components does not affect the mechanical properties of the composite. No significant differences in tensile strength, tensile stiffness or toughness between reference WPC, WPC with gold micro-particles and WPC with gold nano-particles were observed. Similarly, the gold particle size did not affect any of the tensile properties of the resulting WPC composites.

2. The addition of surfactant (tetra-n-octyl ammonium bromide), which may be used in laboratory procedures to obtain gold nano-particles or to disperse gold particles in the polymer matrix, significantly impaired the tensile strength (in the monotonic and cyclic test) of all analyzed WPC composite formulations. Tensile stiffness (initial tangent modulus in monotonic test and equivalent elastic modulus in cyclic test) was significantly affected for most of the WPC groups. More experiments are needed to explore how the surfactant affects the stiffness of WPCs. Toughness or work to maximum load were unaffected by the addition of surfactant.

3. Neither gold micro- nor nano-particles could be dispersed well in the HDPE matrix. A substantial amount of the particles formed agglomerates large enough to be visible as a separate component in the X-ray CT scanning images. However, sufficient amount of gold micro-particles were dispersed well enough in the polymer matrix to provide good contrast between the wood particles and the polymer matrix. Gold nano-particles could not be dispersed well in the polymer

matrix (with or without surfactant) and poor contrast between wood and polymer matrix was obtained.

In summary, technically pure gold micro-particles were found to be an effective contrast agent for X-ray CT scanning of WPCs, they did not impair the tensile properties of the composites. However, considering the high cost of gold particles, this method can only be used for small scale laboratory experiments. For large scale experiments, other methods for improving the X-ray CT scanning contrast should be examined.

CHAPTER 4 -- ACCOUNTING FOR THE WOOD/POLYMER INTERPHASE IN MULTI-SCALE CHARACTERIZATION OF WOOD PLASTIC COMPOSITES USING ADVANCED IMAGING TOOLS

Yi Wang and Lech Muszyński

To be submitted for publication in *Holzforschung*

Accounting for the Wood/Polymer Interphase in Multi-scale Characterization of Wood Plastic Composites Using Advanced Imaging Tools

Yi Wang and Lech Muszyński*

Department of Wood Science & Engineering

Oregon State University

Corvallis, OR 97331

* Corresponding author

119 Richardson Hall, Oregon State University, Corvallis, OR 97331-5751

Email: Lech.Muszynski@oregonstate.edu

Abstract

To improve WPCs mechanical properties and durability and meet building code requirements, a better understanding of their inner structures on different levels is necessary. In this study, imaging tools including high-resolution X-ray CT scanning, optical and electron microcopy were applied to examine WPCs. Digital image processing techniques combined with statistical analysis was applied to develop experimental methodologies for quantitative characterization of WPCs that would properly account for the wood/polymer interphase.

Wood particles (40-50 mesh) are generally composed of several dozens of wood cells. Due to the mechanical processing, wood particles have various shapes. The peripheral wood cells are often squeezed and crushed, in which polymer can penetrate relatively easily during compounding. End opening of wood particles are often closed and blocked with cell wall splinters. The inner wood cells are intact and more difficult for the polymer penetration. The lengths and widths of the 40-50 mesh wood flour have nearly symmetric distribution with medians of 0.77 mm and 0.27 mm respectively. The dominant aspect ratio of wood particles varies from 2 to 4. The majority of the 40-50 mesh wood flour are particles with low aspect ratio and large areas. The nominal wood volume calculated from X-ray CT scanning was lower than the volume calculated from the nominal density of the species, which might be caused by the reduced cell lumens and partial densification from the mechanical processing.

The HSB segmentation of the color micrographs of wood/PVC composite sample slices allowed for effective phase segmentation, and provided an good quantitative approximation of the relative volume fractions of the phases in the composite. Volumetric data from X-ray CT scanning of wood/PVC composite were also effectively separated using the adjusted histogram segmentation method. Volumetric fraction of interphase calculated from HSB segmentation and histogram segmentation method are consistent, and indicated that even without addition of a compatibilizer,

the interphase generated in the compounding process may constitute over 50% of the total wood particle volume.

Imaging tools combined with digital image processing methods are effective for quantitative characterization of wood/PVC composite accounting properly for the existence of interphase between the wood particles and the polymer matrix.

Introduction

Wood plastic composites (WPCs) are relatively new materials composed of wood particles, thermoplastics, and a small amount of modifying additives. WPCs have been successfully used in automobile parts. Perceived as an environmentally sound and low-maintenance building product, WPCs have also been widely used as semi-structural building materials, for instance, decking, fencing, and siding. It was predicted that the use of nonstructural WPCs based on high density polyethylene (HDPE), polypropylene (PP), poly(vinyl chloride) (PVC), and other plastics will continue to grow in the coming years (Dagher 2005; Smith and Wolcott 2006). On the other hand, the market potential for WPCs still remains untapped at less than 5% of the building material (Dagher 2005; Morton et al. 2003). To compete with other predominant building materials (such as solid wood, glulam, and I-joists), it is important that WPCs properties can be improved to satisfy the building code requirements. Challenges include relatively lower tensile strength and lower stiffness, but most importantly more significant long-term creep deformation and creep rupture properties (Dagher 2005; Smith and Wolcott 2006; Wolcott and Smith 2004).

The mechanical and physical properties of WPCs may be engineered to some extent by changing component characteristics and proportions, filler orientation and distribution, and by fine tuning the processing parameters. However, composite design is limited by the naturally variable wood properties and the limited selection of thermoplastics that may be used with wood.

Previous research suggested that the size and aspect ratio of wood particles have significant influence on certain physical and mechanical properties of resulting WPCs. Investigations included bio-fiber/polymer composites made with PE/HDPE (La Mantia and Morreale 2006; Maiti and Singh 1986; Zhu et al. 2001), PP (Myers et al. 1991; Stark and Berger 1997; Stark and Rowlands 2003; Zaini et al. 1996), natural rubber (Hernandez et al. 2004; Ichazo et al. 2006; Ismail et al. 1997), and polybutylene succinate (PBS) (Kim et al. 2005). As long as just effect of particle size was analyzed, the results were contradictory. Some researchers found that finer wood particles resulted increased strength and stiffness of the composites (Ismail et al. 1997; Maiti and Singh 1986; Myers et al. 1991; Takatani et al. 2000), while some others found the opposite effect (Ichazo et al. 2006; Zaini et al. 1996; Zhu et al. 2001). The conclusions are equally unclear regarding the impact properties, with some researchers concluding that coarser particles resulted in increased strength (La Mantia and Morreale 2006; Maiti and Singh 1986; Zaini et al. 1996), while others reported mixed results depending on the test configuration and specimen geometry (notched or unnotched specimens) (Kim et al. 2005; Stark and Berger 1997; Stark and Rowlands 2003; Zhu et al. 2001).

Theoretical analysis and some experimental observations suggest that the particle aspect ratio rather than just size should yield much clearer correlations with mechanical properties of the composites (Stark and Rowlands 2003). It is generally expected that composites filled with fibers have superior mechanical properties to those filled with particles of much lower aspect ratio. The exact mechanisms behind the effects of the bio-particle geometry on the composite micro-mechanics remain unclear.

Research efforts in WPCs have been mostly focused on improving the internal bonding between the particles and the matrix. The hydrophilic wood particles are generally incompatible with hydrophobic thermoplastic polymers. The compatibility between wood and polymer matrix caused a major problem for interfacial adhesion between these two materials in WPCs, this usually resulted in decreased mechanical

properties (Bledzki et al. 1998; Jiang and Kamdem 2004). This incompatibility is usually addressed by the addition of chemical modifiers (coupling agents or compatibilizers) which influence the internal bonding between wood and polymer matrix. On the other hand, modifiers and agents added to act as lubricants, protective treatments or fire retardants may adversely affect the properties of the components or the interphase (Clemons 2002; Colom et al. 2003; Gardner et al. 2004; Geng et al. 2004; Lee et al. 2004; Manchado et al. 2003; Newson and Maine 2004; Wolcott and Smith 2004; Zafeiropoulos et al. 2002). In most studies, the wood/polymer interaction was discussed from the chemical point of view. Although mechanical coupling is considered a major mechanism in adhesion, no known studies have addressed its role in WPCs (Wolcott 2003).

In most composite models, the internal bond area is assumed a clearly defined interface, an imaginary surface forming a common boundary between the phases (a wood particle and the surrounding polymer matrix). Such assumption is a good approximation for composites reinforced with glass or carbon fibers – solid, impermeable and of regular cross sections. Such assumption can hardly be made valid for wood plastic composites, where wood particles are porous, permeable and irregular. Thus in WPCs, the internal bond is believed to be dispersed in the interphase (Michaeli et al. 2000). As opposed to interface, interphase is a three dimensional region on one or both sides of the imaginary contact surface where the phases coexist dispersed in one another, and a more or less gradual change of properties from one phase to another can be observed. Because of its transient nature, the precise location of interphase is not easy to determine. The presence of interphase may also pose a non-trivial difficulty for clear identification of the interface and consequently for precise morphological characterization of the composite.

Depending on the different scales and the properties measured, the term interphase can be used to describe different phases in composites If examined on the molecular level, the wood/polymer interphase is better used to describe the interaction between wood cell wall and polymer molecules, the polymer penetrated into the wood cell lumens is

not considered as interphase. On the other hand, if examined on micro level, the region of wood cells penetrated with polymer matrix (including the wood cell walls and penetrated polymer) can be viewed as an interphase that shows intermittent properties as a whole. In this research, we are looking at the interphase on the micro level.

The effect of interphase on WPCs properties has been examined in many micro-mechanical studies on single-fiber/polymer systems (Egan and Shaler 2000; Eichhorn and Young 2004; Rials et al. 2001; Shaler et al. 1997; Stamboulis et al. 1999; Tze et al. 2007; Tze et al. 2003). These studies provided valuable fundamental background information, including the basic failure behavior of the interphase and the micro-mechanical value, the apparent shear strength for particular compositions. However, these results cannot substitute for a direct in situ knowledge of how larger particles of much more diverse geometry interact with a solid polymer matrix. Such studies also cannot answer the important question of what is the statistical significance of the variability and distribution of filler particles in the material.

Digital images carry plenty of information that can be analyzed and quantified in many ways. It is not surprising that various 2D and 3D imaging tools have been applied to better understand the interfacial characteristics of WPCs destructively or nondestructively. Apart from conventional light microscopy, scanning electron microscopy (SEM) is one of the most commonly used imaging techniques. In numerous research projects investigating interfacial mechanical characteristics of the WPCs, SEM images of the fractured surfaces were taken to examine the interfacial features and predict the bonding strength based on whether the wood particles were pulled out of the matrix or broken (Oksman and Clemons 1998; Ray et al. 2002; Redondo et al. 2003; Rials et al. 2001; Tripathy et al. 2000). Michaeli et al. (2000) used a combination of SEM, transmission electron microcopy (TEM), energy-dispersive X-ray analysis (EDX) and atomic force microscopy (AFM) to detect the fiber/matrix boundary layer of the individual wood fibers coated with coupling agent. Three dimensional images of wood fiber/plastic composites surfaces were obtained

nondestructively using confocal laser scanning microscopy (CLSM), from which the fiber/plastic interphase were successfully visualized and characterized qualitatively (Grigsby et al. 2005). The previous research demonstrated how imaging tools helped to obtain qualitative understanding of the interaction between wood and polymer in WPCs; however, little quantitative characterization with statistical significance was offered or even attempted.

High-resolution X-ray computed tomography (CT) scanning created new opportunities for nondestructive, in situ analysis of particulate composites. X-ray CT scanners are capable of returning digital images carrying spatial information coded in discrete grayscale values representing densities and X-ray attenuations assigned to millions of voxels arranged in arrays (Park et al. 2003; Pétraud et al. 2003). The combination of high-resolution nondestructive imaging techniques like X-ray CT with machine vision tools provides the means for a quantitative characterization of the internal structure of heterogeneous composites as well as an assessment of the deformation and damage that occurs because of climate exposure and loading. X-ray CT techniques have been used in diagnostic medicine, as well as in imaging and the microscopic nondestructive evaluation of materials such as ceramics, electrical insulators, plastics, wood and other materials (Rao et al. 1999; Wang et al. 2007). Machine vision-based characterization of 3D samples of particulate composites and fibrous materials have already been proposed by some researchers (Bertilsson et al. 1992; Kamke and Lee 2007; Peix et al. 1997; Shaler et al. 2003; Thompson et al. 2006; Yang and Lindquist 2000). Most of the proposed algorithms assumed a high contrast and relatively well defined interfaces between component materials.

This study was part of a larger project with an overall objective to investigate correlations between morphology and micro-mechanics in bio-based particulate composites. The specific objective of this study was to establish an effective experimental methodology for quantitative morphological characterization of WPCs that would properly account for the existence of interphase between the wood particles and the polymer matrix.

Materials and Methods

In this study, nondestructive X-ray CT scanning was used for in situ characterization of wood/polymer interphase in wood particles embedded in the polymer matrix in WPC composites. In the compounding process, wood particles are subjected to high temperature and friction, which may cause their morphology to be further modified.

In our preliminary study, wood/PVC composite samples were examined using X-ray CT scanning, in which the gray color shades represent local X-ray attenuations (Figure 4.1a). The grayscale value histogram from the reconstructed image volume is shown in Figure 4.1b. Two distinct peaks are identified as the wood and polymer phase. However, when a segmentation method that simply selects a threshold value at the valley of the histogram was used to separate wood and polymer in the reconstructed image, the calculated wood volume fraction appeared to be grossly underestimated. Apparent wood density was calculated by dividing the known weight fraction content of wood in the composite by the volume fraction content, as defined by the histogram analysis, then multiplying by the known density of the composite. The result was 2500 kg m^{-3}, which is well above the nominal density of the wood cell wall material (about 1500 kg m^{-3}). This led to the conclusion that there must have been an extensive interphase between the wood and polymer matrix in the specimens, which has been neglected in the density histogram assessment.

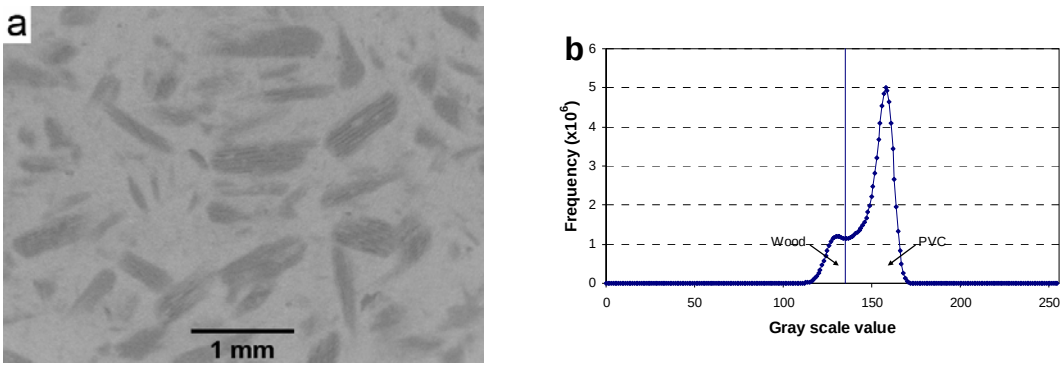

Figure 4.1 Preliminary analysis on the X-ray CT scanning images of wood/PVC composite: (a) Reconstructed slice, (b) Simplistic histogram segmentation.

Wright and Mathias (1993) detected the presence of poly(EHMA) in the wood cell walls of balsa WPC composites using X-ray energy dispersive analysis. This

interphase may contribute to the difficulty in precisely differentiating the particles from the polymer matrix. In order to enhance the precise segmentation of wood particles, in this study CT images of virgin wood particles (before being compounded with polymer) were examined as reference to the data obtained from the composite.

In addition, conventional 2D microscopic techniques (regular light microscopy, fluorescence microscopy, and SEM) were used to provide visual supporting information on the morphology of the wood particles and the wood/polymer interphase at various scale levels.

Materials

Currently about 84% of commercial WPC products use HDPE matrices while PVC and PP share about 9% and 7% respectively of the total WPC market (Morton et al. 2003). However, as discussed in our previous study, the contrast between wood and HDPE (or PP) in the X-ray CT scanning is poor. Although acceptable contrast may be obtained by doping one phase with a contrast agent, much better contrast can be obtained for wood/PVC composite (Wang et al. 2007). Therefore, for this methodological study, PVC was selected for matrix material. The polymer (PVC, density 1400 kg m^{-3}, inherent viscosity 0.74) was purchased from Scientific Polymer based in Ontario, NY.

The wood flour was a commercial pine flour mixture, 40 mesh, donated by American Wood Fibers (Schofield, WI). Prior to use, the wood flour was dried at 103 °C for 24 h and then screened through 50 mesh sieve to remove fines. The remainder was thus designated 40-50 mesh wood flour and was collected for use.

Specimen Preparation

The wood/PVC composite specimens were fabricated in the laboratory using a wood/PVC ratio of 40/60 by weight. The wood flour and PVC were mixed at ambient temperature in batches of 46 g. The mixture was compounded in a Brabender IntelliTorque mixer with bowl mixer and rotor blades attached (C.W. Brabender

Instruments, Inc., S. Hackensack, NJ). The mixer was preheated to 170 ºC before processing. The speed of the rotors in the bowl was 30 rpm. The mixture was blended until a constant torque was reached (which typically took about 5 min) and the blending continued for additional 5 min. The compounded composite was then removed and stored for subsequent compression molding.

A steel mold with the dimension of 101.6 × 101.6 × 2.5 mm^3 was used to compress the mixture into panel sheets in a hot press preheated to 180 °C. The initial pressure was 0.04 MPa and then raised to 0.60 MPa over 2 min and held for an additional 10 min. After that, the mold was cooled under pressure in ambient conditions for 24 h (More details on the specimen fabrication are given in Appendix A.). The wood/PVC composite panels were removed and cut into a cylindrical sample (diameter 9.00 mm, thickness 1.70 mm) for X-ray CT scanning. The composite panels were microtomed to obtain slices and microtomed surfaces for light microscopy and SEM examination.

X-ray CT Scanning

A high-resolution X-ray CT scanner (SCANCO MicroCT medical scanner) located in the Bone Research Laboratory at OSU was used to obtain 3D images wood/PVC composite and wood flour. The cylindrical sample was scanned. For the reference image, wood flour (mass 0.03 g, measured on an analytical lab balance scale, AB104-S/FACT) was contained in a specially designed holder. Both were scanned in X-ray CT scanner at 45 keV and 176 μA, the exposure time for a single projections was 480 ms.

The 3D reconstructions of the specimen cross sections were calculated from projection images taken at 2000 angular positions in 180°. In order to suppress the random noise, the projections for each angular position were calculated as averages from five exposures. The resulting resolution was 6 μm/voxel, the output data composed of reconstructed images was arranged as slice sequence of 16-bit grayscale images.

Optical Microscopy

Regular light microscope and epi-fluorescence microscope were used to examine both wood particles and sections of the wood/PVC composite.

An epi-fluorescence microscope (Nikon ECLIPSE E400) was used to take images (70 ×) of individual wood particles to examine their shape features. In order to examine the sectional profiles of the particles, single wood particles were cross cut with glass knife and fixed on a glass slide with a small droplet of cyanoacrylate adhesive (Supper glue). Epi-fluorescence microscopic images of the cross sections were taken.

For statistical characterization of the particle dimensions, wood flour was dispersed randomly and evenly onto pieces of adhesive tapes in such a way that wood particles were close but not touching each other. The dispersed wood particles were imaged with a stereomicroscope (Nikon SMZ-2T) (no less than 40 wood particles per image). Totally 44 images (1392 × 1040 pixels) were taken. The images were then analyzed using public domain digital image analysis software ImageJ (http://rsb.info.nih.gov/ij/). The particle analysis function of this software returns between other parameters the two principal dimensions (maximum and minimum) of each particle measured along its major axes.

For the microscopic analysis of particle embedded in the polymer matrix, thin slices (30 μm) were microtomed from the wood/PVC composite panel, and stained with an aqueous solution of toluidine blue (0.5%). Stained sections were then rinsed with water, mounted onto glass slides and covered by cover glass. The slices were imaged using regular light microscope (Nikon ECLIPSE E400, without fluorescence light excitation) at 70× magnification. 36 images were taken for analysis (Figure 4.5a shows one of the images).

Scanning Electron Microscopy (SEM)

Single wood particles were selected and analyzed using the SEM facility (AmRay 3300FE) at OSU. A small droplet of cyanoacrylate adhesive was applied onto a cover

glass; wood particles were mounted horizontally or vertically on cover glasses. Then the mounted wood particles were coated with gold and imaged using SEM at magnifications between 218× and 400× (Figure 4.4a,b).

As mentioned above, micrographs of fractured specimen surface are commonly examined in WPC research to evaluate the bonding strength of the interface. In our research, however, the goal of the SEM analysis is to evaluate the wood/polymer interphase in possibly unaffected material. Therefore, in this study, the microtomed wood/PVC composite surfaces were examined. The microtomed surfaces were coated with gold and imaged with SEM at magnifications between 400× and 36,100× (Figure 4.6 and Figure 4.7).

Results and Discussion

Wood Particle Characterization

The results of volumetric and 2D characterization of individual and bulk wood particles are discussed in the following sections.

Wood Particle Volume Characterization Using X-ray CT Scanning

Figure 4.2a shows a reconstructed slice of the wood flour contained in a special holder. The cellular structure of the wood particles, walls and lumens, can be clearly distinguished. The reconstructed images can be thresholded at different gray scale intensity values to get binary images. A gray scale intensity value was selected at which the outline of the wood cell walls in the thresholded binary images can be fitted well with that in the original reconstructed images. The volume of wood cell materials was calculated from counting number of pixels in the binary images qualified as "wood" by thresholding the reconstructed images at the selected gray scale intensity value. With the known mass of the wood flour in the holder (0.03 g), the nominal density of the cell wall material of the wood flour was calculated. However, when the threshold level was selected automatically by the software, the calculated density

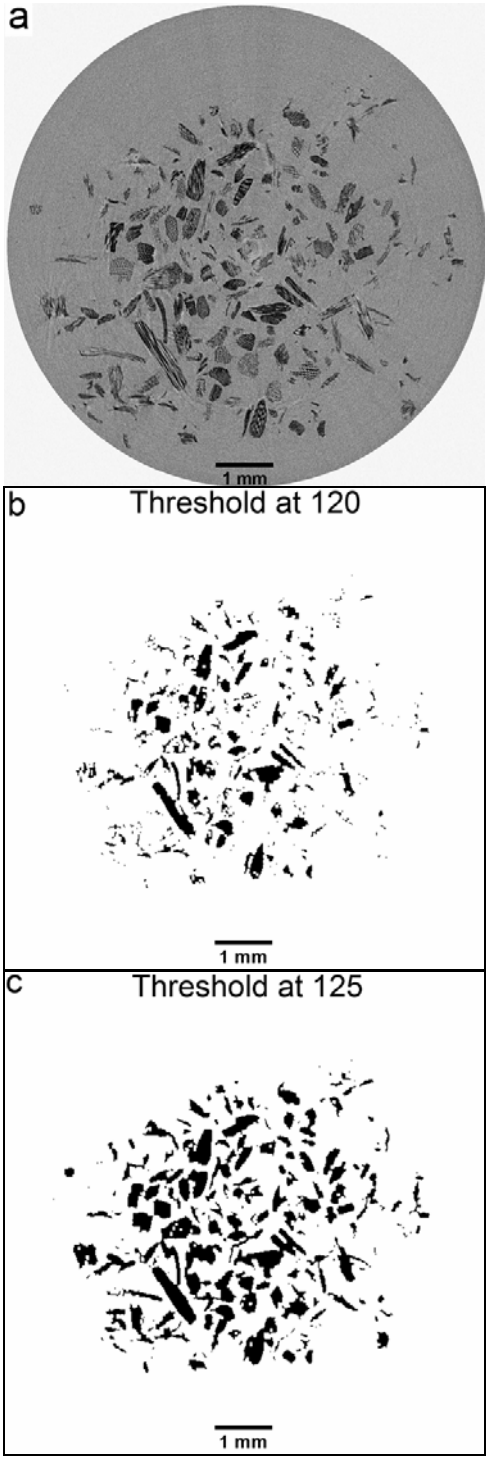

Figure 4.2 Wood particle volume calculation from X-ray CT scanning images: (a) Recontructed slice, (b) Binary image from thresholding at 120 gray scale intensity value, (c) Binary image from thresholding at 125 gray scale intensity value.

was found to be much higher than the wood cell wall material density, and thus rejected as incorrect.

To correctly measure the nominal volume of the wood particles, both cell lumens and walls should be qualified as "wood" in the thresholded image. In order to achieve that, the reconstructed images were treated with morphological closing (a procedure tends to enlarge the boundaries of foreground regions in an image) with a 3 × 3 unit matrix for four iterations. The processed volume was then thresholded at different gray scale intensity values to get binary images (Figure 4.2b,c shows thresholding at gray scale value of 121 and 125 respectively). After comparing these binary images visually with the original grayscale image, it is found that Figure 4.2c can match well with the outline of the wood particles. The nominal density of the wood particles was calculated to be 880 kg m^{-3}. The nominal density calculated from processing X-ray CT scanning image is still higher than the nominal density of pine, which various from 390 to 700 kg m^{-3} (USFPL 1999). On this level however, it cannot be ruled out that the difference results from partial densification of the particles in the manufacturing process. The following microscopic analysis of individual particles was carried out in order to test this hypothesis.

Geometrical Characterization of Wood Particle

Epi-fluorescence microscopic images of individual wood particles were shown in Figure 4.3a-c. Figure 4.3a shows small and blunt particles, with lengths close to the widths (aspect ratios: 1.40 and 2.38, to be discussed later in next section). These shortest particles are often machined into irregular shapes with blunted ends and have relatively large cross section areas and total surface areas. Figure 4.3b shows middle size particles, with relatively larger aspect ratios (4.42 and 3.93). Their surfaces are smooth and with round ends and their cross sections have the dimension of tens of wood cell diameters. Figure 4.3c shows very slim particles with very large aspect ratios (5.89 and 10.57). They often have large sizes in the grain direction and small sizes on the cross section (several wood cells).

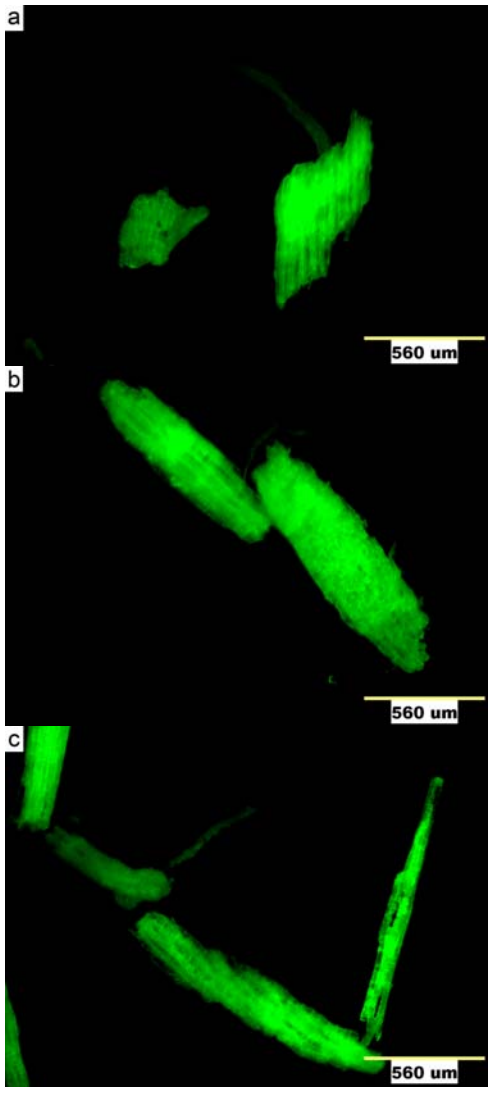

Figure 4.3 Epi-fluorescence microscopic images of single wood particles.

Single wood particles were also examined at higher magnification using SEM and the resulting images were shown in Figure 4.4a,b. Particle in Figure 4.4a has very smooth surface and ends, which is likely a result of repeated hits in the hammermill processing rather than sharp cutting. Figure 4.4b shows particle with different surface features: some cavities on top of the wood particle formed by the machined cell walls and some openings on the particle ends are already visible.

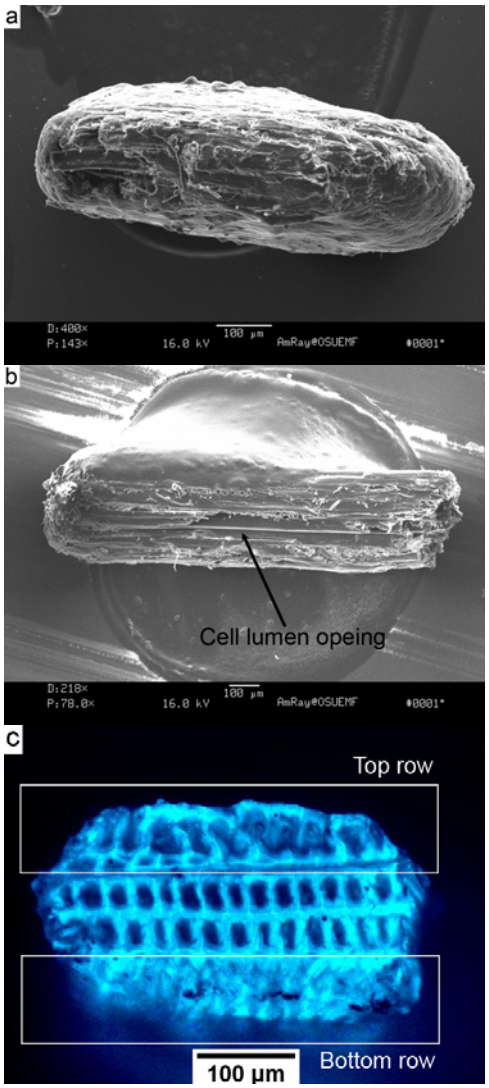

Figure 4.4 Micrographs of single wood particle: (a), (b) SEM images, (c) Epi-fluorescence microgrpah of wood particle cross secton.

Both of the SEM images suggest that due to mechanical processing, wood particle ends and the peripheral cells appear to be ruptured and crushed, which caused some of the cell end openings to be closed and blocked with cell wall splinters. In order to examine the inner structures of the wood particles directly, single wood particles were cut perpendicular to grain direction to expose the cross section. Figure 4.4c shows the epi-fluorescence microscopic image of a wood particle cross section.

The section appears to be composed of four to six rows of cells with about 15 cells in one row. The top rows were crushed to a large extend so that almost all the cell walls were squeezed and the cell lumens were reduced. The bottom row of cells had their walls squeezed towards the interior cells, and there is almost no cell lumen space left. It is evident that these cells experienced great mechanical forces and deformation, but the cell shapes can still be recognized. The fraction of the squeezed wood cell area (including the top row and the bottom row) to the whole cross section area was calculated to be 56%, which is surprisingly high. Although this observation cannot be supported by a statistical proof, crushed peripheral cells appear to be a typical feature of hammermilled particles used in WPCs.

From the above microscopic examination of single wood particles, we found that wood particles were generally machined into different shapes. The peripheral cells on wood particle surface were often squeezed and deformed. This observation seems to confirm that the densification of the peripheral zone of the particles might result in the underestimation of the nominal volume of wood particles from the X-ray CT scanning images.

Wood Particle Size Distribution

The wood particle size distribution was analyzed by processing the microscopic images of dispersed wood flour as described in materials and methods Section 4. Figure 4.5a shows a micrograph of randomly dispersed wood particles captured with a light microscope. Binary images were obtained by thresholding the original micrographs. Background noises were depressed using filtering treatment. With the help of ImageJ software, wood particle length and width were extracted from the binary images. The length, width, and aspect ratio calculated from the 44 images, and the scatter plot of the particle distribution were plotted in Figure 4.5b-d respectively. The length of wood particles had a relatively wide distribution; most fell in the range of 0.20–1.60 mm with median of 0.77 mm. The width had a relatively narrower distribution falling in the range of 0–0.60 mm with median of 0.27 mm. The aspect

ratios were in the range of 1–12, with a peak value between 2 and 3. Zones I, II, and III in Figure 4.5c correspond roughly to the aspect ratios in microscopic images of individual cells shown in Figure 4.3a,b and c respectively. The statistical analysis result is shown in Table 4.1.

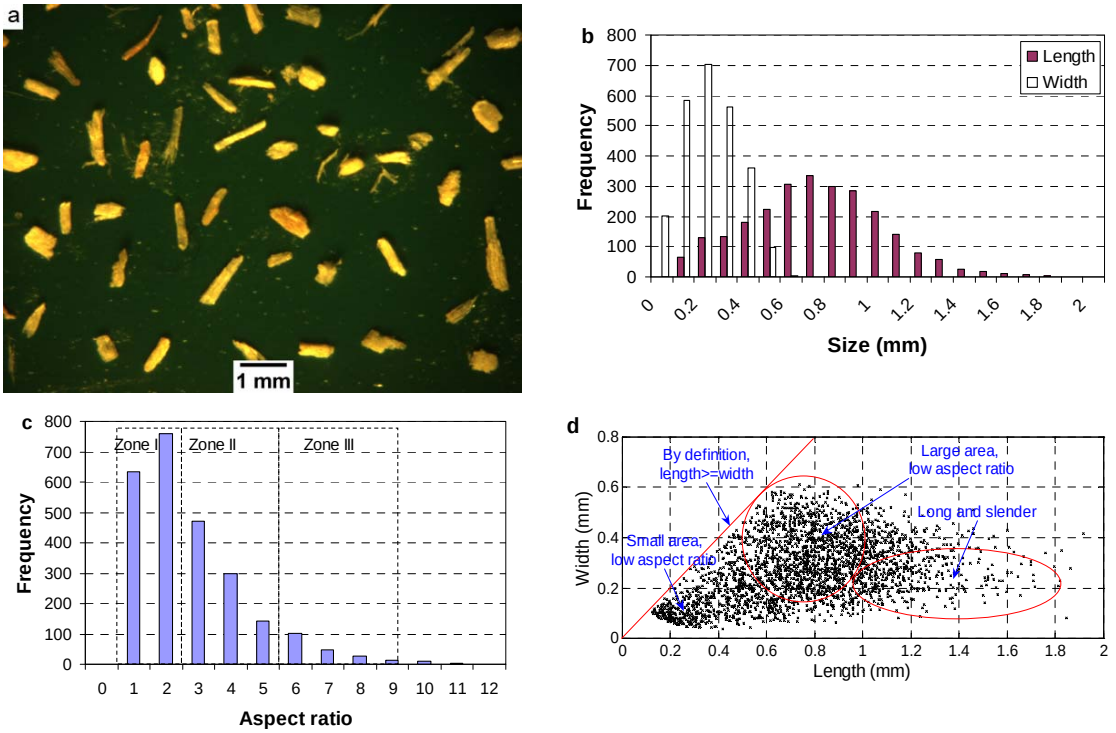

Figure 4.5 Wood particle geometrical characterization based on 44 stereoscopic images: (a) Original image of randomly dispersed wood particles, (b) Length and width distribution, (b) Aspect ratio distribution, (d) Particle size distribution scatter plot.

Table 4.1 Wood particle size distribution parameters.

	Min	Max	Median
Length (mm)	0.13	1.92	0.77
Width (mm)	0.04	0.61	0.27
Aspect ratio	1.03	23.10	2.80

Wood/PVC Composite Characterization

In our preliminary study from X-ray CT scanning of wood/PVC composite, the simplistic segmentation method resulted in highly underestimated wood volume fraction. To investigate the reason for this underestimation, further study was done to

examine the images of wood/PVC composites from X-ray CT scanning and micrographs acquired via conventional microscopy, the results are discussed below.

SEM

The microtomed wood/PVC composite surfaces were examined using SEM to qualitatively characterize the interphase between the wood particle and polymer matrix. Figure 4.6a was focused on a wood particle horizontally embedded in the PVC matrix, so that it was cut along its longitudinal direction. Figure 4.6b,c show the

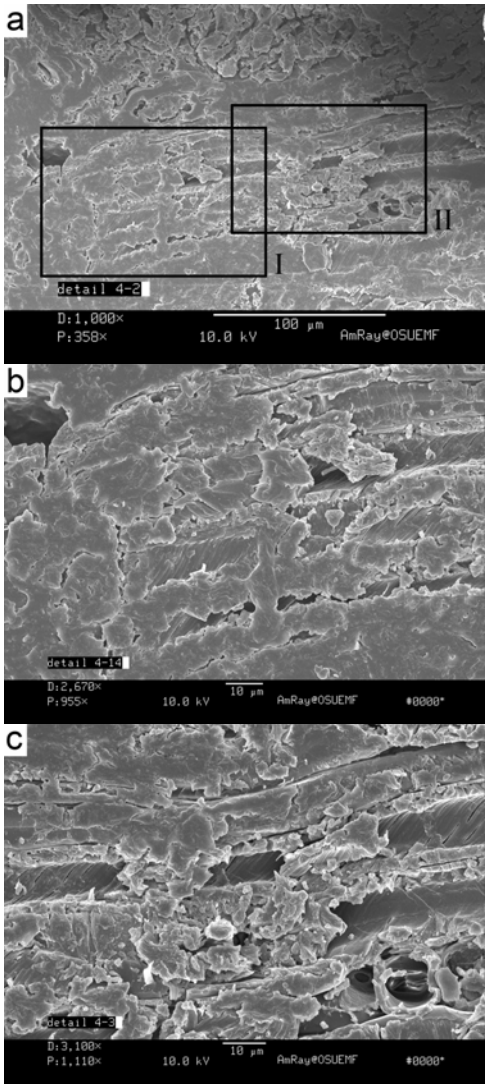

Figure 4.6 SEM images of microtomed wood/PVC composite surface (wood particle was cut parallel to grain).

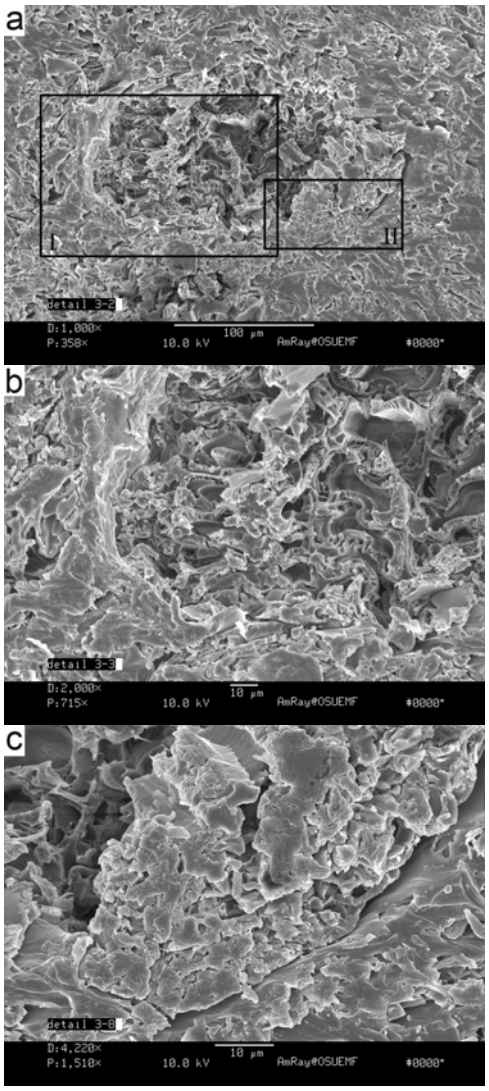

Figure 4.7 SEM images of microtomed wood/PVC composite surface (wood particle was cut perpendicular to grain).

regions of interest I, II respectively. In most part of region I, the boundaries between wood and polymer matrix can barely be identified. Apparently, the shear and pressure of the compounding process managed to force the polymer into the cell lumens to certain length. This is also demonstrated by the smooth and continuous surface after microtoming. In region II, further sections of cell lumens are free of polymer and the contours of the wood particle can be clearly identified. Region I represented the end of the wood particle, with open end lumens and cavities of cell wall on wood particle

surface. Region II represented the middle part of the wood particle, where the incompatibility between the hydrophilic wood cell wall and hydrophobic polymer might cause negative capillary force in the lumen that resisted the polymer penetration. It is also possible that the air trapped in the lumen prevented polymer from further penetration.

Figure 4.7a shows another wood particle positioned vertically and thus cut perpendicular to grain. Figure 4.7b,c show the magnified regions of interest I, II respectively. In region I, the boundary between wood and polymer is relatively clearly visible, however, no gaps could be found between these two phases. Although in this region most cell walls were badly deformed, polymer could not penetrate the squeezed cell lumens. In region II, the boundary between wood and polymer can be detected by a circumferential discontinuity, or a thin gap tracing area along the boundary (or interface). On the other hand, the cell lumens in this area were mostly filled with polymer forming an extensive interphase region.

These SEM images of microtomed wood/PVC composite sections suggested that given the high temperature and shear exerted on the mixture in the compounding process, an extensive wood/polymer interphase can be created even when the bonding is not enhanced with a coupling agent and clearly poor.

Segmentation of Light Microscopic Images

In order to quantitatively characterize the different components in wood/PVC composite, light microscopic images of composite slices were examined (Figure 4.8a-c, 70× magnification, 0.648 μm/pixel). Of total 36 images analyzed for this research, three pictures show here represent sections with various positions of wood particles embedded in the polymer matrix: perpendicular (Figure 4.8a), parallel (Figure 4.8b), and positioned at angle to the cross section (Figure 4.8c). In the images, the clear wood cells are dyed blue, while the matrix shows light brown with many small darker features.

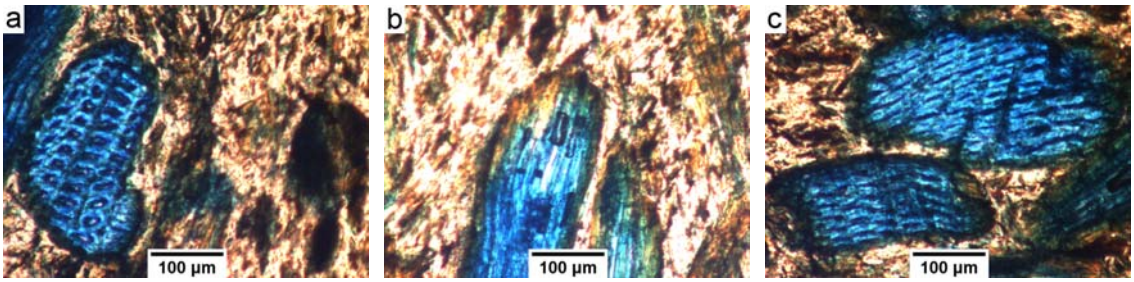

Figure 4.8 Color micrographs of wood/PVC composite slices.

In the particles shown in Figure 4.8a, the outer cells appear to be squeezed, half-collapsed, and possible torn, in a similar manner as those examined separately under the epi-fluorescence microscope (Figure 4.4c). The brown-greenish zone on the perimeter of the particle suggests that the polymer penetrated into the peripheral zone forming an interphase. Figure 4.8b shows two wood particles cut along the cell axis direction. Close to the wood particle surface, wood cells filled with polymer can be clearly observed. Furthermore, the penetration through the tips of the two wood particles can also be identified, with depth of 2–3 times cell diameters, just as observed in the SEM images in Figure 4.6a. This would again indicate that the shear and pressure force and temperature generated during the compounding process forced the polymer into the cell lumens even though the lumens in the virgin particles appeared to be blocked by the end splinters, as shown in SEM images in Figure 4.4a. In Figure 4.8c, wood particles are shown at an angle to their axes directions and wood/polymer interphase was visible in the cell lumens close to particle surfaces.

From these microscopic images, the interphase layer can be clearly distinguished from wood and polymer matrix. Color segmentation in RGB (red, green, and blue) aspects, which was often used to separate different components in color images (Gonzalez and Woods 2001). However, an alternative HSB segmentation method, which analyzes the hue (H), saturation (S), and brightness (B) aspects of the color micrographs, was used here with much better result. Figure 4.9a shows an original color micrograph, Figure 4.9b-d shows the H, S, and B aspects of the original color image represented in gray scale. The histogram of H component (Figure 4.9e) contains three peaks, which

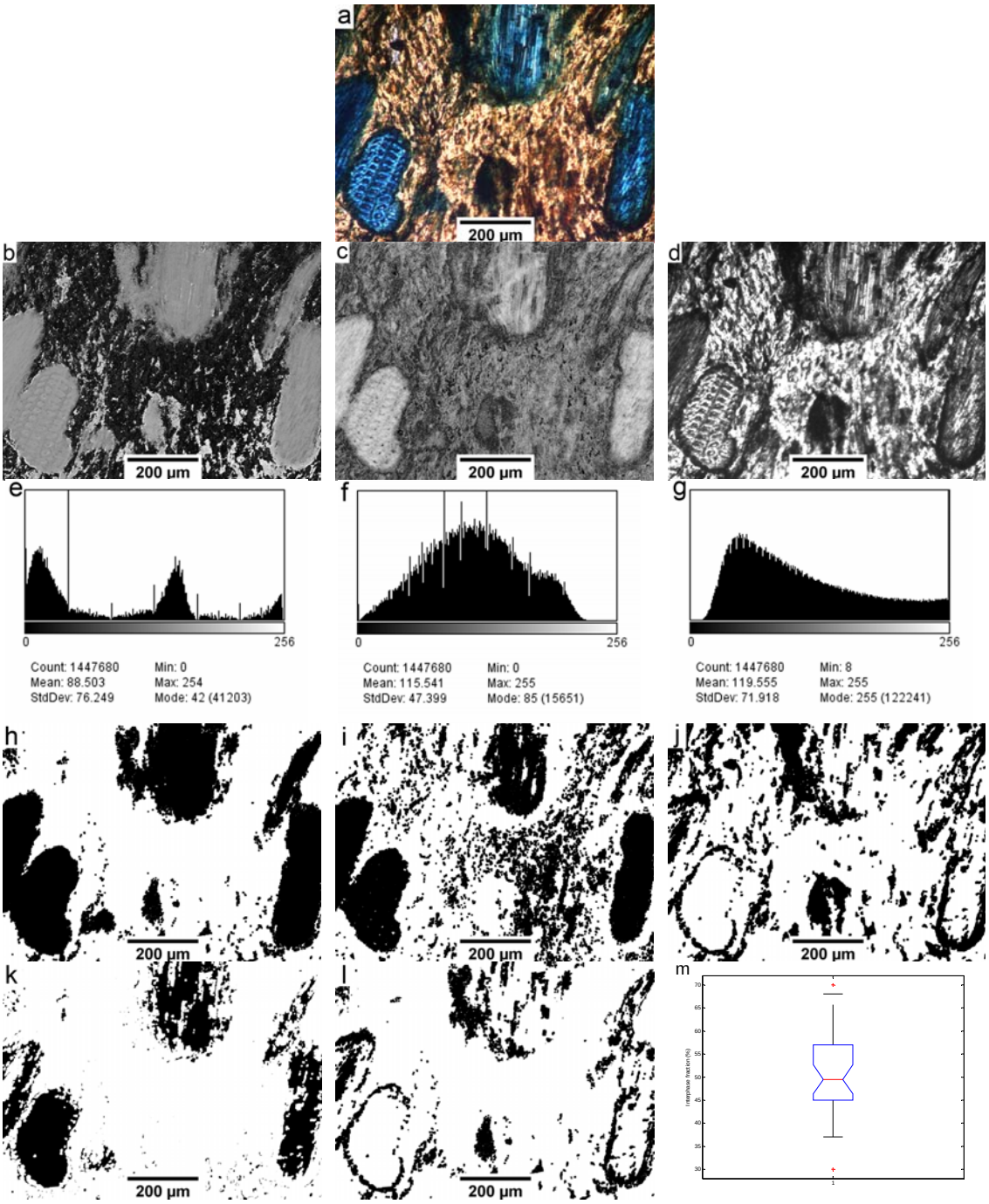

Figure 4.9 HSB color segmentation from micrographs of wood/PVC composite slices: (a) Orignal micrograph, (b)-(d) Hue, saturation, and brightness components, (e)-(g) Histogram of the H, S, and B components, (h)-(j) Binary images of H, S, and B components after being treated with opening procedures, (k) Segmented wood component, (l) Segmented wood/PVC interphase, (m) Boxplot of the interphase fraction calculated from all 36 micrographs.

roughly correspond to the PVC, wood, and wood/PVC interphase respectively. Therefore, the H component was thresholded in such a way that only wood and wood/PVC interphase was selected. To reduce the random noise in the image, the thresholded binary image was processed with three iterations of opening procedure, which tends to remove some of the smaller objects and separate the edges of larger objects touching each other, while preserving the overall areas of the larger objects. The binary image after three iterations of opening was shown in Figure 4.9h. For the S component, the histogram (Figure 4.9f) did not show clearly divided distributions, and no clearly segmented images could be obtained from threshold process. The resulting binary image contained large amount of pixels not clearly related to any phase (Figure 4.9i). In the histogram of the B component, the interphase has lower gray scale intensity values and it corresponds to the only peak in the histogram (Figure 4.9g). Therefore, the interphase can also be clearly segmented from the B component. Figure 4.9j shows the image after treating the thresholded binary image with three iterations of opening procedure. Based on the binary images of interphase (Figure 4.9j) and wood with interphase (Figure 4.9h), the clear wood component not penetrated by the polymer matrix was obtained by subtracting Figure 4.9j from Figure 4.9h, as shown in Figure 4.9k. The interphase was obtained as a logical operation (AND) of Figure 4.9h and Figure 4.9j. The result of the operation is shown in Figure 4.9l.

From the segmented wood and wood/PVC interphase, the fraction of each component was calculated by counting the number of pixels in the binary images. Totally 36 microscopic images of the wood/PVC composite slices were taken, from which the fraction of interphase to wood was calculated. Statistical analysis showed that the calculated interphase ratio (volume of interphase to volume of wood (including “clear” wood and interphase)) had a normal distribution (p-value < 0.01 from Jarque-Bera test with 95% confidence). The mean of the interphase ratio is 51% and the standard deviation is 10%. Figure 4.9m shows the box plot illustrating the distribution of the calculated interphase fraction values.

The average interphase fraction of the particle cross sections (51%) corresponded with the roughly assessed fraction of the peripheral zone of damaged cells observed in Figure 4.4c. Apparently, it is mainly the peripheral zone of thorn and damaged cells that are open for polymer penetration, while the intact central cells remain clear.

Segmentation of X-ray CT Scanning Images

The reconstructed X-ray CT volume was composed of 200 vertical slices (2048 × 2048 pixels). In the images of these slices, the local X-ray attenuation numbers were visualized as pixels of various grayscale intensities. The original grayscale value histogram from entire volume was shown in the solid line in Figure 4.10. It is a bimodal histogram, where one mode corresponds to the wood component and the other to the polymer matrix. However, fitting two normal distributions to this histogram did not bring much better results than dividing the distribution by a simple threshold at the lowest point of the saddle. Clearly, the interphase needed to be accounted for as a separate (third) distribution. The following approach was adapted.

From the X-ray CT scanning of pure wood particles, the gray scale histogram showed normal distribution. Considering the similarities of gray scale intensity value of wood particles, it is reasonable to assume that histogram of the wood content in the WPC composite has symmetric Gaussian distribution. Similarly, the gray scale histogram distribution of polymer content can be assumed to have similar Gaussian distribution, which can be approximated by the normal probability function of: $f(x) = Ae^{-\frac{(x-\mu)^2}{2\sigma^2}}$, where x is the gray level value, f(x) is the probability of a pixel having gray level x, A is the scale parameter, μ and σ are the mean and variance of the distribution (Jain and Dubuisson 1992).

Given the obvious peak position of these two components, their gray scale intensity value distributions can be fitted according to the above formula (shown as component 1,2 in Figure 4.10). When the residue of the two distributions is analyzed, a third distribution is clearly visible (component 3 in Figure 4.10). In the light of the previous

analysis results from SEM and light micrographs of wood/PVC composite slices, it is reasonable to infer that this third distribution corresponds to the wood/PVC interphase. It follows that the "wood" distribution represents just the part of the wood particles that had not been penetrated by the polymer, while the peripheral zone of the particles is classified as the interphase. Only the two added together represent the full volume of the particles in the composite. With the assumption that all these three components (wood, PVC, and wood/PVC interphase) have symmetrical Gaussian distribution, the gray scale intensity value distribution of the interphase was fitted with the above formula (dash line in Figure 4.10). The estimated parameters for these three distributions are listed in Table 4.2.

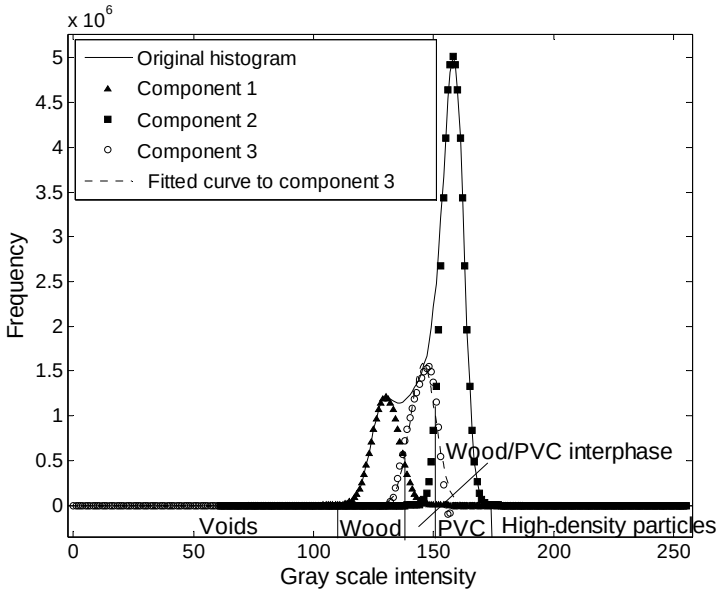

Figure 4.10 Histogram segmentation from X-ray CT scanning of wood/PVC composite.

Table 4.2 Estimated distribution parameters from adjusted histogram segmentation.

	μ	$\mu - 3\sigma$	$\mu + 3\sigma$
Wood	130	113	147
Interphase	158	145	171
PVC	145	129	161

Note: all values presented in 0-255 gray scale intensity values.

Once the parameters of the mixture gray scale intensity value distribution have been estimated, the threshold value can be calculated using Bayes' decision rule with a 0-1 loss function and assuming different prior probabilities for these three components (Jain and Dubuisson 1992). In this study, we used the simple method of choosing the threshold value where the distributions of two neighboring components intersect. Because of the transient nature of the interphase, the three distributions clearly overlap. It means that some pixels in the volume cannot be unambiguously assigned to one of the distributions by the grayscale intensity alone. Therefore, the thresholding methods would be a simplification with certain margin of error.

There are two minor components: voids (or air) and high-density particles (e.g., dirt, minerals, and/or microscopic metal scraps). Voids are the low density content inside wood particles or polymer matrix, generally, they have lower gray intensity values than wood and they correspond to the lower tail of the histogram (gray scale intensity value close to 0). High-density particles are the component the higher tail of the histogram (gray scale intensity value close to 255).

Since the three major components: wood, PVC, and interphase are considered to have Gaussian distribution, the probability that a voxel is out of the $\pm 3\sigma$ range of the distribution belongs to a component is less than 0.5%. Consequently, we can assume that those voxels out of the -3σ range of the gray scale intensity value distribution of wood component represent the voids, while those out of the $+3\sigma$ range of the gray scale intensity value distribution of PVC represent the high-density particles.

Table 4.3 Calculated component volume fractions from adjusted histogram segmentation.

Components	Threshold	Volume fraction (%)
Voids	0-113	3.81
Wood	113-137	18.79
Interphase	137-151	23.93
PVC	151-171	57.23
High-density particles	171-255	1.91

From the above analysis, threshold values for separating different phases (voids, wood, wood/PVC interphase, PVC, and high-density particles) in the wood/PVC composite were calculated and listed in Table 4.3.

Figure 4.11b-f show the binary images obtained using the above thresholding method, they correspond to the voids, wood clear of polymer, wood/PVC interphase, PVC, and high density particles respectively. By counting the number of voxels in each binary image, the fraction of each component to the entire volume was calculated and the relative volume fraction was shown in the last column of Table 4.3. From these volume content fractions, the ratio of interphase content to the total wood particle volume is calculated as a ratio of the interphase content divided by the sum of the interphase and "clear" wood in the WPC. This ratio is calculated to be 54%, which agrees very well with the two earlier estimates based the analysis of two-dimensional images (56% calculated from the wood particle cross section epi-fluorescence micrograph, and 51% calculated from the WPC slice color micrographs).

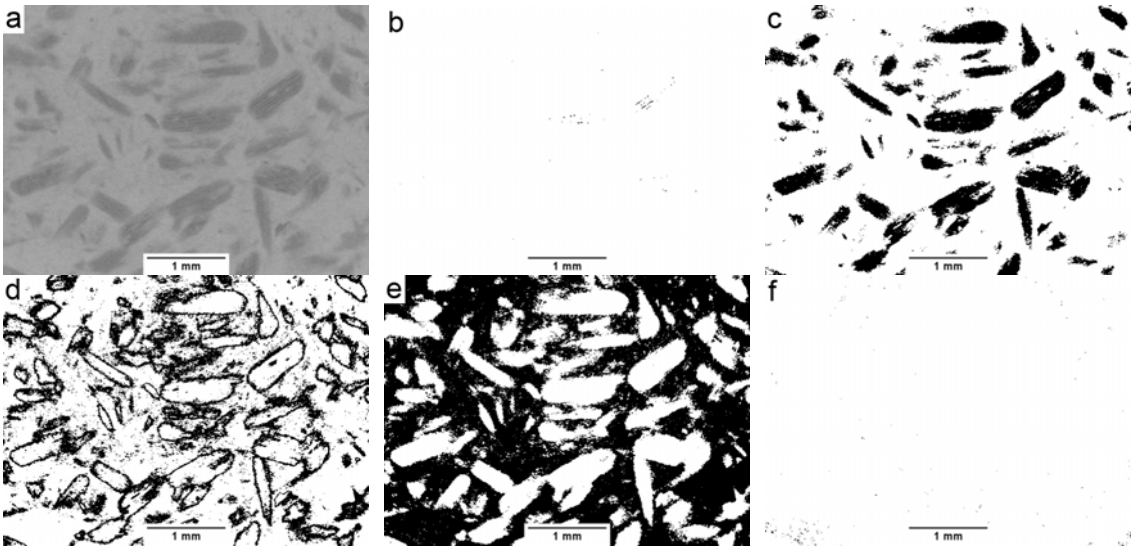

Figure 4.11 Components seperated from X-ray CT scanning images of wood/PVC composite: (a) Reconstructed slice, (b) Voids, (c) Wood, (d) Wood/PVC interphase, (e) PVC matrix, (f) High-density particles.

From Figure 4.11d, we can see that some pixels qualified as interphase are located in the transient area between "clear" wood and polymer matrix, which comprised a significant portion of the total wood particle volume. Some of them however appear to

be dispersed in the matrix. This may result either from thresholding through the ambiguous mixed pixel which belongs to either of the neighboring distributions, or from tracing the content of very fine wood dust trapped in the matrix. Voids and hard particles constitute a minute and dispersed component hardly captured on individual cross sections.

Conclusions

In this study, 2D and 3D imaging tools (optical microscopy, SEM, and X-ray CT scanning) were applied to examine the wood/PVC interface on different scale levels in order to characterize the morphological composition of wood/PVC composite. Following conclusions were drawn from this study:

1. The volume content of wood calculated from X-ray CT scanning was significantly lower than nominal volume fraction calculated from the known weight ratios of the components. The difference is too big to be explained by the partial densification of the particles during the mechanical processing.

2. Examination of 2D micrographs of the composite revealed an extensive interphase zone in the particles, where the wood cell lumens are partially filled with polymer. When the interphase is not accounted for separately in the analysis of CT scans, most of its volume is likely to be interpreted as polymer, which results in serious underestimation of wood content in the composite.

3. The HSB segmentation used in this study allows for effective phase segmentation from the color micrographs of wood/PVC composite sample slices, and provided an approximate quantitative assessment of the relative volumes of the phases ("clear" wood, polymer and the interphase) in the composite.

4. Volumetric data from X-ray CT scanning of wood/PVC composite were effectively separated using an adjusted histogram segmentation method.

5. Volumetric fraction of interphase calculated from HSB segmentation and histogram segmentation of the X-ray CT scanning volumetric data are consistent, and indicated that even without addition of a compatabilizer, the interphase generated in the compounding process may constitute over 50% of the total wood particle volume. Neglecting this fact may lead to significant underestimation of the particle content in the composite.

In summary, on examining images of both wood particles and wood/PVC composites, the existence of the wood/PVC interphase was confirmed. Imaging techniques combined with digital image processing methods are effective tools for quantitative characterization of wood/PVC composite.

CHAPTER 5 -- ASSESSMENT OF ENVIRONMENTAL EXPOSURE EFFECTS ON WOOD PLASTIC COMPOSITE USING X-RAY CT IMAGING

Yi Wang and Lech Muszyński

To be submitted for publication in *Holzforschung*

Assessment of Environmental Exposure Effects on Wood Plastic Composite Using X-ray CT Imaging

Yi Wang and Lech Muszyński*

Department of Wood Science & Engineering

Oregon State University

Corvallis, OR 97331

* Corresponding author

119 Richardson Hall, Oregon State University, Corvallis, OR 97331-5751

Email: Lech.Muszynski@oregonstate.edu

Abstract

Long-term performance of wood plastic composites (WPCs) is one of the most important considerations in new product development. Various destructive methods have been applied to characterize the material structural changes resulting from environmental exposures. However, there is only limited understanding of how the material structure is affected in situ. Further improvement of WPCs durability requires a better understanding of their morphological changes during exposure on the micro level.

In this research, X-ray CT scanning technique was applied to examine the morphological changes in WPCs resulting from accelerated weathering and cyclic loading. Wood/PVC composite specimens were exposed to accelerated weathering (soak-dry and freeze-thaw cycles) and cyclic tensile loading to induce degradation in the material. No significant decrease in elastic modulus was observed at the beginning and end of the cyclic tensile loading, when the deformation was calculated as an average of the strain field measured on the specimen surfaces. For the soak-dry and freeze-thaw treated specimens, significant initial tensile modulus loss was observed over the accelerated. More loss was detected for the first seven cycles than for the last seven cycles. Specimens after accelerated weathering and cyclic tensile loading showed significantly lower residual strength compared with the reference specimens; this indicated damage was accumulated in the specimens after accelerated weathering and cyclic loading.

Introduction

Wood plastic composite (WPC) is the common name for a group of composite comprised of wood flour, thermoplastic polymers, and small amounts of additives. At first wood particles were used as an inexpensive filler for plastics. When the effect of the wood content on stiffness became clearer, attempts were made to use WPCs as a direct lumber substitute. Although WPCs could not compare with solid wood in terms of mechanical properties, their perception as durable and maintenance free products

gained them acceptance in some segments of the market previously dominated by treated wood. Today, most WPC products are being used in exterior applications where water resistance is paramount (Wolcott 2003).

As products and market develop, WPCs are expanding from decking and railing system to fenestration applications and exterior covering applications. For new product designs, long-term performance is one of the most important considerations, especially for structural applications (Smith and Wolcott 2006). In a survey conducted on the WPCs application in the U.S. recreational bridge market, it was found that durability is the most important attribute for recreational bridge decking material, and plays the most important role in new product adoption (McGraw and Smith 2007).

Generally, in-service conditions can expose WPCs to various degrading factors. In the past decade, extensive investigations have been done to examine how WPCs were affected by moisture (Balatinecz and Park 1997; Clemons and Ibach 2004; Lin et al. 2002; Stark 2001; Tajvidi and Ebrahimi 2003), temperature change (Karbhari et al. 2002; Pilarski and Matuana 2005, 2006), ultraviolet (UV) radiation (Matuana and Kamdem 2002; Matuana et al. 2001; Selden et al. 2004; Stark and Matuana 2003; Stark et al. 2004), atmospheric gases (oxygen and pollutants), mechanical and biological degrading agents, such as fungi, bacteria and termites, and so on (Mankowski and Morrell 2000; Pendleton et al. 2002). The effects of natural exposures on WPCs were also examined in other investigations (Oberdorfer and Golser 2005; Schauwecker et al. 2006).

Degradation occurred during exposures can be detected from specimen mechanical property loss (e.g. loses in strength or stiffness), physical property change (density and color change) or visual inspection of the changes in surface morphology. Different methods have been utilized to characterize the structural changes in WPC resulting from weathering exposures. Chemical characterization methods, including contact angle measurement (Matuana and Kamdem 2002), spectroscopic techniques (Fabiyi et al. 2005), thermal analysis (Selden et al. 2004) were mostly used to examine the

chemical composition changes of the weathered specimens. Microscopic techniques, such as scanning electron microscopy (SEM) (Stark et al. 2004), optical microscopy (Lundin et al. 2001) were used as qualitative tools to study the morphological changes from the images of the weathered or fractured specimen surfaces. Porosity of the weathered WPCs were measured by probing the pores with mercury (Pilarski and Matuana 2006). All these methods provided valuable information on the material structural changes during the weathering process. However, this knowledge cannot substitute for a direct, in situ understanding of how wood particles interact with a solid polymer matrix and how the environmental exposure affects the interaction.

On the micro-mechanical level, the spatial distributions of components, particle alignments, and void spaces are affected by various processing and in-use service regimes. Severe weathering cycles, surface wear and/or mechanical loading can result in a variety of damage mechanisms ranging from distributed micro-cracking to localized crack bands and macro-cracks either within the polymer matrix or the wood particle; or as failure at the wood/polymer interface (Landis et al. 2004). As these internal fractures accumulate with time they mechanically weaken the internal structure and breach the protective layers of polymer, which exposes the wood particles to further degradation.

As a nondestructive evaluation method, X-ray computed tomography (CT) technique provides a great opportunity for a nondestructive in situ analysis of particulate composites structures. X-ray CT scanners are capable of returning digital images carrying spatial information coded in millions discrete grayscale values (voxels) arranged in arrays, which represent local densities and X-ray attenuations (Park et al. 2003; Pétraud et al. 2003). X-ray scanning techniques have been used in diagnostic medicine for about 40 years with a typical resolution around 300 μm. With the development of the high-resolution radiation facilities and high computation capacities, X-ray microtomography technique has been applied extensively in material science and civil engineering research. The combination of high-resolution

nondestructive imaging techniques like X-ray micro-tomography (XMT) with machine vision tools provides the means for a quantitative morphological characterization of heterogeneous composites as well as an assessment of the deformation and damage resulting from climate exposure and mechanical loading. In fact, machine vision-based methods have been used for imaging and microscopic nondestructive characterization of 3D samples of certain particulate composites and fibrous materials (Bertilsson et al. 1992; Kamke and Lee 2007; Landis et al. 2004; Peix et al. 1997; Wang and Muszynski 2007; Wang et al. 2007; Yang and Lindquist 2000).

The objective of this study was to investigate effective methods for quantitative characterization of the morphological changes in WPCs resulting from accelerated weathering and cyclic mechanical loading, and to correlate the structural changes to the mechanical property loss resulting from these degradation treatments. Further objective was to investigate the potential correlations between the amount of damage introduced by accelerated weathering exposure to that from cyclic loading.

Materials and Methods

Materials

Currently about 84% of commercial WPC products use HDPE matrices while PVC and PP share about 9% and 7% respectively of the total WPC market (Morton et al. 2003). However, our previous study demonstrated that there is very poor contrast between wood and HDPE (or PP) in the X-ray CT scanning. Much better contrast can be obtained from wood/PVC composite (Wang et al. 2007). In this study, PVC was selected as the polymer component to make WPC.

The wood flour was a commercial pine flour mixture, 40 mesh, donated by American Wood Fibers (Schofield, WI). Prior to use, the wood flour was dried at 103 °C for 24 h and then screened through 50 mesh sieve to remove fines. The remaining phase was designated 40-50 mesh wood flour and was collected for use. The polymer was Polyvinyl Chloride (PVC, density 1400 kg/m^3, inherent viscosity 0.74), purchased

from Scientific Polymer based in Ontario, NY. The wood-PVC composite specimens for this study were manufactured in the laboratory using a wood/PVC weight ratio of 40/60.

Specimen Preparation

The wood/PVC composite specimens were fabricated in the laboratory using a wood/PVC weight ratio of 40/60. The wood flour and PVC were mixed at ambient temperature in batches of 46 g. The mixture was compounded in a Brabender IntelliTorque mixer with bowl mixer and rotor blades attached (C.W. Brabender Instruments, Inc., S. Hackensack, NJ). The mixer was preheated to 170 ºC before processing. The speed of the rotors in the bowl was 30 rpm. The mixture was blended for 5 min until a constant torque was reached and the blending continued for 5 min. The contents were then removed and stored for subsequent compression molding.

A steel mold with the dimensions of 101.6 × 101.6 × 2.5 mm^3 was used to compress the mixture into boards in a hot press preheated to 180 °C. The initial pressure was 0.04 MPa and then raised to 0.6 MPa over 2 min and held for an additional 10 min. After that, the mold was gradually cooled under pressure in ambient conditions for 24 h (The sample fabrication procedure is described in detail in the Appendix A.).

To introduce significant weathering degradation effect to the specimens in possibly short time and to gain the best X-ray CT scanning resolution, small size specimens were examined in this research. After being removed from the mold, the WPC panels were cut and machined into dog-bone shaped specimens (narrow cross section area of 8.0 mm × 2.5 mm) Specimens were divided into three groups for soak-dry cycling (S group), freeze-thaw cycling (F group), and cyclic mechanical loading (C), with six specimens in each group. To efficiently exposure wood particles to the environments, the soak-dry and freeze-thaw weathering specimens were sanded using #120 sanding paper to remove the thin layer of polymer on specimen surface.

Accelerated Weathering

Two accelerated weathering procedures were used to simulate damages caused by long-term natural exposure: soak-dry cycling and freeze-thaw cycling. The cycling procedures were developed in our preliminary study for capacity of inflicting significant degradation in relatively short time. The weathering procedures (soak-dry and freeze-thaw cycling) are shown in Figure 5.1 and Figure 5.2 respectively.

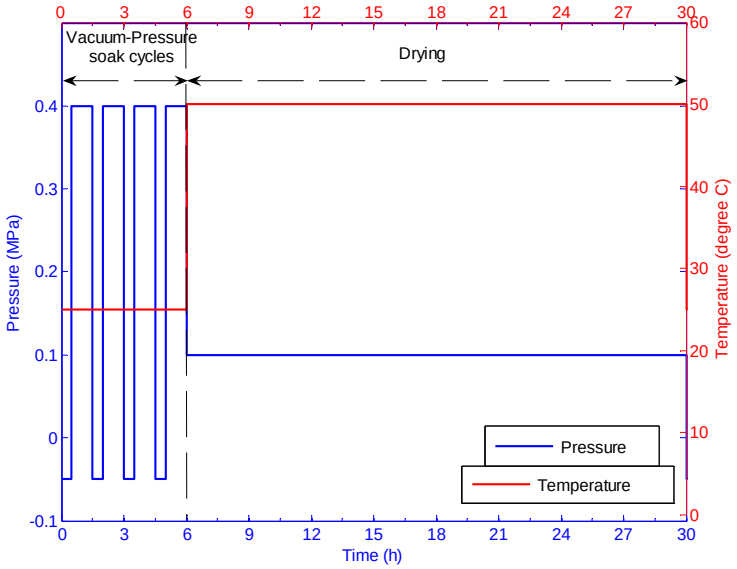

Figure 5.1 One full cycle of the cyclic soak-dry weathering.

Before soak-dry and freeze-thaw weathering, composite samples were soaked in water for eight vacuum-pressure soaking cycles with pressure of -0.05 MPa (for 30 min) and 0.4 MPa (for 60 min) alternatively.

The soak-dry cycling procedure consisted of the following steps: (1) Four vacuum-pressure soaking cycles with pressure of -0.05 MPa (for 30 min) and 0.4 MPa (for 60 min) alternatively; (2) Oven dry under 50 °C for 24 h. Steps (1) and (2) compose one full soak-dry cycle, as shown in Figure 5.1.

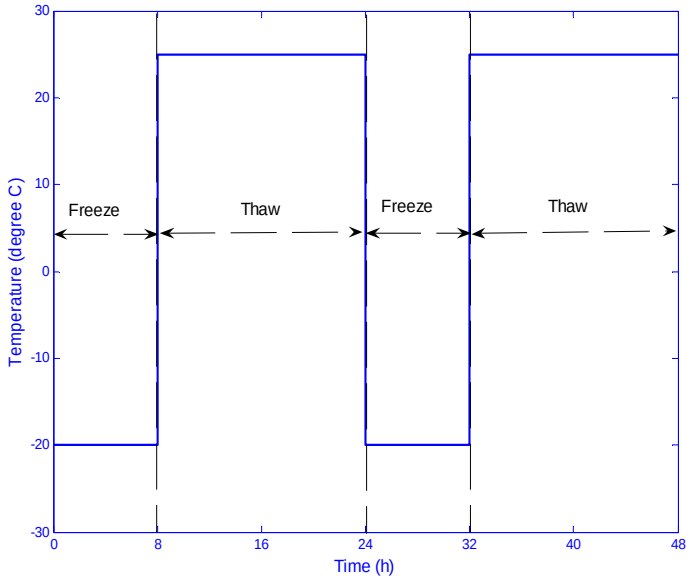

Figure 5.2 Two full cycles of the cyclic freeze-thaw weathering.

The freeze-thaw cycling procedure consisted the following steps: (1) Freeze under -20 °C for 8 h; (2) Thaw under ambient lab temperatures (25 ± 0.5 °C) for 16 h. Steps (1) and (2) compose one freeze-thaw cycle (Figure 5.2 shows two full freeze-thaw cycles).

Cyclic Mechanical Loading

In order to investigate potential correlations between the damage introduced by cyclic loading and the damage generated by accelerated weathering exposure, the third group of specimens (C group) was subjected to cycles of incremental tensile loading. The cyclic loading was performed in the displacement control mode at a constant rate of 0.5 mm min^{-1}. The specimens were pre-stressed to 0.5 MPa before the cyclic loading began. In the first four cycles the stress was cycled between 0.5 MPa and 5.0 MPa. Beginning with the fifth cycle, the peak stress was increased by 3 MPa for each consecutive cycle with the minimum stress kept at 0.5 MPa. Nominal average tensile stress values were calculated from the real time load cell force readings and the initial individual cross section measurements for each specimen. The cyclic loading diagram was shown in Figure 5.3. The mechanical tests were done on Instron 5582 universal testing machine.

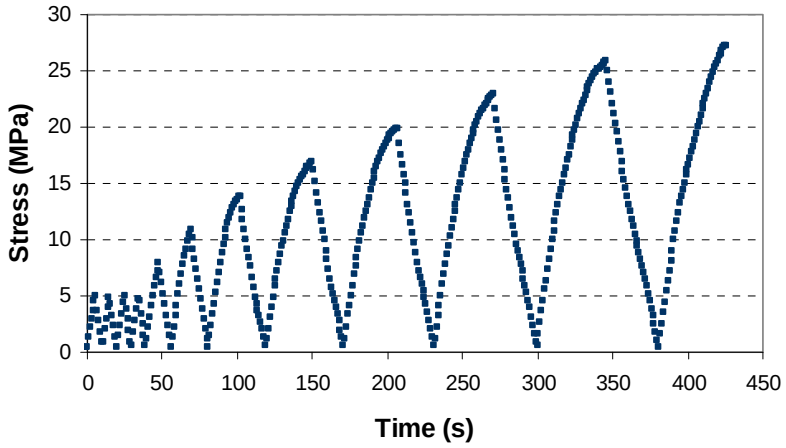

Figure 5.3 Cyclic loading diagram.

Deformations and strains on specimen surface were measured with optical equipment based on the digital image correlation method (Vic-3D by Correlated Solutions, Inc., West Columbia, SC). The system included two horizontally configured digital cameras, an image acquisition unit, and VIC-3D analytical software. During the tests, sequential images were recorded every 0.5 s until failure. Then the displacement and strain fields for areas of interest on the specimen surfaces were calculated by comparing the images of deformed specimens with the reference undeformed images. In order to enhance the analysis, a random black and white speckle pattern was applied on the specimen surfaces before testing using a black and white paint spray. Since in this study only the total deformations were of interest, uniform strain and stress distributions were assumed and the average strain values from the full-field strain distributions were used for further analysis.

Elastic modulus is one of the most important material mechanical properties. Since WPCs are viscoelastic materials, which show nonlinear mechanical behavior, in this study, tangent modulus and secant modulus were calculated to evaluate the mechanical properties of WPC specimens for each full loading cycle. Three types of modulus were of interest: secant modulus (Es) of each cycle, tangent modulus at the start point of each cycle (Etstart), and tangent modulus at the peak point of each cycle (Etend). The tangent moduli (Etstart and Etend) were calculated from the slope of the

line tangent to the stress-strain curve at the start and peak point of each cycle, and the secant modulus (Es) were calculated from the slope of the line drawn connecting the start and the end point of each cycle, as shown in Figure 5.4. Results from preliminary study showed that virgin wood/PVC composite specimens (without exposures) generally failed in between the 10^{th} and the 12^{th} cycles, so the cyclic loading was stopped before the 10^{th} peak, and the specimens were removed for X-ray CT scanning.

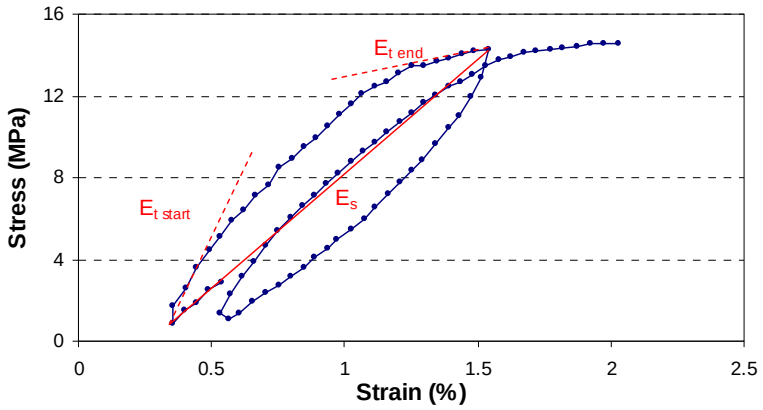

Figure 5.4 Calculation of tangent and secant modulus in cyclic tensile loading.

Measurement of Mechanical Degradation

As the result of accelerated weathering and cyclic loading, material degradation damage can be detected as bulk mechanical property losses. In this study, to quantify the effect of degrading treatments, initial tensile modulus of specimens were measured via low level tensile tests (max load up to approximately 100 N), in such a way that the loading is in the elastic range and no damage is introduced to the specimens. The tensile tests were performed in the displacement control mode at a constant rate of 0.5 mm min^{-1}. An Instron 5582 universal testing machine was applied to do tensile tests. The deformations and strains were measured using digital image correlation method. The modulus measurement of S and F groups was performed on three stages: before weathering, after first seven cyclic weathering, and after 14 cyclic weathering.

To better understand the degradation effect of the accelerated weathering and cyclic tensile loading on the material strength, the residual strength after these treatments were measured from monotonic tensile test. The monotonic tensile tests were performed in the displacement control mode at a constant rate of 0.5 mm min^{-1}.

X-ray CT Scanning

The degradation effects of accelerated weathering and cyclic loading on wood/PVC composite samples were assessed from 3D scans of the specimens from the Fein Focus FXE-160.20 custom X-ray system in the Department of Mechanical Engineering at OSU. The system includes a micro focus X-ray source, rotational sample stage, and a detector connected to a digital camera. The 3D reconstructions of the specimen cross sections were calculated from projection images taken at 1600 angular positions. The resulting resolution was 12 μm, the output data composed of reconstructed images was arranged as slice sequence of 8-bit grayscale images.

The void content ratio was evaluated by thresholding out the lowest density distribution from the volumetric data. The threshold level was determined from the volume grayscale histogram following the procedure described in the previous chapter (Wang and Muszynski 2007).

Results and Discussion

Cyclic Tensile Loading

The secant and tangent modulus of specimens subjected to cyclic loading (C group) in each of the nine cycles are shown in Figure 5.5. The moduli were calculated from the mean strain value for the entire area of interest on specimen surface, ignoring local strain concentration. The statistical analysis comparing the modulus in the fourth and ninth cycle is shown in Table 5.1. The statistical significance level is 0.05.

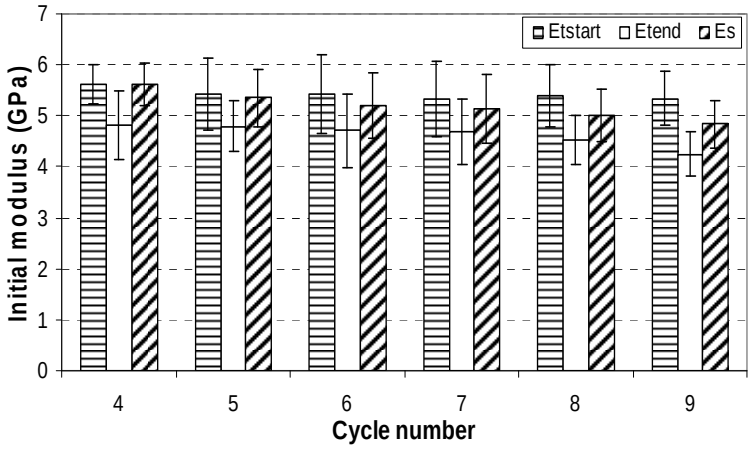

Figure 5.5 Secant and tangent modulus of reference group in each cycle of loading.

Table 5.1 Statistical comparison between modulus in the fourth and the ninth cycle of loading.

	Two-sided p-value	Significantly different?	Difference (GPa)
E_{tstart}	0.44	No	0.27
E_{tend}	0.09	No	0.56
E_s	0.03	Yes	0.78

For the secant and tangent modulus in all cycles, a weak decreasing trend could be observed as the cycle number increased. However, only the loss of the secant modulus appeared statistically significant. Even in this case, the p-value is relatively high, which indicated the relatively low significance. Therefore, there is no significant decrease of the tangent and secant modulus from the fourth peak to ninth peak. However, if we examine the full field strain distribution on specimen surface at the peaks of each cycle (Figure 5.6), we can find strain concentration in some local regions (the yellow to orange areas). These areas are the possible places of micro-damage accumulation and become the weak regions of the specimen, where cracks initiate.

Modulus Loss in Accelerated Weathering

In Figure 5.7, the initial tensile modulus (E) of S and F groups measured at the three weathering stages are compared. The results of statistical analysis at 5% significance level are shown in Table 5.2. The subscript S and F represent soak-dry, freeze- thaw

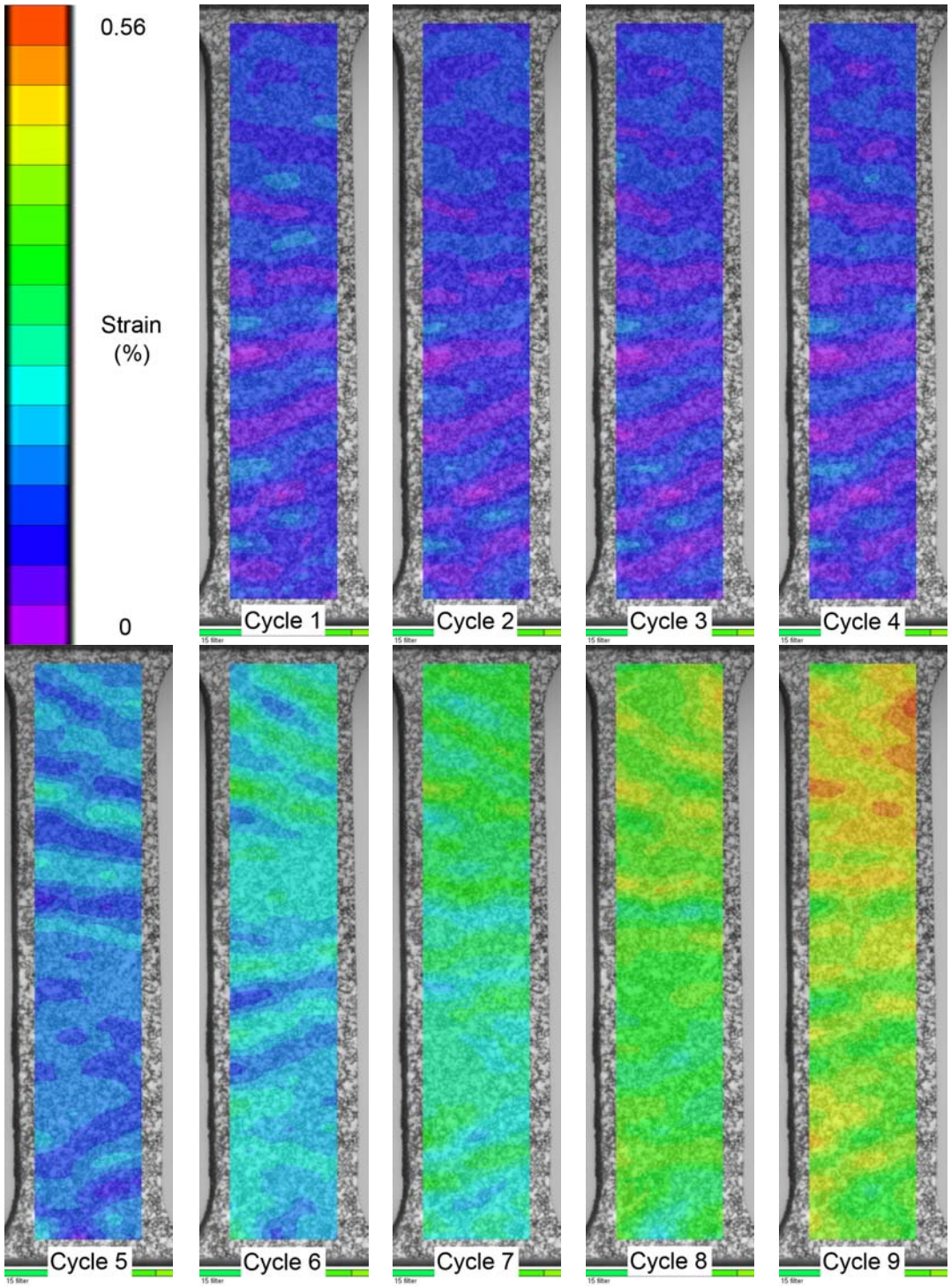

Figure 5.6 Surface strain distribution map at the peak of each cycle.

groups respectively, the subscript B, M, and E represent before weathering, after 7 cycles of weathering, and after 14 cycles of weathering respectively. For example, the symbol E_{SB} and E_{FM} represent the initial modulus of the soak-dry group before weathering and freeze-thaw group in the middle of weathering.

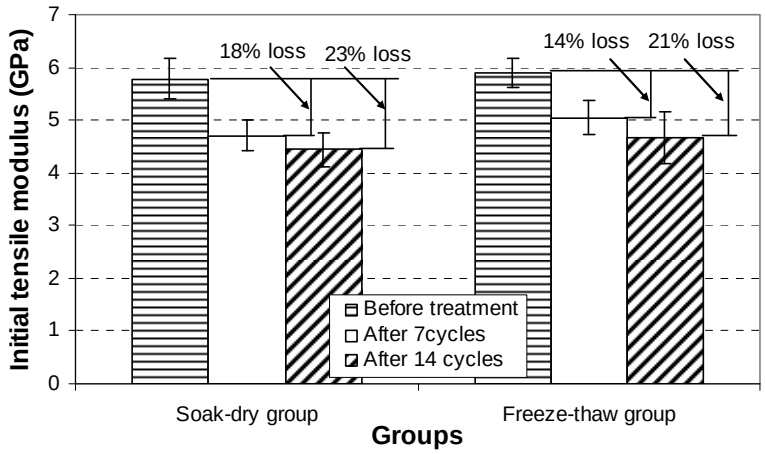

Figure 5.7 Initial tensile modulus at different weathering stages.

Table 5.2 Statistical analysis of the initial tensile modulus at different weathering stages.

	Two-sided p-value	Significantly different?	Difference (GPa)
Soak-dry weathering			
E_{SB} vs. E_{SM}	<0.01	Yes	1.08
E_{SM} vs. E_{SE}	0.17	No	0.26
Freeze-thaw weathering			
E_{FB} vs. E_{FM}	<0.01	Yes	0.89
E_{FM} vs. E_{FE}	0.16	No	0.37

Note: The subscript S and F represent soak-dry, freeze-thaw groups respectively, B, M, E represent before weathering, in the middle of soak-dry and freeze-thaw cycles, and the end of the weathering respectively.

Both soak-dry and freeze-thaw groups showed similar amount of initial modulus loss over the weathering. In the first seven cycles of weathering, S and F group observed significant decrease in modulus (18 % and 14 % respectively), however, the following seven cycles of the weathering resulted in 5% and 7% decrease of the modulus respectively.

Residual Strength after Accelerated Weathering and Cyclic Loading

The measured residual strength of the specimens are shown in Figure 5.8 and the statistical analysis results at 5% significance level were shown in Table 5.3.

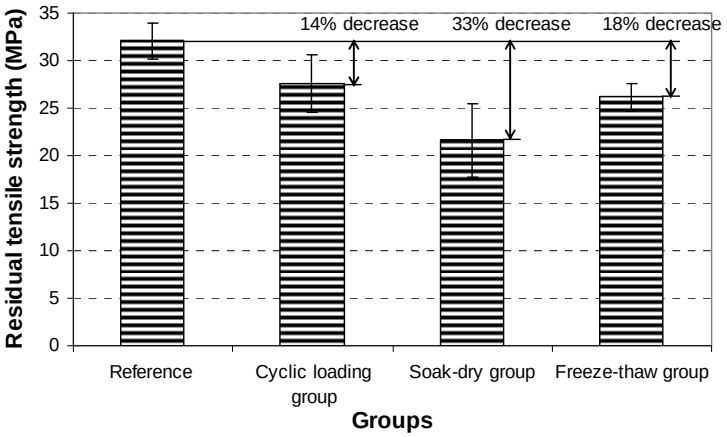

Figure 5.8 Residual strength after accelerated weathering and cyclic loading.

Table 5.3 Statistical analysis of the measured residual strength.

	Two-sided p-value	Significantly different?	Difference (GPa)
R vs. C	<0.01	Yes	4.47
R vs. S	<0.01	Yes	10.44
R vs. F	<0.01	Yes	5.89

Note: R represents reference group, C represents cyclic loading group, S represents soak-dry group, and F represents freeze-thaw group.

The groups subjected to cyclic loading and weathering exposure showed significantly lower strength compared to the reference group, which gave further proof of the mechanical property loss after these treatments.

Preliminary Conclusions

In this study, wood/PVC composites were treated with accelerated soak-dry and freeze-thaw exposure, and cyclic tensile loading. X-ray CT scanning was applied to examine the internal structure changes during the treatment. The following preliminary conclusions were drawn from this study:

1. No significant decrease in elastic modulus (tangent modulus and secant modulus, based on average strain) was observed at the beginning and end of the cyclic tensile loading.

2. Similar amount of initial tensile modulus loss was observed for the soak-dry and freeze-thaw treated groups over the accelerated weathering. More loss was detected for the first seven cycles than the last seven cycles.

3. Specimens after accelerated weathering and cyclic tensile loading showed significantly lower residual strength compared with the reference specimens, which indicated damage has been accumulated in the specimens after accelerated weathering and cyclic loading.

Work in Progress

To-date, all specimens were scanned before and after the accelerated weathering and cyclic loading. However, the reconstruction of the volumetric data from the scans has not been completed yet. The completion of the reconstruction of all samples is scheduled for late September 2007, therefore, further analysis falls out of the time frame of this thesis. Once the reconstruction is complete, the reconstructed 3D images will be analyzed using the grayscale histogram segmentation method (described in Chapter 5 in this thesis) to determine the voids content in the specimens at different treatment stages. The void content will be analyzed statistically and correlated to the mechanical property loss. Further results will be presented in the manuscript for publication.

CHAPTER 6 – GENERAL CONCLUSIONS

In this research, advanced imaging tools, including X-ray CT scanning, optical and electron microscopy were applied to obtain comprehensive morphological characteristics and evaluation of micro-damage accumulations in wood plastic composites (WPCs) subjected to accelerated environmental exposure and mechanical loading. The following is a summary of the conclusions drawn from this research:

1. Literature review:

    1.1. Extensive research has been conducted to examine the effects of bio-fiber sizes on the properties of the resulting reinforced plastic composites, and it is generally accepted that wood particle with larger aspect ratio can provide better mechanical properties. However, the exact mechanisms behind the effects of the bio-particle geometry on the composite micro-mechanics remain unclear.

    1.2. In most studies, the wood/polymer interaction was discussed from the chemical point of view (the chemistry of bonding in the imaginary wood/polymer interface). Although mechanical interlocking is commonly considered a major mechanism in adhesion, no known studies have addressed its role in WPCs (Wolcott 2003)

    1.3. Although many interesting techniques have been successfully applied for characterization of the wood/polymer bond area, none offered the capacity of nondestructive in situ evaluation comparable to X-ray CT techniques. However, the full potential of this XCT has not been fully utilized in the area of morphological characterization of WPCs.

2. On examining the effects of adding surfactant and gold particles of two different sizes on the tensile properties of wood/HDPE composites and X-ray CT scanning contrast, the following conclusions were drawn:

2.1. The addition of small amounts (1% weight) of technically pure gold particles to WPC formulations in order to improve the X-ray CT scanning contrast between components does not affect the mechanical properties of the composite. The gold particle size did not affect any of the tensile properties of the resulting WPC composites.

2.2. The addition of surfactant (tetra-n-octyl ammonium bromide), which may be used in laboratory procedures to obtain gold nano-particles or to disperse gold particles in the polymer matrix, significantly impaired some of the tensile properties of the composite. Further experiments are needed to explore how the surfactant affects the stiffness of WPCs.

2.3. Neither gold micro- nor nano-particles could be dispersed well in the HDPE matrix. A substantial amount of the particles formed agglomerates large enough to be visible as a separate component in the X-ray CT scanning images. However, sufficient amount of gold micro-particles were dispersed well enough in the polymer matrix to provide good contrast between the wood particles and the polymer matrix. Gold nano-particles could not be dispersed well in the polymer matrix (with or without surfactant) and poor contrast between wood and polymer matrix was obtained.

In summary, technically pure gold micro-particles were found to be an effective contrast agent for X-ray CT scanning of WPCs, they did not impair the tensile properties of the composites.

3. 2D and 3D imaging tools (optical microscopy, SEM, and X-ray CT scanning) were applied to examine the wood/PVC interface on different scales levels in order to characterize the morphological composition of wood/PVC composite. Following conclusions were drawn:

3.1. The volume content of wood calculated from X-ray CT scanning was significantly lower than nominal volume fraction calculated from the known

weight ratios of the components. The difference is too big to be explained by the partial densification of the particles during the mechanical processing.

3.2. Examination of 2D micrographs of the composite revealed an extensive interphase zone in the particles, where the wood cell lumens are partially filled with polymer. When the interphase is not accounted for separately in the analysis of CT scans, most of its volume is likely to be interpreted as polymer, which results in serious underestimation of wood content in the composite.

3.3. The HSB segmentation used in this study allows for effective phase segmentation from the color micrographs of wood/PVC composite sample slices, and provided an approximate quantitative assessment of the relative volumes of the phases ("clear" wood, polymer and the interphase) in the composite.

3.4. Volumetric data from X-ray CT scanning of wood/PVC composite were effectively separated using an adjusted histogram segmentation method.

3.5. Volumetric fraction of interphase calculated from HSB segmentation and histogram segmentation method are consistent, and indicated that even without addition of a compatibilizer, the interphase generated in the compounding process may constitute over 50% of the total wood particle volume.

In summary, on examining images of both wood particles and wood/PVC composites, the existence of the wood/PVC interphase was confirmed. Imaging techniques combined with digital image processing methods are effective tools for quantitative characterization of wood/PVC composite.

4. Wood/PVC composites were treated with accelerated soak-dry and freeze-thaw exposure, and cyclic tensile loading, X-ray CT scanning was applied to examine

the internal structure changes during the treatment, following preliminary conclusions were drawn:

4.1. No significant decrease in elastic modulus (tangent modulus and secant modulus, based on average strain) was observed between the beginning and end of the cyclic tensile loading.

4.2. Similar amount of initial tensile modulus loss was observed for the soak-dry and freeze-thaw treated groups over the accelerated weathering. More modulus loss was detected for the first seven cycles than the last seven cycles.

4.3. Specimens after accelerated weathering and cyclic tensile loading showed significantly lower residual strength compared with the reference specimens, which indicated damage has been accumulated in the specimens after accelerated weathering and cyclic loading.

In summary, X-ray CT scanning is a promising and effective nondestructive technique for three dimensional in situ examination and morphological characterization of WPCs and other heterogeneous bio-based composites of similar composition. The experimental methodologies employing various imaging tools (including X-ray CT scanning and 2D microscopy) and digital image processing methods are capable of characterizing WPCs, its component phases and the interphase returning statistically meaningful quantitative data.

BIBLIOGRAPHY

ASTM standard (2004) D 638-03, Standard test method for tensile properties of plastics.

ASTM standard (2005) E 2126-05, Standard test methods for cyclic (reversed) load test for shear resistance of walls for buildings.

Balatinecz, J. J., Park, B.-D. (1997) Effects of temperature and moisture exposure on the properties of wood-fiber thermoplastic composites. J. Thermoplast. Compos. Mater. 10:476-487.

Bayraktar, E., Antolonovich, S., Bathias, C. (2006) Multiscale study of fatigue behaviour of composite materials by X-rays computed tomography. Int. J. Fatigue 28:1322-1333.

Berger, M. J., Stark, N. M. (1997) Investigations of species effects in an injection-molding-grade, wood-filled polypropylene. In: Proceedings of the fourth international conference on woodfiber-plastic composites, Madison, WI. pp. 19-25.

Bertilsson, H., Franzén, B., Klason, C., Kubát, J., Kitano, T. (1992) The influence of processing on fiber orientation and creep in short carbon-fiber reinforced low density polyethylene and polycarbonate. Polym. Compos. 13:121-132.

Bledzki, A. K., Reihmane, S., Gassan, J. (1998) Thermoplastics reinforced with wood fillers: A literature review. Polym. Plast. Technol. Eng. 37:451-468.

Brust, M. (1994) Synthesis of thiol-derivatised gold nanoparticles in a two-phase liquid-liquid system. J. Chem. Soc., Chem. Commun. 7:801-802.

Carmeliet, J., Delerue, J. F., Vandersteen, K., Roels, S. (2004) Three-dimensional liquid transport in concrete cracks. Int. J. Numer. Anal. Met. 28:671-687.

Chapman, H. N., Williams, S., Jacobsen, C. (1994) Imaging of 30 nm gold spheres by dark-field scanning transmission X-ray microscopy. In: Proceedings of the 52nd Annual Meeting of the Microscopy Society of America, New Orleans, LA, USA. pp. 52-53.

Clemons, C. (2002) Wood-plastic composites in the United States: The interfacing of two industries. Forest. Prod. J. 52:10-18.

Clemons, C. M., Ibach, R. E. (2004) Effects of processing method and moisture history on laboratory fungal resistance of wood-HDPE composites. Forest. Prod. J. 54:50-57.

Colom, X., Carrasco, F., Pages, P., Canavate, J. (2003) Effects of different treatments on the interface of HDPE/lignocellulosic fiber composites. Compos. Sci. Technol. 63:161-169.

Craven, J. P., Cripps, R., Viney, C. (2000) Evaluating the silk/epoxy interface by means of the microbond test. Composites Part A 31:653-660.

Dagher, H. J. (2005) Structural applications of wood-plastic composites: Code challenges and opportunities. In: Proceedings of the 3rd International Conference on Advanced Engineered Wood Composites, Bar Harbor, ME, USA.

DeRosa, A. (2004) Trex agrees to settle class-action lawsuit. Plastics News 16:1-40.

Egan, A., Shaler, S. M. (2000) Fracture and mechanics of fracture for resin coated single wood fibres. In: Proceedings of the Fourth Panel Products Symposium, Llandudno, Wales, UK. pp. 95-103.

Eichhorn, S. J., Young, R. J. (2003) Deformation micromechanics of natural cellulose fibre networks and composites. Compos. Sci. Technol. 63:1225-1230.

Eichhorn, S. J., Young, R. J. (2004) Composite micromechanics of hemp fibres and epoxy resin microdroplets. Compos. Sci. Technol. 64:767-772.

Fabiyi, J. S., McDonald, A. G., Wolcott, M. P. (2005) Chemical changes that occur during weathering of wood-plastic composites. In: Proceedings of the eighth international conference on woodfiber-plastic composites, Madison, WI. pp. 191-196.

Gardner, D. J., Son, J., O'Neill, S., Tze, W. T., Tim, G. R. (2004) Study of the crystallization behavior and material properties of extruded polyolefin wood-plastic composite lumber as a function of post die process conditions. In: Proceedings of the Progress in Woodfibre-Plastic Composites, Toronto, Canada. 15 pp.

Geng, Y., Li, K., Simonsen, J. (2004) Effects of a new compatibilizer system on the flexural properties of wood-polyethylene composites. J. Appl. Polym. Sci. 91:3667-3672.

Geng, Y., Simonsen, J., Muszynski, L. (2005) Unpublished data.

Gonzalez, R. C., Woods, R. E. 2001. Digital image processing. Prentice Hall, Upper Saddle River, NJ.

Grieken, P. E. V., Markowicz, A. A. 1993. Handbook of X-ray spectrometry: Methods and techniques. Marcel Dekker Inc., New York.

Grigsby, W., Thumm, A., Klepser, H. (2005) Assessing interfacial behaviors of natural fiber-plastic composites by fluorescent microscopy. In: Proceedings of the eighth international conference on woodfiber-plastic composites, Madison, WI. pp. 145-151.

Hernandez, M., Ichazo, M., Gonzalez, J., Albano, C. (2004) Influence of type of filler on natural rubber properties. In: Proceedings of the Annual Technical Conference - ANTEC, Chicago, IL. pp. 2738-2742.

Hristov, V., Vasileva, S. (2003) Dynamic mechanical and thermal properties of modified poly(propylene) wood fiber composites. Macromol. Mater. Eng. 288:798-806.

Hubbell, J. H., Seltzer, S. M. (1996) Tables of X-ray mass attenuation coefficients and mass energy-absorption coefficients from 1 keV to 20 MeV for elements Z = 1 to 92 and 48 additional substances of dosimetric interest. Ionizing Radiation Division, Physics Laboratory National Institute of Standards and Technology Gaithersburg, MD 20899. Available: http://physics.nist.gov/PhysRefData/XrayMassCoef/cover.html. Last Access: 12/14/2006.

Ichazo, M. N., Hernandez, M., Albano, C., Gonzalez, J. (2006) Curing and physical properties of natural rubber/wood flour composites. Macromol. Symp. 239:192-200.

Ismail, H., Rozman, H. D., Jaffri, R. M., Mohd Ishak, Z. A. (1997) Oil palm wood flour reinforced epoxidized natural rubber composites: The effect of filler content and size. Eur. Polym. J. 33:1627-1632.

Jacob, M., Joseph, S., Pothan, L. A., Thomas, S. (2005) A study of advances in characterization of interfaces and fiber surfaces in lignocellulosic fiber-reinforced composites. Compos. Interfaces 12:95-124.

Jacob, M., Thomas, S., Varughese, K. T. (2004) Mechanical properties of sisal/oil palm hybrid fiber reinforced natural rubber composites. Compos. Sci. Technol. 64:955-965.

Jain, A. K., Dubuisson, M.-P. (1992) Segmentation of X-ray and C-scan images of fiber reinforced composite materials. Pattern Recognition 25:257-270.

Jiang, H., Kamdem, D. P. (2004) Development of poly(vinyl chloride)/wood composites. A literature review. J. Vinyl Addit. Technol. 10:59-69.

Johnson, D. A., Johnson, D. A., Urich, J. L., Rowell, R. M., Jacobson, R., Caufield, D. F. (1999) Weathering characteristics of fiber-polymer composites. In:

Proceedings of the fifth international conference on woodfiber-plastic composites, Madison, WI. pp. 203-209.

Joseph, K., Varghese, S., Kalaprasad, G., Thomas, S., Prasannakumari, L., Koshy, P., Pavithran, C. (1996) Influence of interfacial adhesion on the mechanical properties and fracture behaviour of short sisal fibre reinforced polymer composites. Eur. Polym. J. 32:1243-1250.

Joseph, S., Sreekala, M. S., Oommen, Z., Koshy, P., Thomas, S. (2002) A comparison of the mechanical properties of phenol formaldehyde composites reinforced with banana fibres and glass fibres. Compos. Sci. Technol. 62:1857-1868.

Kamke, F. A., Lee, J. N. (2007) Adhesive penetration in wood - a review. Wood Fiber Sci. 39:205-220.

Karbhari, V. M., Rivera, J., Zhang, J. (2002) Low-temperature hygrothermal degradation of ambient cured E-glass/vinylester composites. J. Appl. Polym. Sci. 86:2255-2260.

Ketchman, R. A., Carlson, W. D. (2001) Acquisition, optimization and interpretation of X-ray computed tomographic imagery: Applications to the geosciences. Comput. Geosci. 27:381-400.

Kim, H.-S., Yang, H.-S., Kim, H.-J. (2005) Biodegradability and mechanical properties of agro-flour-filled polybutylene succinate biocomposites. J. Appl. Polym. Sci. 97:1513-1521.

Kumar, R. P., Thomas, S. (2001) Interfacial adhesion in sisal fiber/SBR composites: An investigation by the restricted equilibrium swelling technique. J. Adhes. Sci. Technol. 15:633-652.

La Mantia, F. P., Morreale, M. (2006) Mechanical properties of recycled polyethylene ecocomposites filled with natural organic fillers. Polym. Eng. Sci. 46:1131-1139.

Landis, E. N., Shaler, S. M., Muszynski, L., Cheng, Q. (2004) Microtomographic investigations of damage in wood composites. In: Proceedings of the 3rd International Conference of the European Society for Wood Mechanics, Villa Real, Portugal. pp. 151-158.

Lee, S.-Y., Yang, H.-S., Kim, H.-J., Jeong, C.-S., Lim, B.-S., Lee, J.-N. (2004) Creep behavior and manufacturing parameters of wood flour filled polypropylene composites. Compos. Struct. 65:459-469.

Lin, Q., Zhou, X., Dai, G. (2002) Effect of hydrothermal environment on moisture absorption and mechanical properties of wood flour-filled polypropylene composites. J. Appl. Polym. Sci. 85:2824-2832.

London, B., Yancey, R. N., Smith, J. A. (1990) High-resolution X-ray computed tomography of composite materials. Mater. Eval. 48:604-608.

Lundin, T., Falk, R. H., Felton, C. (2001) Accelerated weathering of natural fiber-thermoplastic composites: Effects of ultraviolet exposure on bending strengthand stiffness. In: Proceedings of the 6th International Conference on Woodfiber-Plastic Composites, Madison, WI. pp. 87-93.

Luo, S., Netravali, N. (2001) Characterization of henequen fibers and the henequen fiber/poly (hydroxybutyrate-co-hydroxyvalerate) interface. J. Adhes. Sci. Technol. 15:423-437.

Macedo, A., Vaz, C. M. P., Pereira, J. C. D., Naime, J. M., Cruvinel, P. E., Crestana, S. (2002) Wood density determination by X- and gamma-ray tomography. Holzforschung 56:535-540.

Maiti, S. N., Singh, K. (1986) Influence of wood flour on the mechanical properties of polyethylene. J. Appl. Polym. Sci. 32:4285-4289.

Manchado, M. A. L., Arroyo, M., Biagiotti, J., Kenny, J. M. (2003) Enhancement of mechanical properties and interfacial adhesion of PP/EPDM/flax fiber composites using maleic anhydride as a compatibilizer. J. Appl. Polym. Sci. 90:2170-2178.

Mankowski, M., Morrell, J. J. (2000) Patterns of fungal attack in wood-plastic composites following exposure in a soil block test. Wood Fiber Sci. 32:340-345.

Matuana, L. M., Kamdem, D. P. (2002) Accelerated ultraviolet weathering of PVC/wood-flour composites. Polym. Eng. Sci. 42:1657-1666.

Matuana, L. M., Kamdem, D. P., Zhang, J. (2001) Photoaging and stabilization of rigid PVC/wood-fiber composites. J. Appl. Polym. Sci. 80:1943-1950.

McGraw, D. F., Smith, P. M. (2007) Opportunities for woodfiber-plastic composites in the U.S. Recreational bridge market. Forest. Prod. J. 57:76-83.

Michaeli, W., Münker, M., Krumpholz, T. (2000) Characterisation of the fibre/matrix adhesion with different microscopic analysing methods on natural fibre-reinforced thermosets. Macromol. Mater. Eng. 284-285:25-29.

Morris, P. I., Cooper, P. (1998) Recycled plastic/wood composite lumber attacked by fungi. Forest. Prod. J. 48:86-88.

Morse, D. H., Antolak, A. J., Mills, B. E. (2004) High-resolution radiography for detecting and measuring micron-scale features. In: Proceedings of the 2004 ASME International Mechanical Engineering Congress and Exposition, Anaheim, CA, United States. pp. 89-95.

Morton, J., Quarmley, J., Rossi, L. (2003) Current and emerging applications for natural & wood fiber composites In: Proceedings of the 7th International Conference on Woodfiber-Plastic Composites, Madison, WI. pp. 3-6.

Muszynski, L. (2007) Imaging WPCs: X-ray computed tomography, few other promising techniques and why you should pay attention. In: Proceedings of the Wood Plastics Composites Workshop: WPC's 2007 - The changing technology in WPCs, Seattle, WA. 9 pp.

Myers, G. E., Chahyadi, I. S., Coberly, C. A., Ermer, D. S. (1991) Wood flour/polypropylene composites: Influence of maleated polypropylene and process and composition variables on mechanical properties. Int. J. Polymer. Mater. 15:21 - 44.

Newson, W. R., Maine, F. W. (2004) Advances in new WPC technologies. In: Proceedings of the Progress in Woodfibre-Plastic Composites, Toronto, ON. 17 pp.

Oberdorfer, G., Golser, M. (2005) Analysis of environmental impact on highly filled wood plastic composites by laboratory simulation and full-scale testing. In: Proceedings of the eighth international conference on woodfiber-plastic composites, Madison, WI. pp. 197-205.

Oksman, K., Clemons, C. (1998) Mechanical properties and morphology of impact modified polypropylene-wood flour composites. J. Appl. Polym. Sci. 67:1503-1513.

Park, B.-D., Wi, S. G., Lee, K. H., Singh, A. P., Yoon, T.-H. (2003) Characterization of rice husks using microscopic and micro-analytical techniques for rice husk/thermoplastic composites. In: Proceedings of the 7th International Conference on Woodfiber-Plastic Composites, Madison, WI. pp. 323-331.

Patterson, J. (2001) New opportunities with wood-flour-foamed PVC. J. Vinyl Addit. Technol. 7:138-141.

Peix, G., Cloetens, P., Murielle, P.-S., Buffiere, J.-Y., Baruchel, J., Peyrin, F., Schlenker, M. (1997) Hard X-ray phase tomographic investigation of materials

using fresnel diffraction of synchrotron radiation. In: Proceedings of the SPIE-The International Society for Optical Engineering. pp. 149-157

Pendleton, D. E., Hoffard, T. A., Adcock, T., Woodward, B., Wolcott, M. P. (2002) Durability of an extruded HDPE/wood composite. Forest. Prod. J. 52:21-27.

Pétraud, M., Labbé, N., Lartigue, J.-C., De Jéso, B., Sébe, G. (2003) Nuclear magnetic resonance relaxometry applied to wood fibers. In: Proceedings of the 7th International Conference on Woodfiber-Plastic Composites, Madison, WI. p. 358.

Pilarski, J. M., Matuana, L. M. (2005) Durability of wood flour-plastic composites exposed to accelerated freeze-thaw cycling. Part I. Rigid pvc matrix. J. Vinyl Addit. Technol. 11:1-8.

Pilarski, J. M., Matuana, L. M. (2006) Durability of wood flour-plastic composites exposed to accelerated freeze-thaw cycling. II. High density polyethylene matrix. J. Appl. Polym. Sci. 100:35-39.

Pothan, L. A., Neelakantan, N. R., Rao, B., Thomas, S. (2004) Stress relaxation behavior of banana fiber-reinforced polyester composites. J. Reinf. Plast. Compos. 23:153-165.

Pothan, L. A., Thomas, S. (2003) Polarity parameters and dynamic mechanical behaviour of chemically modified banana fiber reinforced polyester composites. Compos. Sci. Technol. 63:1231-1240.

Rao, D. V., Cesareo, R., Brunetti, A. (1999) Computed tomography with image intensifier: Imaging and characterization of materials. Nucl. Instrum. Methods Phys. Res., Sect. A 437:141-151.

Ray, D., Sarkar, B. K., Rana, A. K. (2002) Fracture behavior of vinylester resin matrix composites reinforced with alkali-treated jute fibers. J. Appl. Polym. Sci. 85:2588-2593.

Redondo, S. U. A., Gonçalves, M. C., Yoshida, I. V. P. (2003) Eucalyptus kraft pulp fibers as an alternative reinforcement of silicone composites. II. Thermal, morphological, and mechanical properties of the composites. J. Appl. Polym. Sci. 89:3739-3746.

Rials, T. G., Wolcott, M. P., Nassar, J. M. (2001) Interfacial contributions in lignocellulosic fiber-reinforced polyurethane composites. J. Appl. Polym. Sci. 80:546-555.

Rossi, L. M. (2005) Wood-plastic composites: Putting innovation on a faster track. In: Proceedings of the eighth international conference on woodfiber-plastic composites, Madison, WI. pp. 3-6.

Rowell, R. M. (2006) Advances and challenges of wood polymer composites. In: Proceedings of the 8th Pacific Rim Bio-based Composites Symposium, Kuala Lumpur, Malaysia. 11 pp.

Salvo, L., Cloetens, P., Maire, E., Zabler, S., Blandin, J. J., Buffiere, J. Y., Ludwig, W., Boller, E., Bellet, D., Josserond, C. (2003) X-ray micro-tomography an attractive characterisation technique in materials science. Nucl. Instrum. Methods Phys. Res., Sect. B 200:273-286.

Schauwecker, C., Morrell, J. J., McDonald, A. G., Fabiyi, J. S. (2006) Degradation of a wood-plastic composite exposed under tropical conditions. Forest. Prod. J. 56:123-129.

Schilling, P. J., Karedla, B. P. R., Tatiparthi, A. K., Verges, M. A., Herrington, P. D. (2005) X-ray computed microtomography of internal damage in fiber reinforced polymer matrix composites. Compos. Sci. Technol. 65:2071-2078.

Selden, R., Nystrom, B., Langstrom, R. (2004) UV aging of poly(propylene)/wood-fiber composites. Polym. Compos. 25:543-553.

Selke, S. E., Wichman, I. (2004) Wood fiber/polyolefin composites. Composites Part A 35:321-326.

Shaler, S. M., Egan, A., Mott, L., Landis, E. (1997) Fracture and micromechanics of resinated fibers. In: Proceedings of the 4th International Conference on Woodfiber-Plastic Composites, Madison, WI. pp. 32-39.

Shaler, S. M., Landis, E., Muszynski, L., Vasic, S., Cheng, Q. (2003) Damage assessment in wood-plastic composites by means of material level microstructural characterization. In: Proceedings of the seventh international conference on woodfiber-plastic composites, Madison, WI. pp. 151-156.

Sherman, L. M. (2004) Wood-filled plastics they need the right additives for strength, good looks and long life. Plast. Technol. 50:52-59.

Simonsen, J., Jacobsen, R., Rowell, R. (1998) Wood-fiber reinforcement of styrene-maleic anhydride copolymers. J. Appl. Polym. Sci. 68:1567-1573.

Smith, P. M., Wolcott, M. P. (2006) Opportunities for wood/natural fiber-plastic composites in residential and industrial applications. Forest. Prod. J. 56:4-11.

Song, I., Little, D., Masad, E., Lytton, R., You, Z., Rowe, G., Roque, R., Kim, R., Huang, S., Dongre, R. (2005) Comprehensive evaluation of damage in asphalt mastics using X-ray CT, continuum mechanics, and micromechanics. In: Proceedings of the Technical Sessions-Asphalt Paving Technology: Association of Asphalt Paving, Long Beach, CA, United States. pp. 885-920.

Stamboulis, A., Baillie, C., Schulz, E. (1999) Interfacial characterisation of flax fibre-thermoplastic polymer composites by the pull-out test. Angew. Makromol. Chem. 272:117-120.

Stark, N. (2001) Influence of moisture absorption on mechanical properties of wood flour-polypropylene composites. J. Thermoplast. Compos. Mater. 14:421-432.

Stark, N. (2005) Effect of weathering variables on the lightness of high-density polyethylene woodflour composites. In: Proceedings of the eighth International conference on woodfiber-plastic composites, Madison, WI. pp. 207-212.

Stark, N. M., Berger, M. J. (1997) Effect of particle size on properties of wood-flour reinforced polypropylene composites. In: Proceedings of the fourth international conference on woodfiber-plastic composites, Madison, WI. pp. 134-143.

Stark, N. M., Matuana, L. M. (2003) Ultraviolet weathering of photostabilized wood-flour-filled high-density polyethylene composites. J. Appl. Polym. Sci. 90:2609-2617.

Stark, N. M., Matuana, L. M., Clemons, C. M. (2004) Effect of processing method on surface and weathering characteristics of wood-flour/HDPE composites. J. Appl. Polym. Sci. 93:1021-1030.

Stark, N. M., Rowlands, R. E. (2003) Effects of wood fiber characteristics on mechanical properties of wood/polypropylene composites. Wood Fiber Sci. 35:167-174.

Stock, S. R. (1999) X-ray microtomography of materials. Int. Mater. Rev. 44:141-164.

Tajvidi, M., Ebrahimi, G. (2003) Water uptake and mechanical characteristics of natural filler-polypropylene composites. J. Appl. Polym. Sci. 88:941-946.

Takatani, M., Ito, H., Ohsugi, S., Kitayama, T., Saegusa, M., Kawai, S., Okamoto, T. (2000) Effect of lignocellulosic materials on the properties of thermoplastic polymer/wood composites. Holzforschung 54:197-200.

Thompson, K. E., Willson, C. S., Zhang, W. (2006) Quantitative computer reconstruction of particulate materials from microtomography images. Powder Technol. 163:169-182.

Tripathy, S. S., Landro, L. D., Fontanelli, D., Marchetti, A., Levita, G. (2000) Mechanical properties of jute fibers and interface strength with an epoxy resin. J. Appl. Polym. Sci. 75:1585-1596.

Tze, W. T. Y., O'Neill, S. C., Tripp, C. P., Gardner, D. J., Shaler, S. M. (2007) Evaluation of load transfer in the cellulosic-fiber/polymer interphase using a micro-Raman tensile test. Wood Fiber Sci. 39:184-195.

Tze, W. T. Y., O'Neill, S. C., Gardner, D. J., Tripp, C. P., Shaler, S. M. (2003) Coupling polystyrene and cellulose fibers with hydrophilic and hydrophobic silanes: Effects on interfacial properties. In: Proceedings of the 7th International Conference on Woodfiber-Plastic Composites, Madison, WI. pp. 29-35.

USFPL. 1999. Wood handbook-wood as an engineering material U.S. Department of Agriculture, Forest Service, Forest Products Laboratory., Madison, WI.

Valadez, G. A., Cervantes-Uc, J. M., Olayo, R., Herrera-Franco, P. J. (1999) Effect of fiber surface treatment on the fiber-matrix bond strength of natural fiber reinforced composites. Composites Part B 30:309-320.

Velde, K. V. D., Kiekens, P. (2001) Influence of fiber surface characteristics on the flax/polypropylene interface. J. Thermoplast. Compos. Mater. 14:244-260.

Wang, L., Paul, H. S., Harman, T., D'Angelo, J. (2004) Characterization of aggregates and asphalt concrete using X-ray computerized tomography a state of the art report. In: Proceedings of the Asphalt Paving Technology, Baton Rouge, LA, United States. pp. 467-500.

Wang, Y., Muszynski, L. (2007) Accounting for the wood/polymer interphase in multi-scale characterization of wood plastic composites using advanced imaging tools. Holzforschung. To be submitted for publication.

Wang, Y., Muszynski, L., Simonsen, J. (2007) Gold as an X-ray CT scanning contrast agent: Effect on the mechanical properties of wood plastic composites. Holzforschung. Submitted for publication. Manuscript # HOLZ-D-07-00041.

Willis, K. L., Abell, A. B., Lange, D. A. (1998) Image-based characterization of cement pore structure using Wood's metal intrusion. Cem. Concr. Res. 28:1695-1705.

Wolcott, M. P. (2003) Production methods and platforms for wood plastic composites. In: Proceedings of the non-wood substitutes for solid wood products conference Melbourne, Australia. 12 pp.

Wolcott, M. P., Smith, P. M. (2004) Opportunities and challenges for wood-plastic composites in structural applications. In: Proceedings of the Progress in Woodfibre-Plastic Composites, Toronto, ON. 10 pp.

Wright, J. R., Mathias, L. J. (1993) Physical characterization of wood and wood-polymer composites: An update. J. Appl. Polym. Sci. 48:2225-2239.

Yang, H., Lindquist, B. W. (2000) Three-dimensional image analysis of fibrous materials. In: Proceedings of the SPIE - The International Society for Optical Engineering, San Diego, CA, USA. pp. 275-282.

Zafeiropoulos, N. E., Baillie, C. A., Hodgkinson, J. M. (2002) Engineering and characterisation of the interface in flax fibre/polypropylene composite materials. Part II. The effect of surface treatments on the interface. Composites Part A 33:1185-1190.

Zaini, M. J., Fuad, M. Y. A., Ismail, Z., Mansor, M. S., Mustafah, J. (1996) Effect of filler content and size on the mechanical properties of polypropylene/oil palm wood flour composites. Polym. Int. 40:51-55.

Zhou, X. P., Li, R. K. Y., Xie, X. L., Tjong, S. C. (2003) Reinforcement of polypropylene using sisal fibers grafted with poly(methyl methacrylate). J. Appl. Polym. Sci. 88:1055-1064.

Zhu, X., Zhou, H., Wei, H., Zheng, Y., Zhang, Z. (2001) Mechanical and fluid properties of wood flour/high density polyethylene composite. Beijing Huagong Daxue Xuebao(Ziran Kexueban)/Journal of Beijing University of Chemical Technology 28:56-58.

APPENDICES

Appendix A: Working Instruction for Wood Plastic Composite Specimen Fabrication

Objective:

Manufacture wood plastic composite (WPC) samples via pressure molding process.

Responsibility:

Project manager or designee: Yi Wang

References:

1. Instruction Manual of 3-Piece Mixer/Measuring Head. [C.W.BRABENDER INSTRUMENTS, Inc.]

2. Instruction Manual of Plasti-Corder® Torque Rheometer.[C.W.BRABENDER INSTRUMENTS, Inc.]

3. Instruction Manual of WINMIX Mixer Program for Windows. [C.W.BRABENDER INSTRUMENTS, Inc.]

4. Instruction Manual of CARVER® Automatic Hot Press (Model: Auto "M", Catalog No.: 3891), and of CARVER® Manual Press (Model: "Mini C", Catalog No.: 3850).

Data Forms:

Composite Recipe Spreadsheet:

The net chamber volume of the C.W.BRABENDER 3-Piece Mixer is 60 ml, of which 80% (48 ml) should be filled. For HDPE/wood flour blends at 40:60 weight raito, the weight of the wood flour and polymer mixture should be roughly 46 g.

For example, if a WPC sample (weight ratio of wood flour: additive: HDPE = 40: 1: 59) is to be made, the weight of wood flour, additive and HDPE should be 18.4 g, 0.46 g, 27.14 g respectively.

Set the FORCE Parameter for CARVER® Automatic Hot Press:

The FORCE value is the load applied between the lower platen and the top platen of the hot press, so the FORCE should be set as: FORCE (lb) = pressure actually applied to specimen sheet (psi) × area of the mold (in^2). For example, if the actual pressure on specimen sheet is 75 psi and the dimension of the mold is 5.50 × 5.24 in^2, the parameter of FORCE should be set as: FORCE = 50 psi × 5.50 ×5.24 in^2 = 1441 lb.

Calculate the Pressure for CARVER® Automatic Manual Press:

The pressure value P_{gauge} (psi) on the pressure gauge is the force (lb) on unit area (in^2) of the hydraulic ram, with the radius of 3 in. The area of the ram is: $S_{ram} = \pi \times (1.5in)^2 = 7.0685in^2$. If P_{actual} is the actual pressure applied on specimen sheet, S_{mold} is the area of the mold, then the pressure value P_{gauge} can be calculated as below: $P_{gauge} = \frac{P_{actral} \times S_{mold}}{S_{ram}}$. For example, if the actual pressure on specimen sheet is 50 psi, and the dimension of the mold is 5.50 × 5.24 in^2, the pressure value P_{gauge} is:

$$P_{gauge} = \frac{50psi \times 5.50 \times 5.24in^2}{7.0685in^2} = 203.86psi$$

Instruction:

Scope:

This document describes the steps for manufacturing WPC samples via pressure molding, which includes the operation of C.W.BRABENDER INSTRUMENTS, Inc. to mix wood flour and polymer, molding specimen sheets in the hydraulic hot press and specimen preparation.

Equipment and Materials and Personal Protection Equipment Needed:

Personal Protection Equipments:

Chemical goggles, thermally protective gloves, lab coat.

Equipments and Materials Needed:

1. C. W Brabender Plasticoder mixer
2. CARVER® Automatic Hot Press
3. CARVER® Manual Press
4. Miniature table saw
5. Beaker with a mixing stick
6. Lab balance (0.001g)
7. Brass brush & brass blade (see Figure A.1)
8. Rubber hammer
9. Miscellaneous: aluminum foil, screw

Figure A.1 Cleaning tools for Brabender mixer

Materials:

1. Wood flour
2. Polymer (PE) pellets
3. Polystyrene for easier cleaning of the mixer (Some difficult-to-clean materials might stick to the blade and the chamber wall of the mixer. In this case, polystyrene, which is easily removed from the mixer after melting, can be added into the mixer and melted, after being blended thoroughly with the residuals; they can be removed more easily, so the chamber can be cleaned more effectively)
4. One sheet of aluminum foil
5. Dry lubricant

Procedures:

Making Wood Flour and Plastic Mixture (C.W.BRABENDER):

1. Calculate the weight of the wood flour and polymer according to the mixture composition.
2. Weigh wood flour and polymer in separate beakers using lab balance.
3. Mix the wood flour and the polymer in one beaker and blend it thoroughly using glass stick.
4. Turn on the main power (located on the front of the instrument, see Figure A.2) of the mixer, adjust the control mode to “computerized” mode (refer to the instruction 6.0-7.0 on p.14-18 of reference 3.2)

Figure A.2 Control panel of Brabender mixer

5. Turn on the computer and start the WINMIX program.

6. Select the menu “File”-“New” to open the parameter window, insert project name in the “Order” field, and your name in the “Operator” field (refer to instruction 3.2.1 on p.5-6 of reference 3.3).

7. Set the test parameters: mixer speed, temperature and mixing time (refer to instruction 3.2.1 on p.5-6 of reference 3.3).

8. Save the settings file to your folder (refer to instruction 3.2.3 on p.7 of reference 3.3).

9. Select the menu “Run”-“Start test” to start the test, a window shown the temperatures is displayed (see Figure A.3).

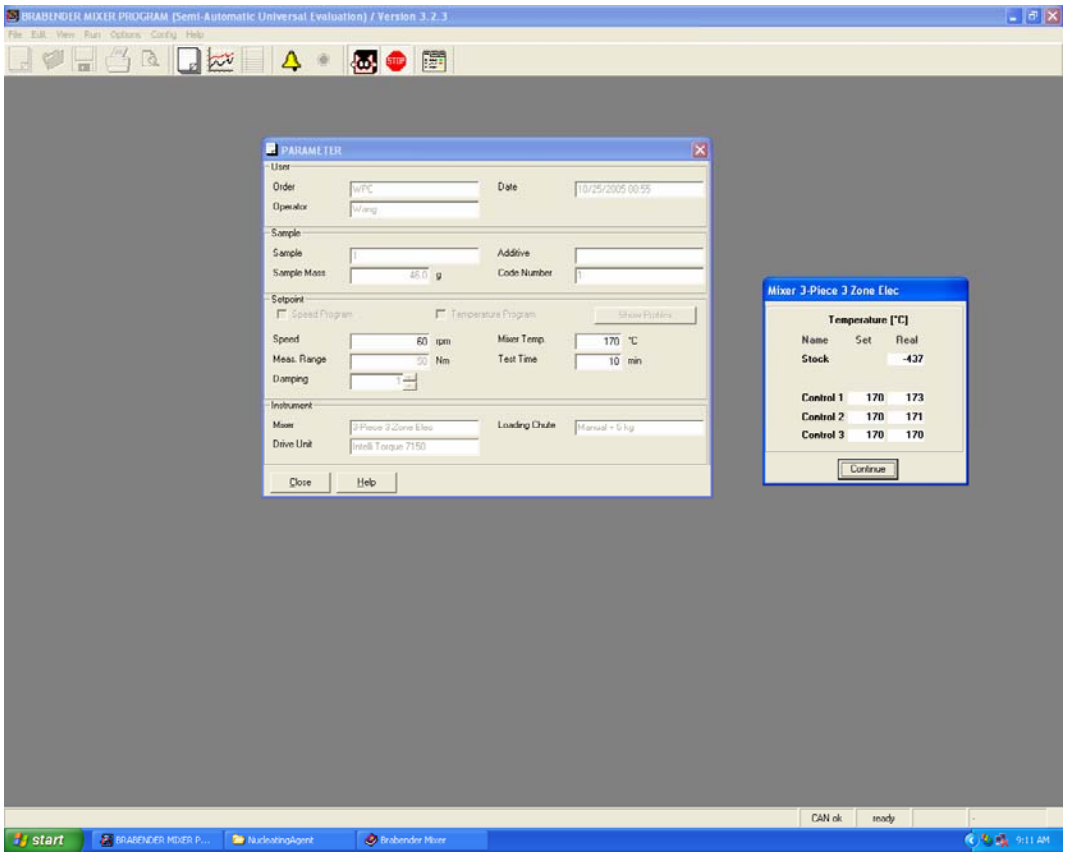

Figure A.3 WINMIX program interface

10. Wait until the temperature reaches the set value (about 15 minutes).

11. When the temperature reaches the set values, click the “Continue” button to start the test.

12. Load the mixer with the wood flour and polymer mixture in the order specified. For HDPE/wood flour, add the HDPE first, wait until it melts; then add the wood flour (refer to instruction 5.0.10-5.0.13 on p.12-13 of reference 3.1).

13. Press the “Start” key on the control keypad (located on the front of the instrument, see Figure A.2) toolbar to start mixing.

14. Wait until the mixer stops automatically after the set time expires (if it does not, press the red “Stop” key on the control keypad, see Figure A.2).

15. After completion of the test, select “File”-“Save as” to save the test graph file.

16. Dissemble the mixer (refer to instruction 6.1-6.2 on p.14 of reference 3.1).

17. Scrape all the process surfaces with brass blade and brass brush.

18. Place the mixed material into the small drawer on the front of the instrument (Figure A.4), and press the retained sample into flat form for later use. Be careful, it is hot.

Figure A.4 Drawer for containing compounding materials

19. Immediately after removing all usable material from the mixer, thoroughly clean all the parts (refer to instruction 5.0.16-5.0.21 on p.13 of reference 3.1).

20. If more specimens are to be made, allow the mixer temperature to stabilize prior to starting a new test.

21. If the experiment is finished, exit the WINMIX program and turn off the computer, turn of the main power on the mixer.

Making Specimen Sheet by Pressing (CARVER® Automatic Hot Press and CARVER® Manual Press)

1. Make sure the safety shield door on the hot press is in the closed position (see Figure A.5).

2. Turn on the power of CARVER® Automatic Press by pushing down the "Power" switch, begin to preheat by pushing down the "Heat" switch (See Figure A.5), set the desired platen temperature (refer to instruction 3.5-3.6 on p.35 of reference 3.4, also see Figure A.6), the platen begins to be preheated.

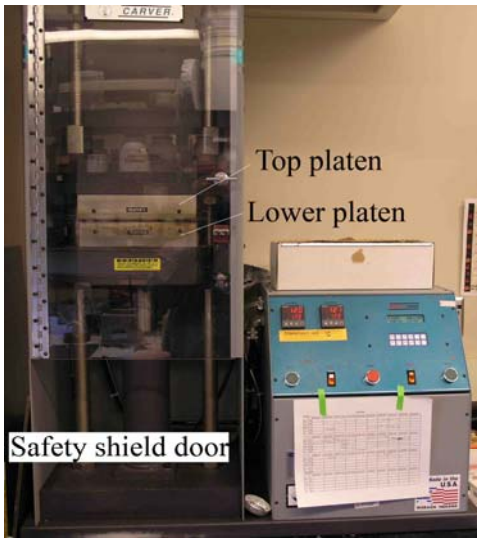

Figure A.5 CARVER hot press

Figure A.6 Control panel of CARVER hot press

3. Set up the pressing parameters by storing a recipe, the parameters include "Force", "Pump speed", "The time base", and "The dwell time" (refer to instruction 3.2.7 on p.17 of reference 3.4).

4. Recall the stored recipe and make it current (refer to instruction 3.2.8 on p.17-18 of reference 3.4).

5. Press the "Auto" key on the keypad to set the instrument in Automatic Mode.

6. Spray some dry lubricant (Tel-X) on the inner surface of the mold.

7. Fill the mold with mixed wood flour/polymer mixture from the Brabender mixer.

8. Close the mold and tighten the screws.

9. Wait until the platens reach the set temperature (about 10 min).

10. Open the safety shield door and place the mold on the lower platen of the hot press.

11. Place one piece of aluminum foil on the top of the mold to prevent the squeezed-out mixture from sticking to the top.

12. Close the safety shield door, and push down the "Close" buttons simultaneously until the upper surface of the mold is 5-10 mm below the lower surface of the top platen.

13. Preheat the mold for 10 min.

14. Close the press and apply pressure on the mold (refer to instruction 4.2.1 on p.38 of reference 3.4). The platen will stop automatically once the pressure is applied to the mold, and automatic pressing begins.

15. Wait until the dwell time is complete.

16. Open the press.

17. Stop heating the platen by pushing down the “Heat” switch on the front of the instrument.

18. Turn off the power of the hot press by pushing down the “Heat” switch.

19. Ease the pressure valve of the CARVER® Manual Press (on the front of the instrument, see Figure A.7) and make sure the platens are open.

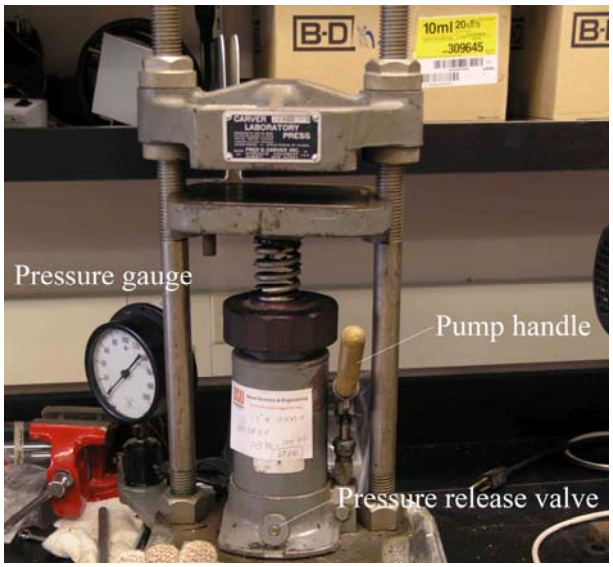

Figure A.7 CARVER cold press

20. Open the safety shield door of the hot press and move the mold (together with the aluminum foil) from the lower platen to the lower platen of CARVER® hot press.

21. Close the pressure release valve of the manual press.

22. Close the platen of the manual press using the pump handle until the set pressure (the same as in the hot press) is reached.

23. Leave the mold in the manual press until cool down (or overnight).

24. Open the pressure release valve and remove the mold from the press.

25. Un-tighten the screws in the mold frame.

26. Use rubber hammer to hit the bottom of the mold and make the specimen out of the mold

27. Clean the mold carefully with brass brush and brass blade.

Hazard Assessment Statement

Hazard Assessments for Personal Protective Equipment: The Laboratory Operations Manager maintains Hazard Assessments and makes them available to all laboratory employees. Individual employees working on the project outlined by this WI are responsible for familiarizing themselves with the Hazard Assessments pertaining to the chemicals, processes, and equipment referred to in this WI.

Appendix B: MATLAB Code for Correlating DIC Analog Force Data to Real Time Load Data from Mechanical Testing Machine

```
function [dt,dn] = finddt(time1,load,time2,force,eyy,area)

%This is the program to correlate the DIC analog force data to the real time load data from the mechanical testing machine. Input “time1”, “load” are the real time and load values recorded by the mechanical testing machine; “time2”, “force” are the time and force data transferred from analog data to DIC; “eyy” is the strain value calculated from DIC software, and “area” is the specimen cross section area.

dt = -20;

dn = 0.1;

ssd = sum((interp1(time1,load,time2+dt*ones(size(time2)),'cubic')-dn*force).^2);

for t = -20:0.5:20

   for n = 0.1:0.1:3

      ssd1 = sum((interp1(time1,load,time2+t*ones(size(time2)),'cubic')-n*force).^2);

      if ssd1 <= ssd

         ssd = ssd1; dt = t; dn= n;

      end

      end

end

plot(time1,load,'r',time2,force,'b',time2+dt*ones(size(time2)),

interp1(time1,load,time2+dt*ones(size(time2)),'cubic'),'ms');

h = legend('Load','Force',2); xlabel('time'); ylabel('force');

disp('dt='); disp(dt); disp('dn='); disp(dn);
```

```
figure;

plot(eyy*100,interp1(time1,load,time2+

dt*ones(size(time2)),'cubic')/area,'-*');

xlabel('Strain (%)'); ylabel('Stress (Mpa)');
```

Appendix C: HSB Color Segmentation Results from Micrographs of Wood/PVC Composite Slices

Images of Segmented Wood and Wood/PVC Interphase

Note: The images are arranged in the sequence of: original micrograph (a), segmented wood component (b), segmented wood/PVC interphase (c).

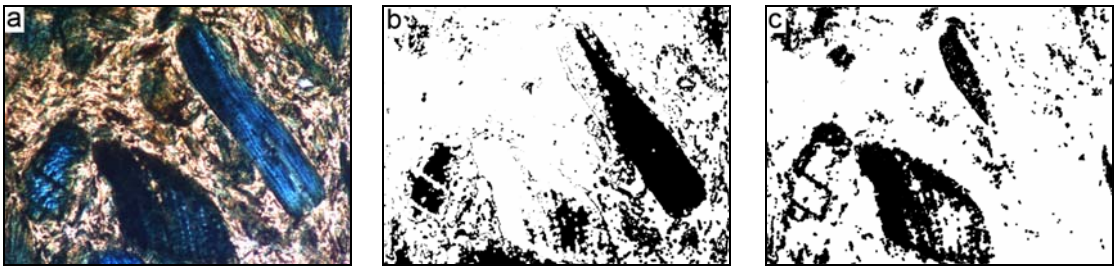

Figure C.1 HSB color segmentation results from slice # 1.

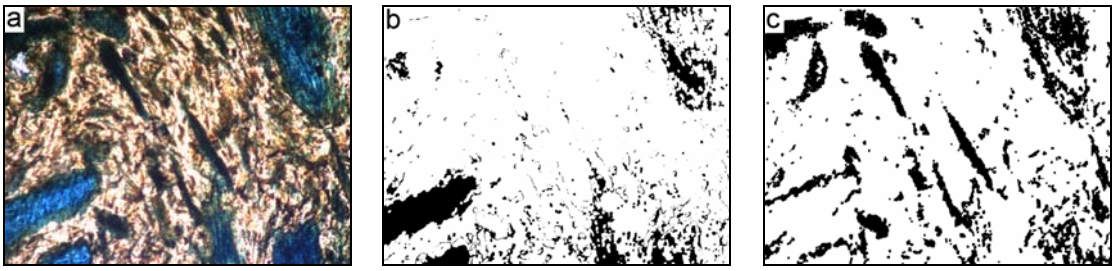

Figure C.2 HSB color segmentation results from slice # 2.

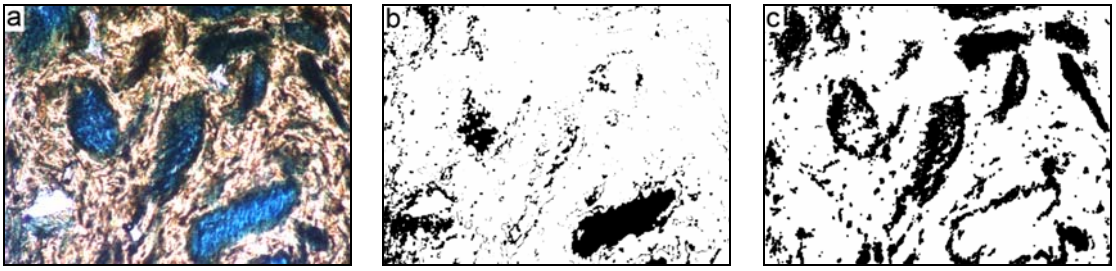

Figure C.3 HSB color segmentation results from slice # 3.

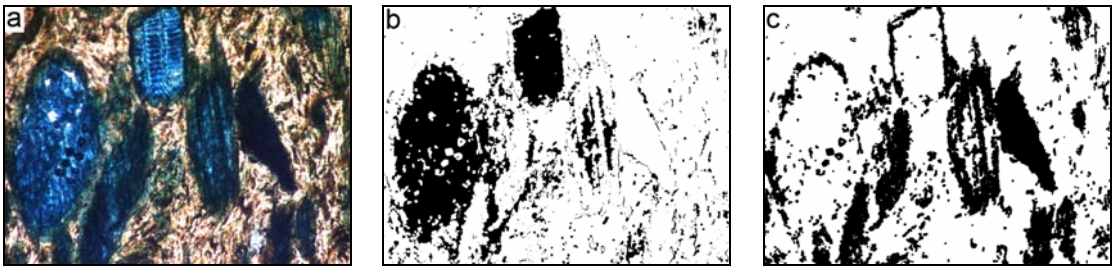

Figure C.4 HSB color segmentation results from slice # 4.

Figure C.5 HSB color segmentation results from slice # 5.

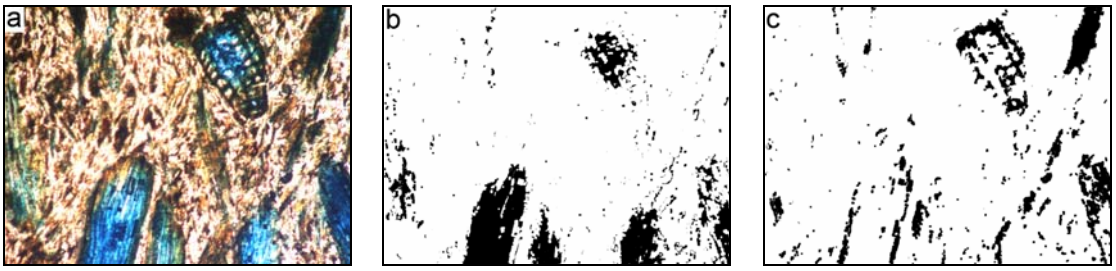

Figure C.6 HSB color segmentation results from slice # 6.

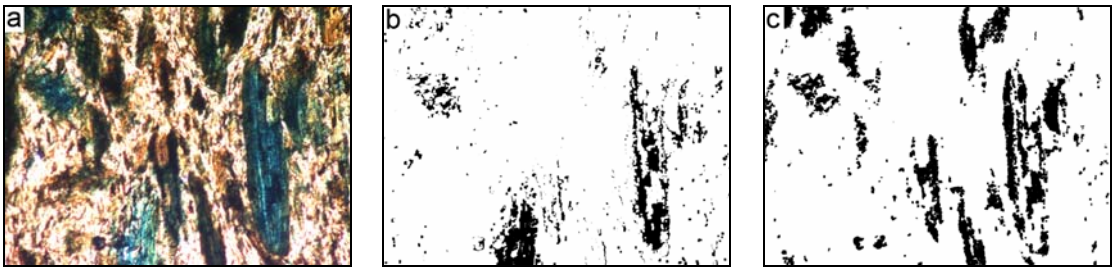

Figure C.7 HSB color segmentation results from slice # 7.

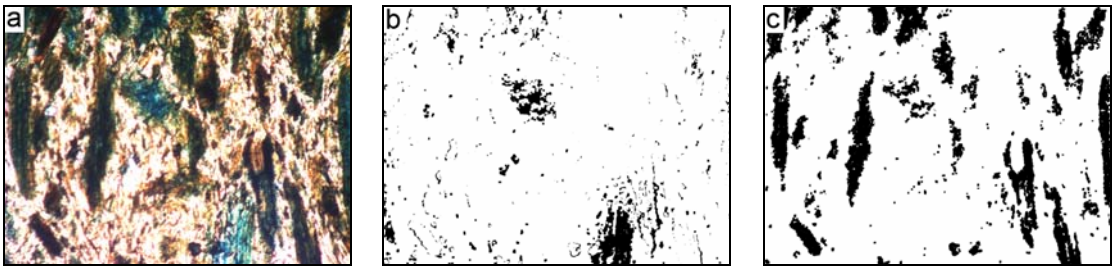

Figure C.8 HSB color segmentation results from slice # 8.

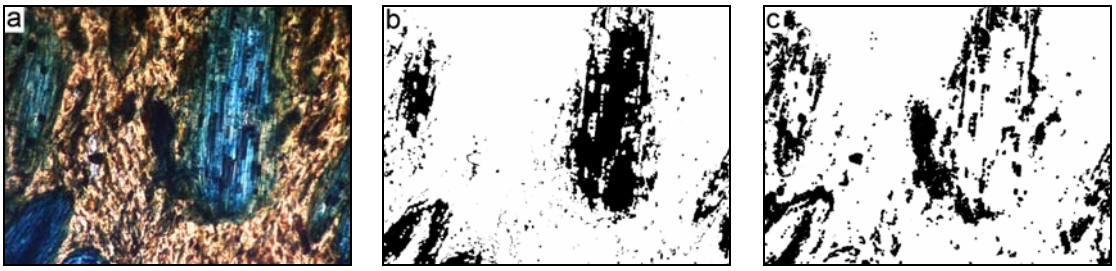

Figure C.9 HSB color segmentation results from slice # 9.

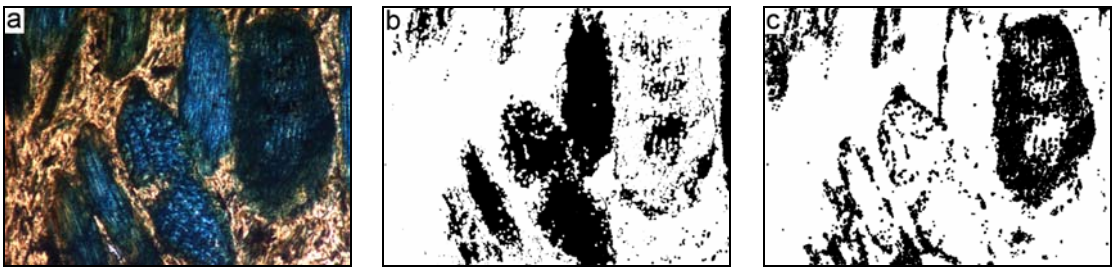

Figure C.10 HSB color segmentation results from slice # 10.

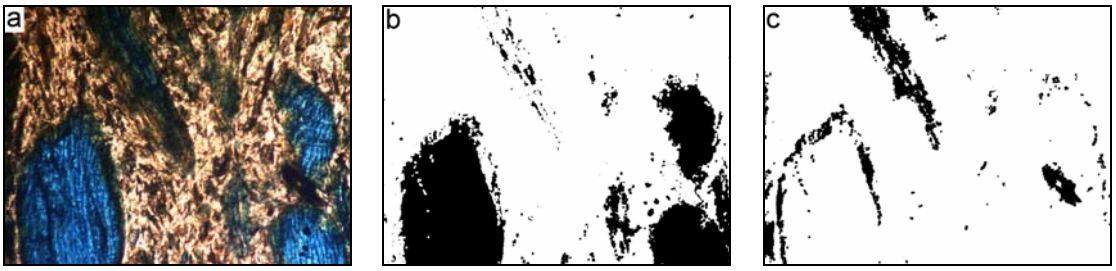

Figure C.11 HSB color segmentation results from slice # 11.

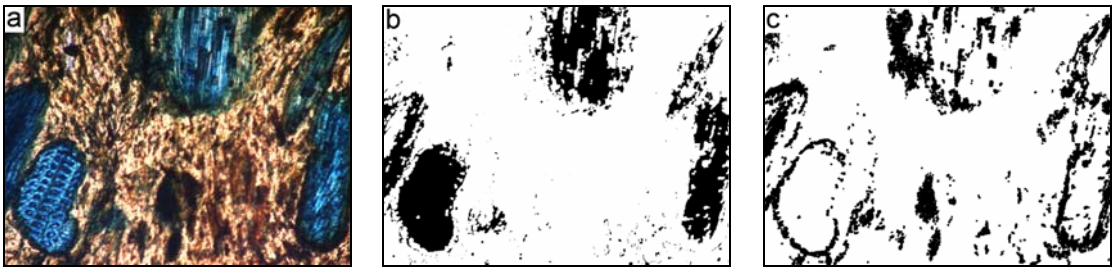

Figure C.12 HSB color segmentation results from slice # 12.

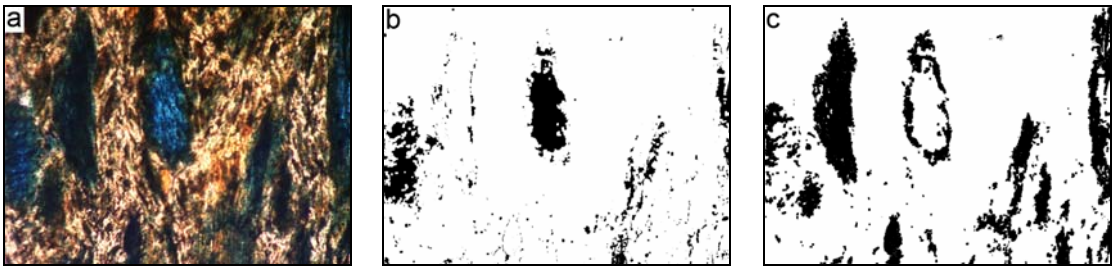

Figure C.13 HSB color segmentation results from slice # 13.

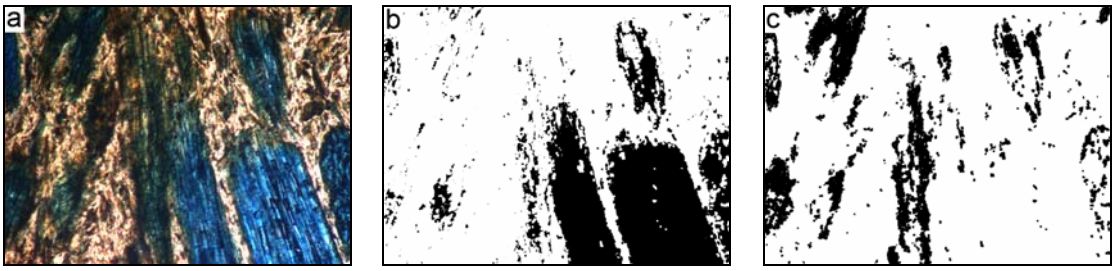

Figure C.14 HSB color segmentation results from slice # 14.

Figure C.15 HSB color segmentation results from slice # 15.

Figure C.16 HSB color segmentation results from slice # 16.

Figure C.17 HSB color segmentation results from slice # 17.

Figure C.18 HSB color segmentation results from slice # 18.

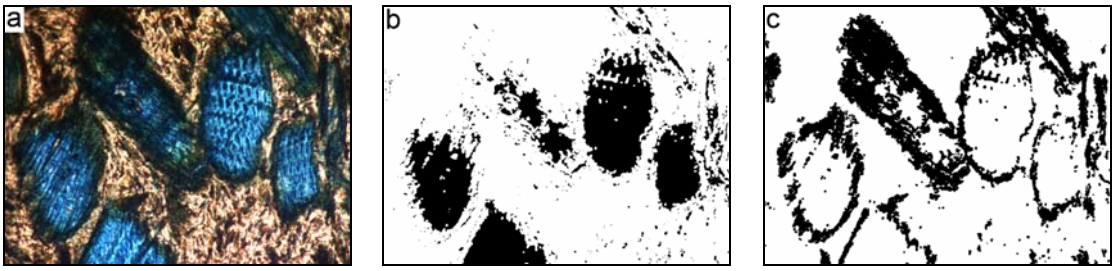

Figure C.19 HSB color segmentation results from slice # 19.

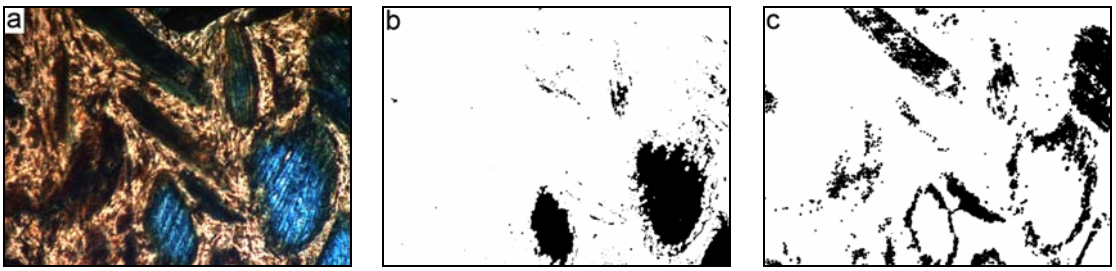

Figure C.20 HSB color segmentation results from slice # 20.

Figure C.21 HSB color segmentation results from slice # 21.

Figure C.22 HSB color segmentation results from slice # 22.

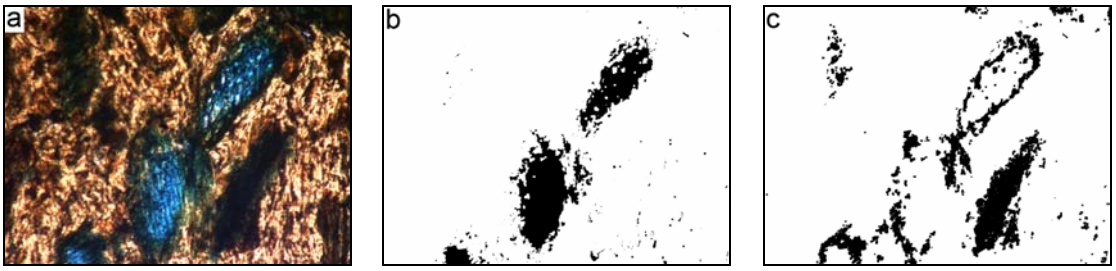

Figure C.23 HSB color segmentation results from slice # 23.

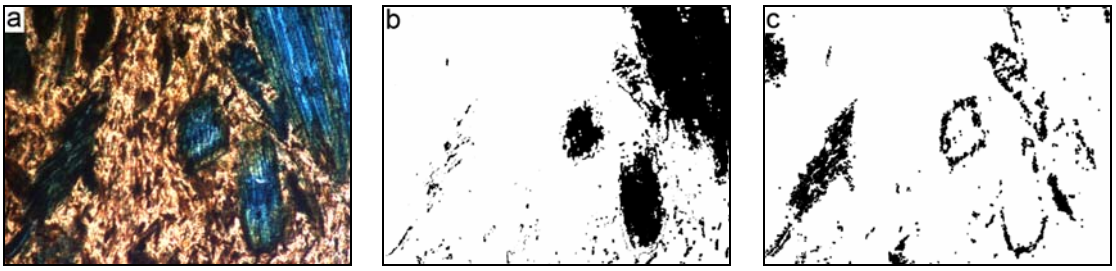

Figure C.24 HSB color segmentation results from slice # 24.

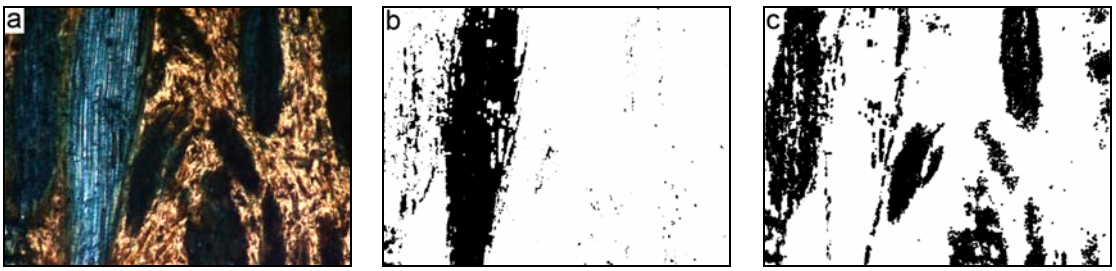

Figure C.25 HSB color segmentation results from slice # 25.

Figure C.26 HSB color segmentation results from slice # 26.

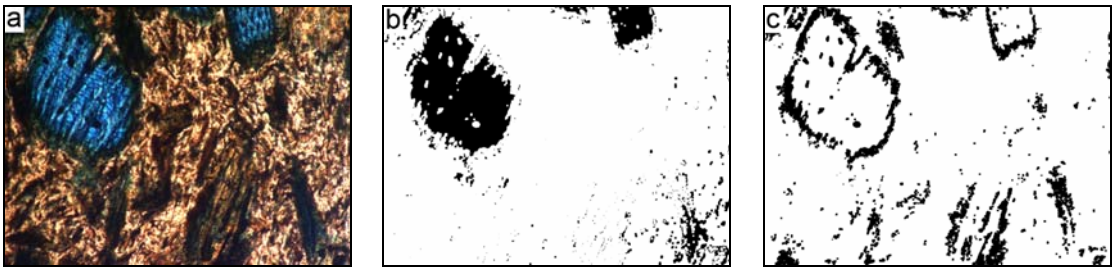

Figure C.27 HSB color segmentation results from slice # 27.

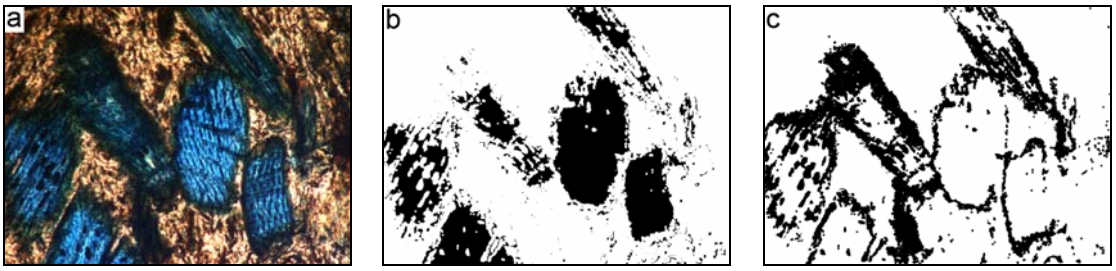

Figure C.28 HSB color segmentation results from slice # 28.

Figure C.29 HSB color segmentation results from slice # 29.

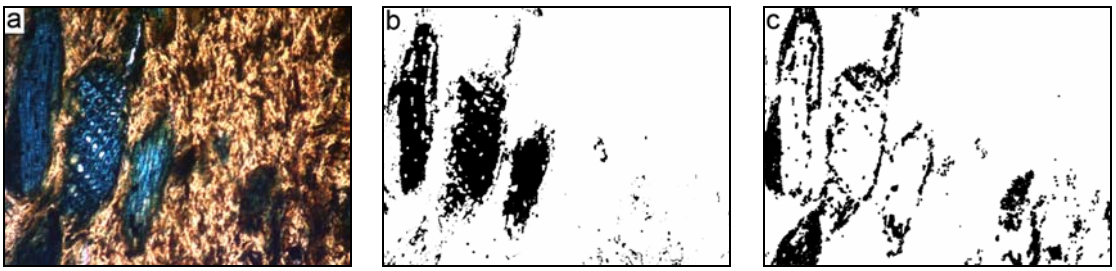

Figure C.30 HSB color segmentation results from slice # 30.

Figure C.31 HSB color segmentation results from slice # 31.

Figure C.32 HSB color segmentation results from slice # 32.

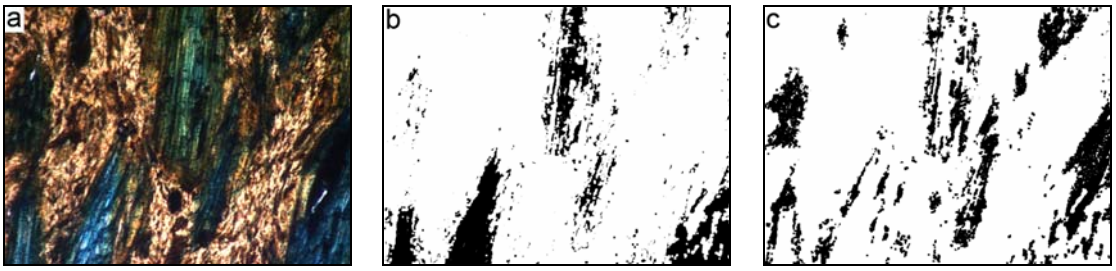

Figure C.33 HSB color segmentation results from slice # 33.

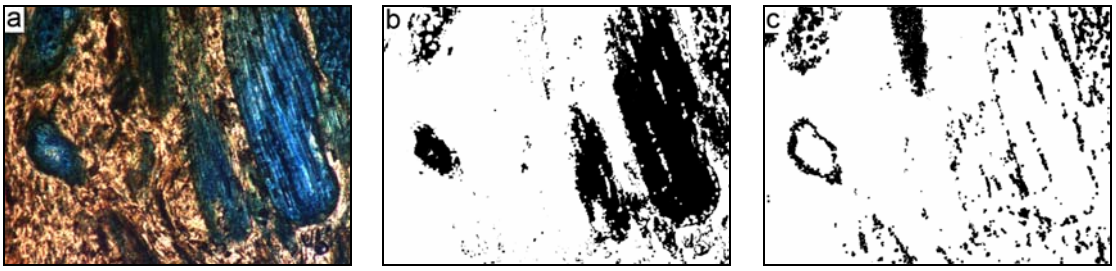

Figure C.34 HSB color segmentation results from slice # 34.

Figure C.35 HSB color segmentation results from slice # 35.

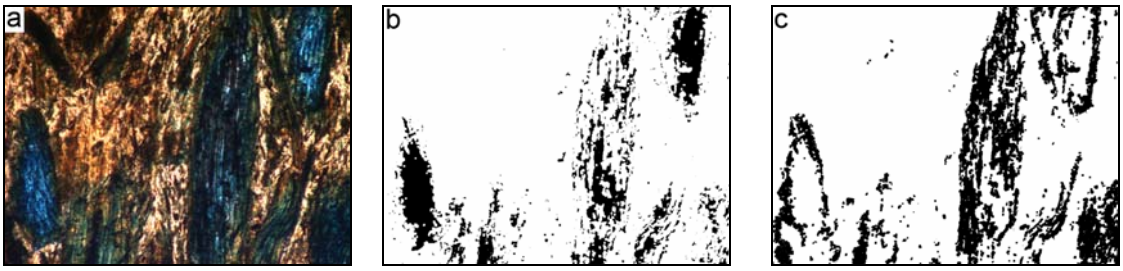

Figure C.36 HSB color segmentation results from slice # 36.

Analysis Results of HSB Segmentation

Table C.1 Analysis results from HSB color segmentation of micrographs of wood/PVC composite slices

Image No.	Hue component threshold		Number of pixels from H1	Brightness component threshold		Number of pixels from B1	Number of pixels from H1 AND B1	Interphase/wood fraction (%)
	Lower threshold	Upper threshold		Lower threshold	Upper threshold			
1	81	254	599574	16	79	359111	258890	43.2
2	92	254	364146	12	97	361339	183290	50.3
3	56	245	504429	23	134	502121	327832	65.0
4	77	254	738544	20	89	467511	370491	50.2
5	74	254	907590	18	143	571273	503347	55.5
6	43	254	314237	20	118	335910	140489	44.7
7	44	254	315577	20	98	400358	213816	67.8
8	49	254	336404	17	108	394350	235270	69.9
9	69	254	576497	9	84	528533	283201	49.1
10	58	254	788244	7	61	502987	373129	47.3
11	53	254	466834	8	53	478507	208581	44.7
12	60	254	533750	8	75	422297	241217	45.2
13	57	254	382479	8	70	482144	260214	68.0
14	60	254	619385	10	72	409822	231899	37.4
15	56	254	339302	10	78	386875	126658	37.3
16	54	254	433830	12	67	334356	201525	46.5
17	56	254	302816	12	62	390382	163913	54.1
18	60	254	798526	9	72	444304	293244	36.7
19	60	254	701212	8	79	567983	364641	52.0
20	57	254	388851	5	72	619860	229656	59.1
21	59	254	337381	7	74	514956	219497	65.1
22	52	254	593731	12	63	378809	235834	39.7

Table C.1 (continued) Analysis results from HSB color segmentation of micrographs of wood/PVC composite slices

Image No.	Hue component threshold		Number of pixels from H1	Brightness component threshold		Number of pixels from B1	Number of pixels from H1 AND B1	Interphase/wood fraction (%)
	Lower threshold	Upper threshold		Lower threshold	Upper threshold			
23	46	254	268764	8	68	491136	146826	54.6
24	46	254	418976	8	62	492412	191422	45.7
25	50	254	652382	4	63	665399	389580	59.7
26	60	254	506517	5	67	611742	278829	55.0
27	53	254	372692	8	58	378581	165932	44.5
28	59	254	693391	9	68	527361	327339	47.2
29	45	254	497614	7	64	504110	225620	45.3
30	46	254	414176	9	64	369817	189402	45.7
31	54	254	457830	10	69	453523	208626	45.6
32	62	254	388110	10	54	421798	219944	56.7
33	56	254	431622	7	62	508050	245287	56.8
34	59	254	577572	10	60	314673	170835	29.6
35	51	254	537565	7	67	496614	295225	54.9
36	52	254	484695	10	62	529339	295332	60.9

Note: H1 designates the image obtained from opening the thresholded binary image from hue component, B1 designates the image obtained from opening the thresholded binary image from brightness component

Appendix D: SEM Images of Microtomed Wood/PVC Composite Surface

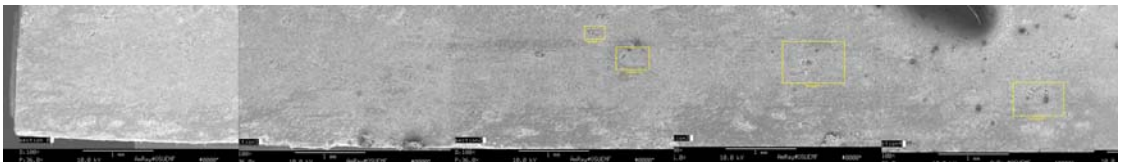

Figure D.1 Whole cross section (including four regions: Section 2-1, 2-2, 3-1, 4-1).

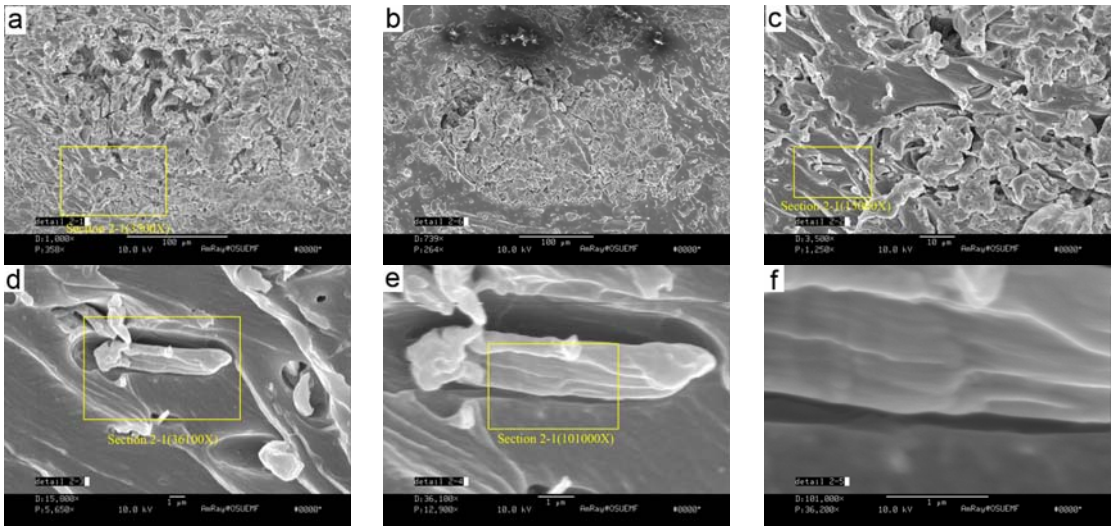

Figure D.2 Magnified images of Section 2-1, 2-2.

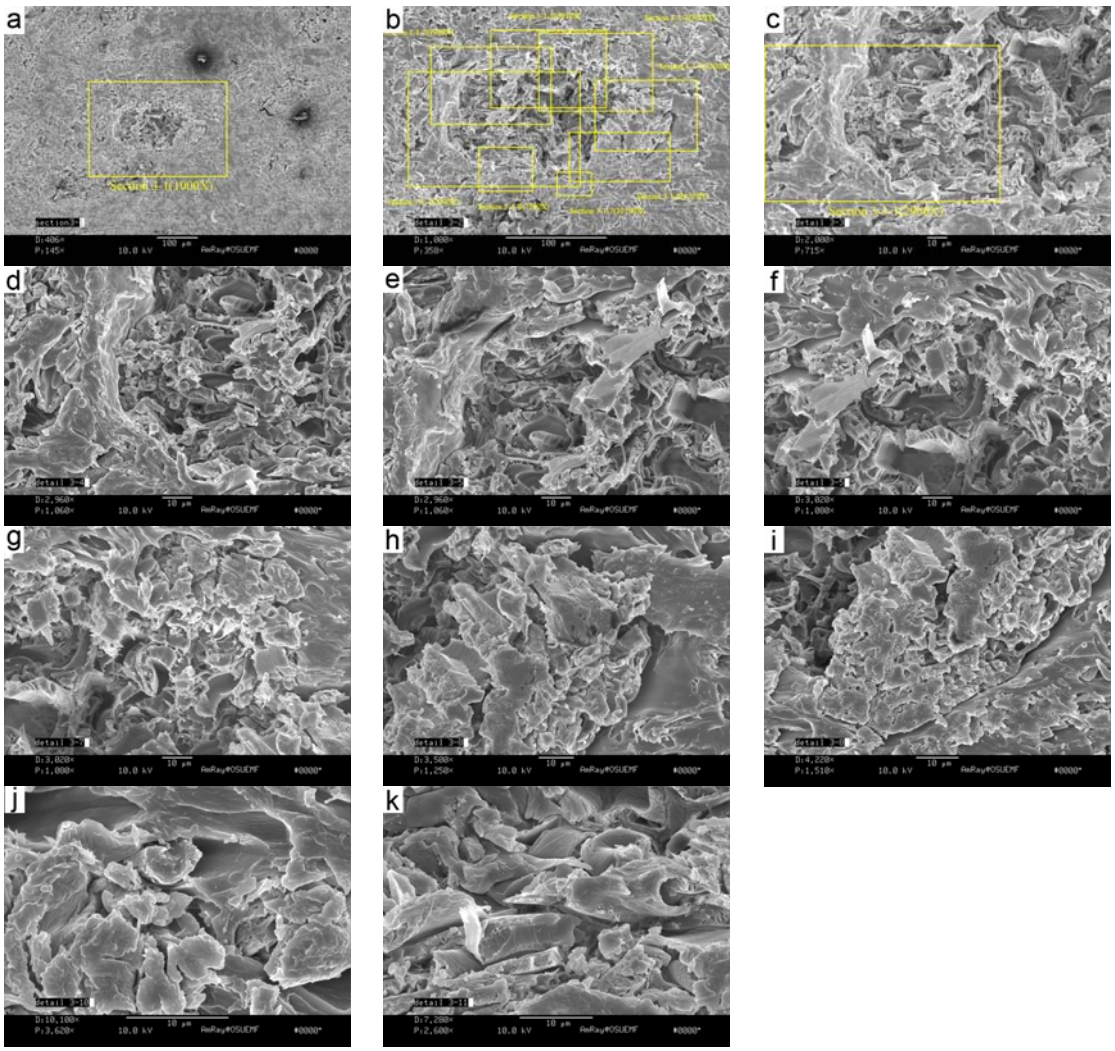

Figure D.3 Magnified images of Section 3-1.

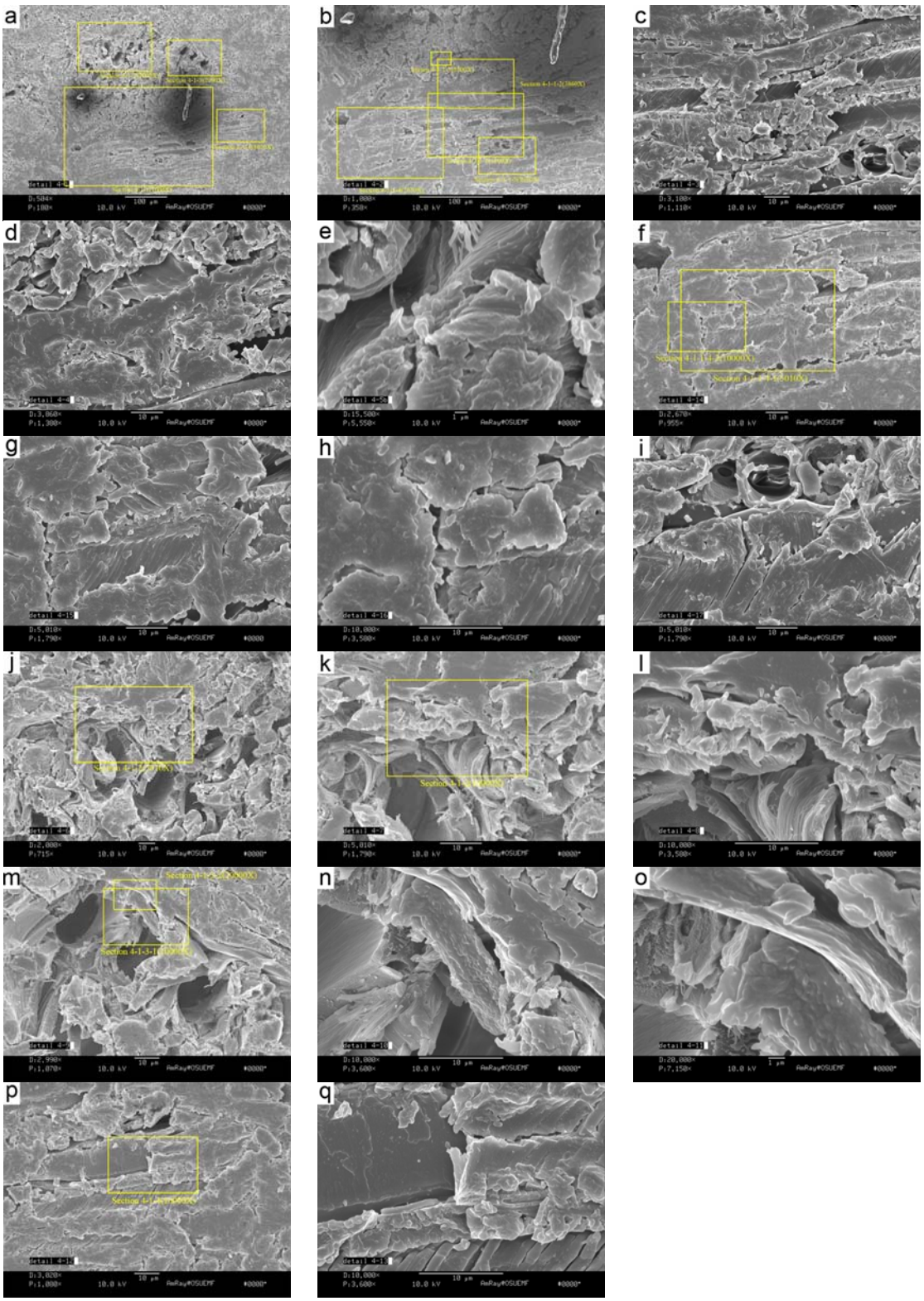

Figure D.4 Magnified images of Section 4-1.

Appendix E: SEM Images of Fractured Wood/PVC Composite Surface

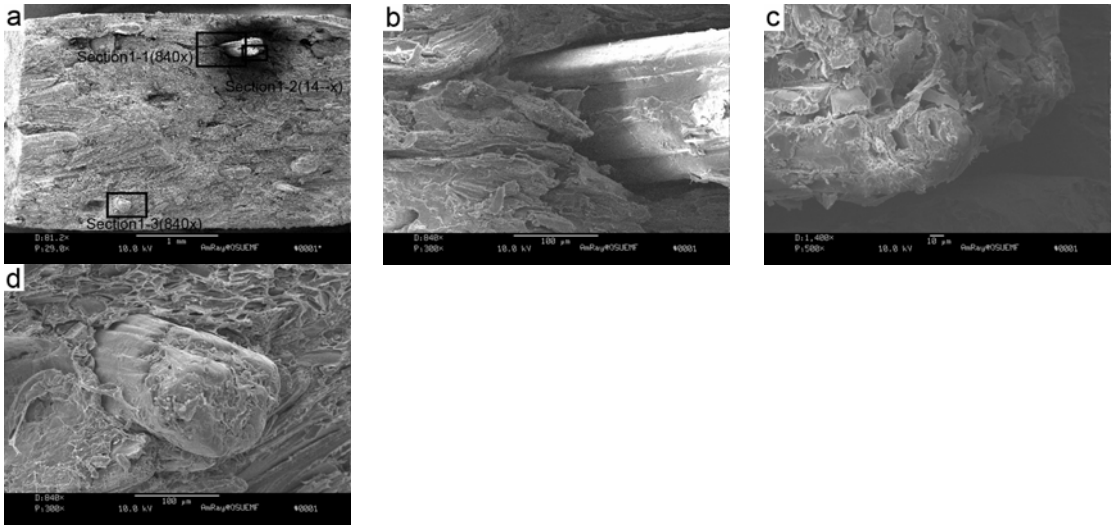

Figure E.1 Magnified images of Section 1.

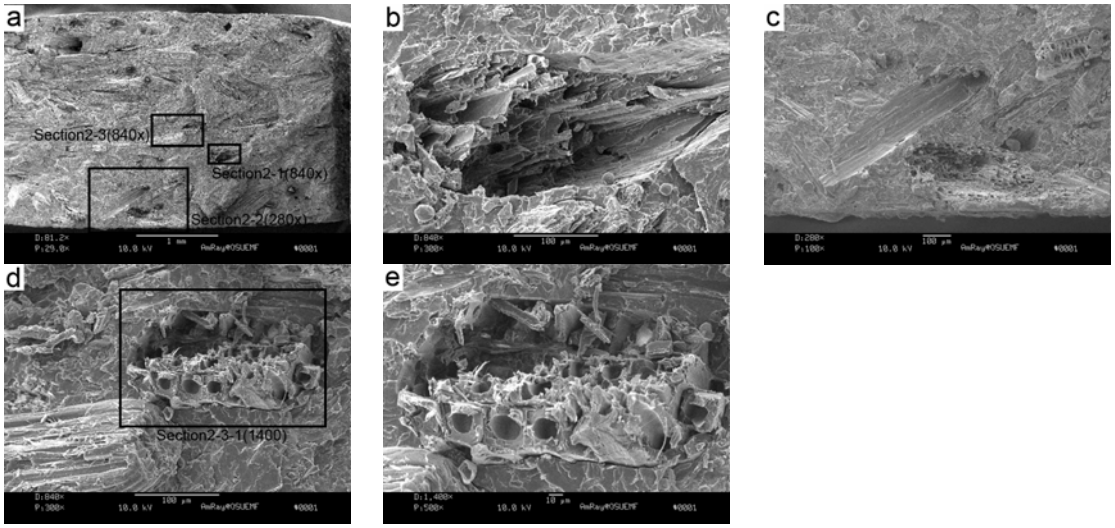

Figure E.2 Magnified images of Section 2.

Appendix F: Surface Strain Distribution Map in Cyclic and Monotonic Tensile Loading

Note: For the cyclic loading, the color bar is shown behind the maps; for the monotonic loading, the color bar is shown beside the map.

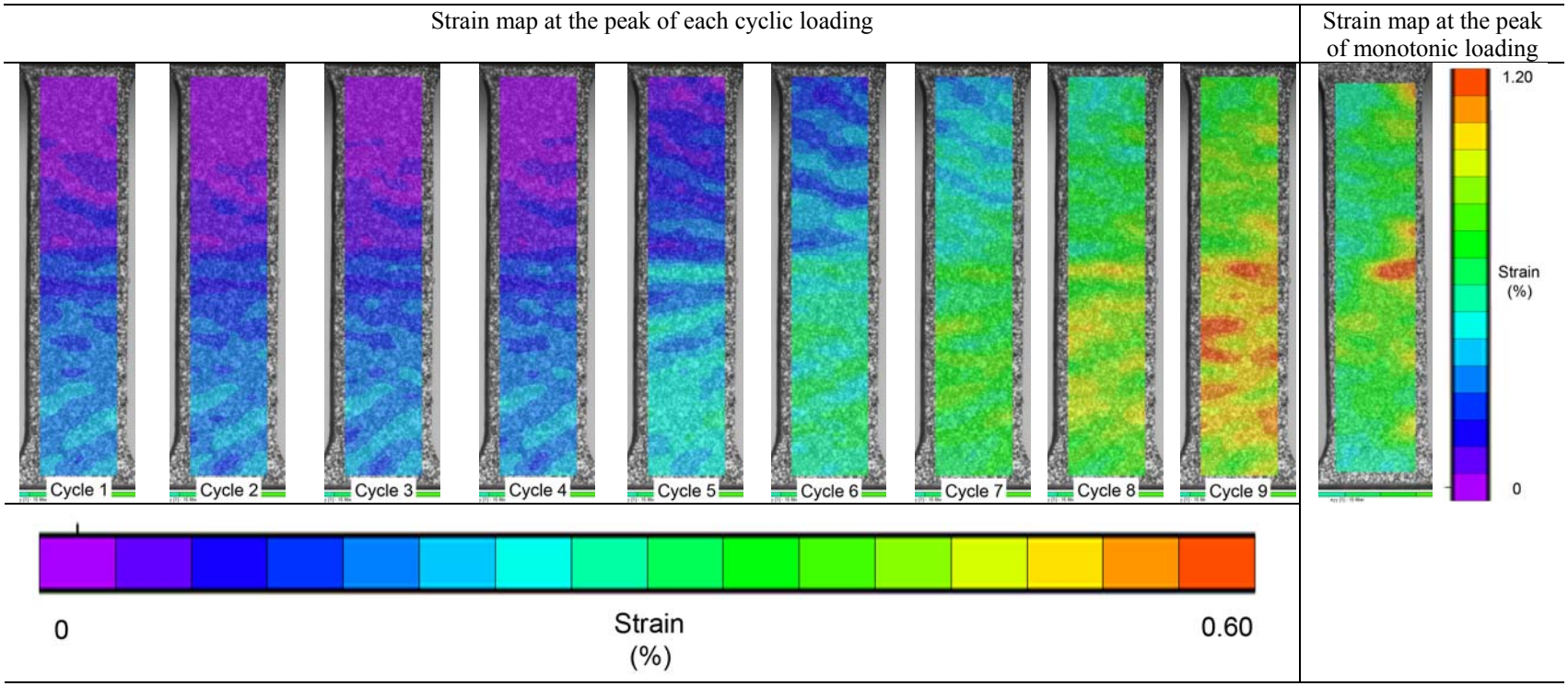

Figure F.1 Specimen C-1.

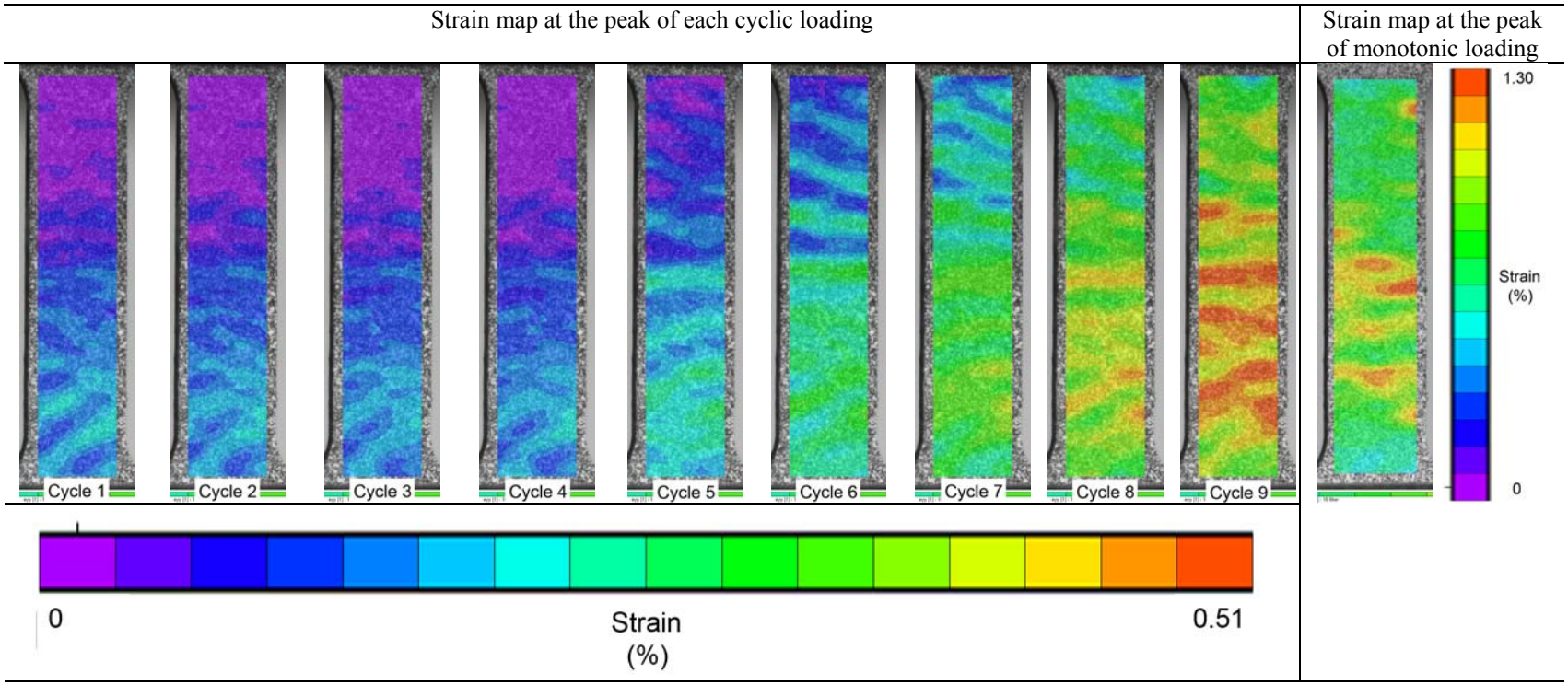

Figure F.2 Specimen C-2.

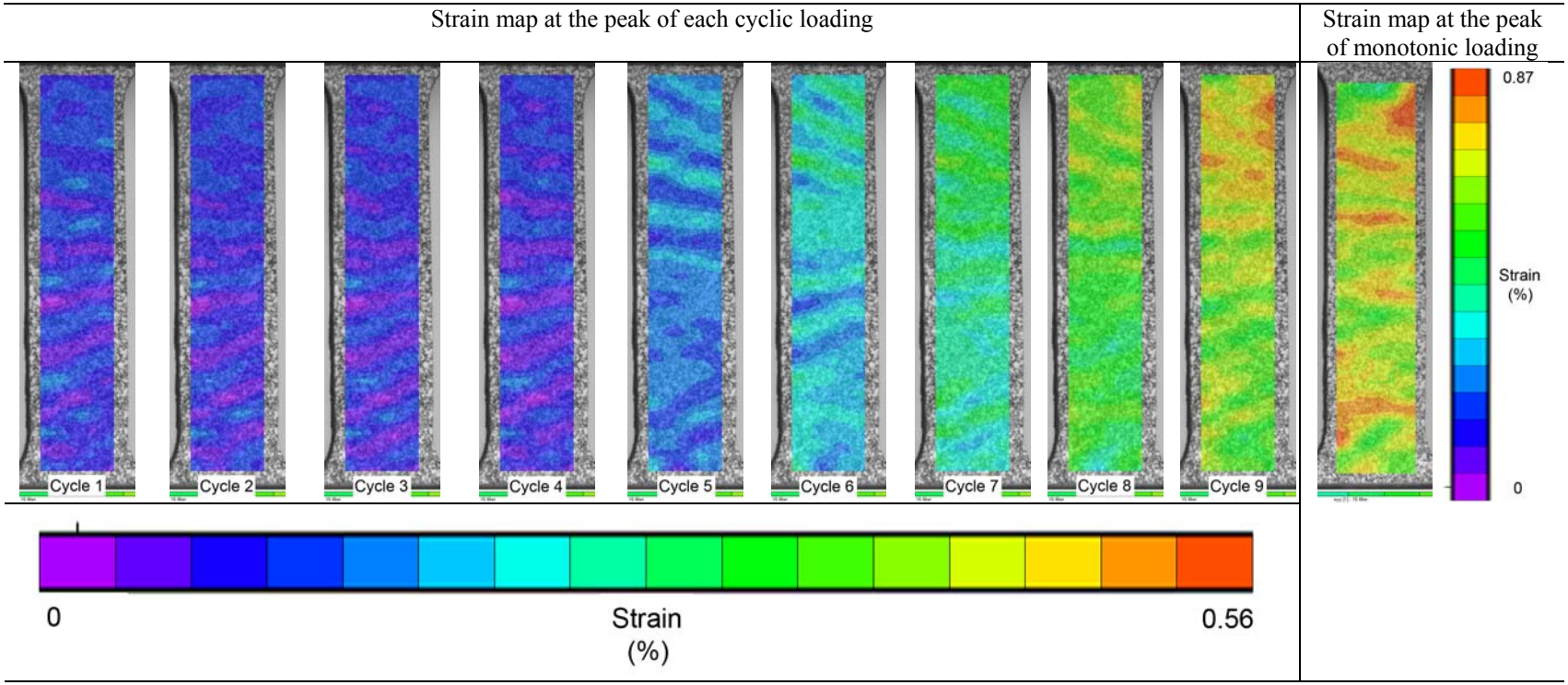

Figure F.3 Specimen C-3.

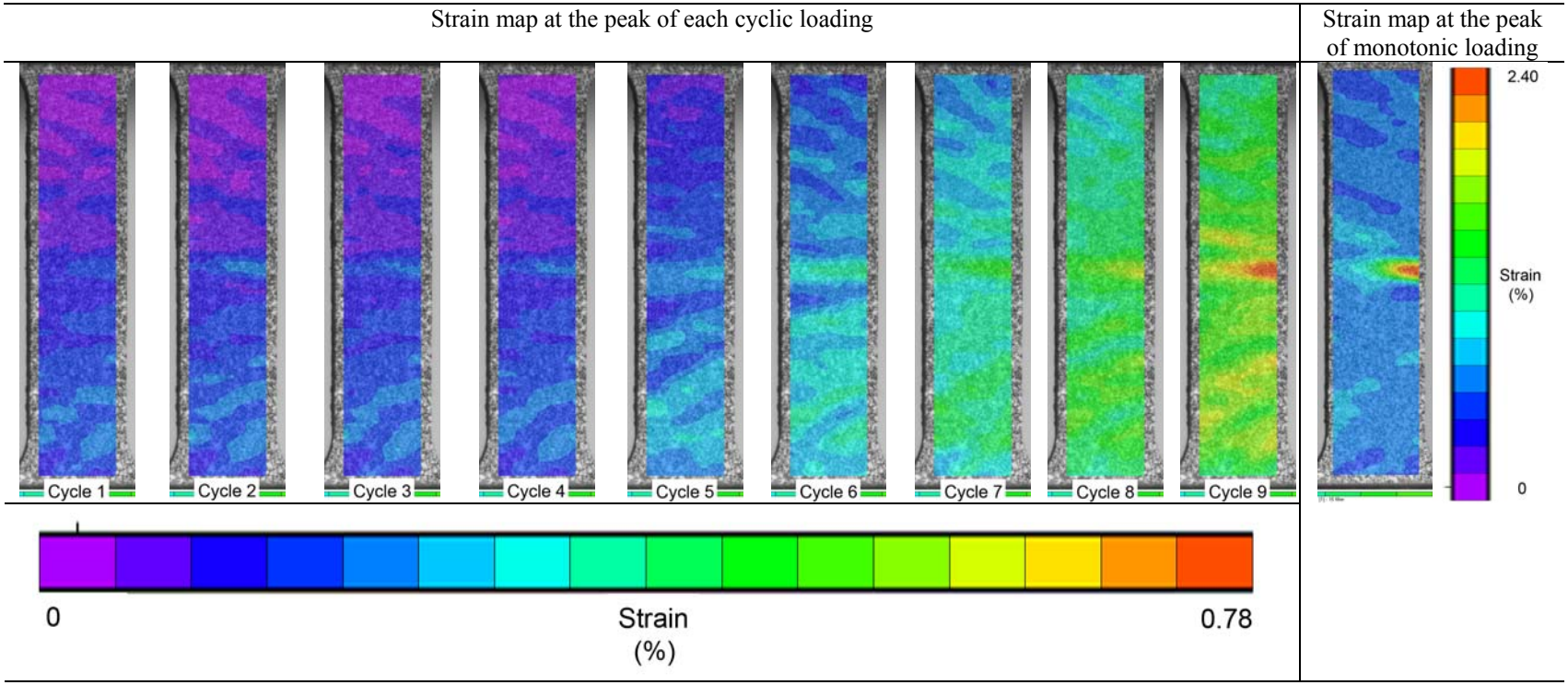

Figure F.4 Specimen C-4.

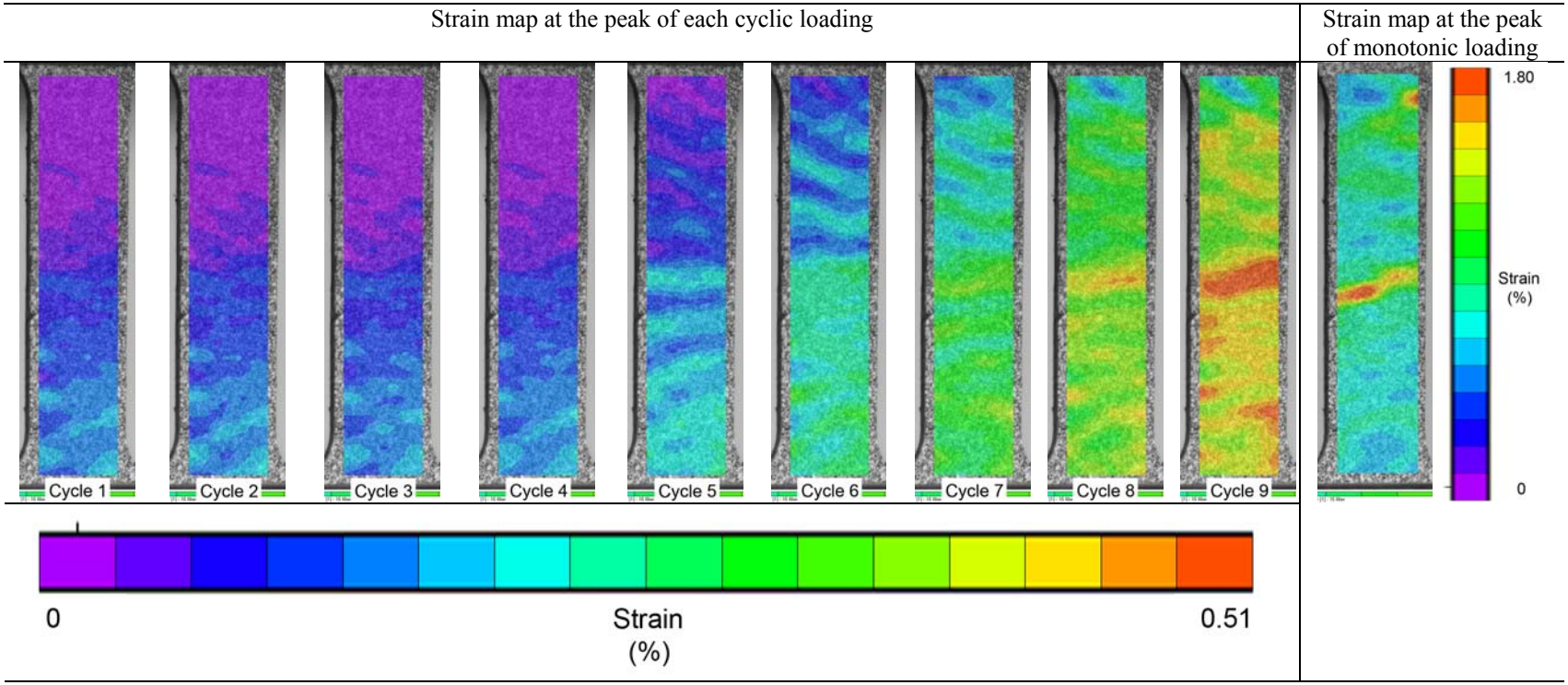

Figure F.5 Specimen C-5.

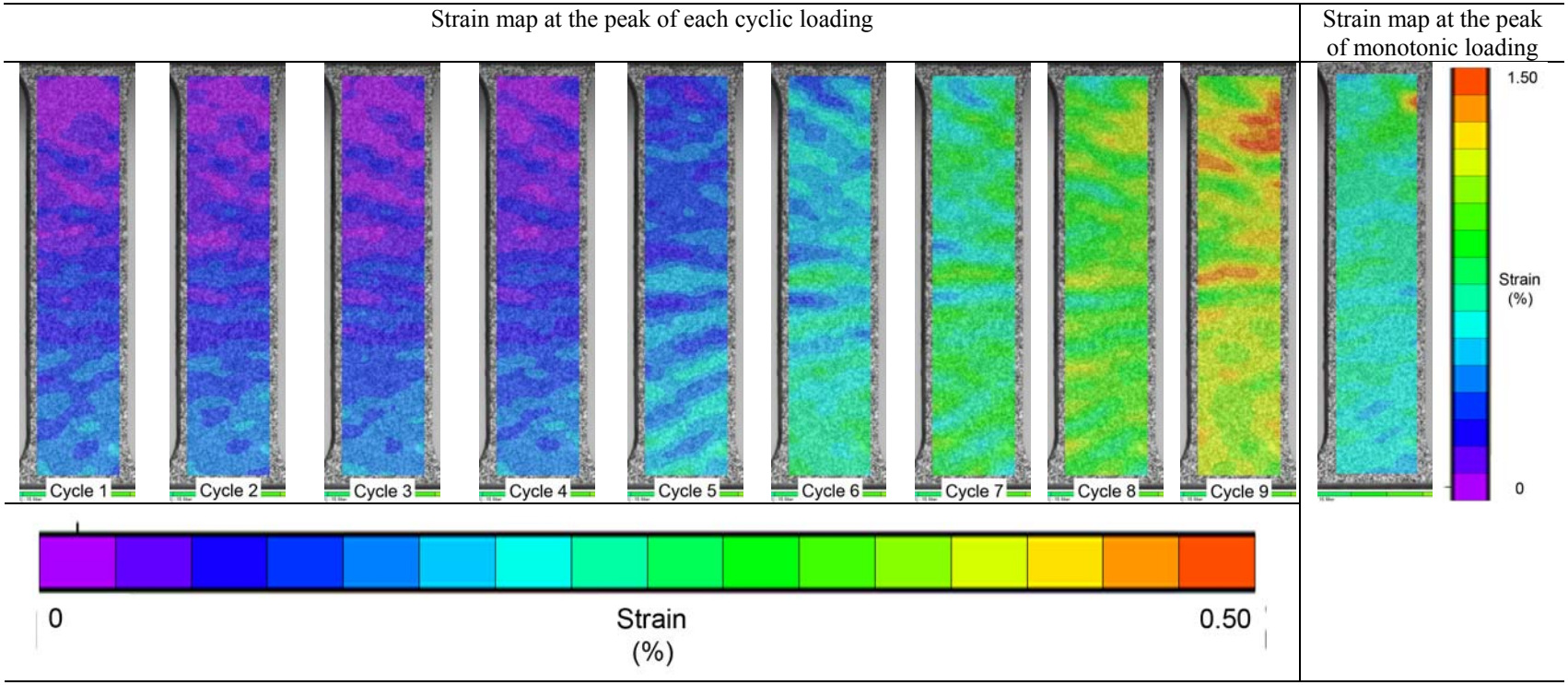

Figure F.6 Specimen C-6.